“When, Where, and How will Wetlands be Resilient to Climate Change”:

Estimating wetland resilience and carbon sequestration to anthropogenic disturbances across different geographies.

By

Pranjal Dwivedi

A dissertation submitted in partial satisfaction of the

requirements for the degree of

Doctor of Philosophy

in

Environmental Science, Policy, and Management

in the

Graduate Division

of the

University of California, Berkeley.

Committee in charge:

Professor Céline Pallud, Chair

Professor Ronald Amundson

Professor Dennis Baldocchi

Summer 2024

Abstract

“When, Where, and How will Wetlands be Resilient to Climate Change”:

Estimating wetland resilience and carbon sequestration to anthropogenic disturbances across different geographies.

By

Pranjal Dwivedi

Doctor of Philosophy in Environmental Science, Policy, and Management

University of California, Berkeley

Professor Céline Pallud, Chair

It is undeniable that climate change is one of the most pressing challenges facing humanity in the 21st century and that climate is changing at an unprecedented rate, primarily due to human activities such as burning fossil fuels, deforestation, and land-use changes. These activities have contributed to an unprecedented increase in greenhouse gas (GHG) emissions, most notably carbon dioxide (CO_2) responsible for bulk of the temperature increase[1], but also methane (CH_4) and nitrous oxide (N_2O), possessing greenhouse warming potentials 28 and 273 times of carbon dioxide, and increase global temperatures.

Wetland or soil carbon storage and GHG emissions are not comparable to fossil carbon emission inherently due to differences in the durability of the carbon impacts and likelihood that those impacts are reversed[2]. Fossil carbon emissions, in contrast to wetland greenhouse gas emissions, result from combustion of geologically sequestered carbon that had been stored for thousands to millions of years. Approximately 20-35% of emitted fossil carbon will remain for over 3000 years in the atmosphere with clear and quantifiable climate impacts[3]. However, natural climate solutions are “by nature” not guaranteed to be permanent. Carbon sequestration in soils and wetlands employ photosynthesis to move atmospheric carbon to biomass and belowground carbon pools, which can endure in storage anywhere from months to millennia[4]. Even if a carbon sequestration practice such as improved agricultural management, or construction and maintenance of wetlands were guaranteed to be maintained for many decades, natural or anthropogenic events may disrupt the system and release the carbon back to the atmosphere, reversing sequestration. However, even if these sequestration rates are

temporary and reversible they can still lead to negative radiative forcing reducing or delaying peak global temperatures depending on anthropogenic emissions trajectories[5,6]. Increasing wetland/soil carbon is unequivocally beneficial from a holistic perspective[7–9], with an added bonus of contributing to cooling the climate whenever the flux of GHGs out of the atmosphere and is higher than the flux in the opposite direction.

Wetlands, in particular, have emerged as a significant piece of the puzzle in the fight against climate change[10]. Wetlands are among the most productive and diverse ecosystems on Earth, providing a wide range of ecosystem services, including carbon sequestration, flood control, water purification, and wildlife habitat. Despite covering only around 6% of the Earth's land surface, wetlands store a disproportionate amount of carbon, with some estimates suggesting that they could store up to a third of the world's soil carbon[11,12]. However, wetlands are also one of the most threatened ecosystems on the planet, with an estimated 35% of the world's wetlands having been lost since 1970[13]. This loss has been primarily driven by human activities such as drainage for agriculture, urbanization, and pollution[14]. As wetlands are drained or degraded, the accreted peat and organic matter stored is mineralized and goes back into the atmosphere as carbon dioxide, contributing to further warming of the planet.

However, to effectively protect and restore wetlands, we need a more sophisticated understanding of how they respond to anthropogenic disturbances, such as fires[15], pollution[16], increasing sea levels and temperatures[17,18]. Studying wetlands and their response to anthropogenic perturbations is important for several reasons. First, it helps us to identify the drivers of wetland loss and degradation and develop targeted interventions to address these threats. Second, it allows us to quantify the carbon storage potential of different wetland types and regions, which is essential for informing natural climate solution strategies. Third, it helps us to assess the effectiveness of wetland conservation and restoration efforts and adapt our approaches as needed.

In this dissertation, I investigated the impact of anthropogenic disturbances on wetland soil response from two different geographies: a burned subalpine wetland in Wyoming, and three wetland sites comprising a salinity gradient in the Sacramento-San Joaquin Delta. To achieve this, I carried out experiments of increasing complexity, beginning from simple slurry-based experiments to sophisticated flow-through reactor experiments. I simulated disturbance events; namely monthly temperature variations in chapter 1, increased nitrate loadings and salinity concentrations in chapters 2 and 3 and altered root exudate regimes using model compounds in

chapter 4. Through my work, I was able to report the effects of both changing porewater/soil chemistry and plant inputs on greenhouse gas emissions and dissolved carbon fluxes.

Contents

Chapter 1: Short-term impacts of fire and rising temperatures on carbon storage and greenhouse gas fluxes in subalpine wetlands.

1. Introduction

Wildfires have been an ever present part of ecosystem disturbances throughout our geological history and are increasingly considered crucial to the proper functioning of ecosystems and to building resilience and evolutionary pressure for flora and fauna[19]. They are known to directly impact soils through the formation of pyrogenic carbon[20], which has implications for biological, physical, and chemical processes taking place in soils. Pyrogenic carbon (pyC) describes thermally altered carbon produced by the incomplete combustion of organic matter during fires[20 21]. It is estimated to comprise anywhere between 0 and 60% of total soil organic matter across grasslands, forests, agricultural soils, and wetlands[22 23]. Pyrogenic carbon is an important slow-cycling constituent of the carbon cycle[2 24] that can support microbial respiration[25] and can be used as an amendment to support carbon sequestration in soils and soils[26]. Due to its chemical recalcitrance, it has a longer half-life than non-thermally altered organic carbon[24,27]. Despite its chemical complexity and stability, recent research on organic matter decomposition dynamics in highly complex soil continuums has challenged our long-standing view of the stability of such organic matter compounds and fractions[28,29]. A recent study found increases in water extractable organic carbon and higher carbon dioxide fluxes for burned soils compared to unburned soils, along with specific metabolites implicated in microbial processing of organic carbon[30]. Elevated post-fire inputs of pyrogenic carbon can also impact cycling of native soil carbon through changes in dissolved organic carbon (DOC) export and greenhouse gas (GHG) production through "positive priming" effects, especially in the short-term[31,32]. Soil carbon priming is a phenomenon in which the addition of fresh organic matter to soil stimulates the decomposition of pre-existing soil organic matter (SOM)[33]. This process can lead to a short-term increase in carbon dioxide (CO_2) emissions from the soil, as the microbial community becomes more active and breaks down both the fresh organic matter and the older, more stable SOM[34]. Furthermore, the ability of pyC to act as an electron snorkel[35], the ability to absorb and shuttle electrons, can speed up mineral dissolution through the reduction of Fe(III) oxides and affect CO_2, methane (CH_4) and nitrous oxide (N_2O) production, especially in anoxic environments prevalent in wetlands. Loss in soil carbon due to DOC export and subsequent microbial

processing to carbon dioxide can be expected to vary by depth due to differences in soil organic carbon/total iron content, bulk density, abundance of Fe(III)-reducing bacteria, and pyrogenic carbon diffusive transport, which will increase redox potential due to its electron snorkelling ability and impact greenhouse gas fluxes from deep soils. This would alter the ability of these wetland systems, often thought as sinks of carbon[11,12], to sequester carbon post wildfire events.

On larger scales, wildfires, and subsequent input of pyrogenic carbon, are also known to increase[36–40], decrease[37,41–43] or not alter[44,45] DOC concentrations and greenhouse gas emissions reported immediately post-fire in streams and wetlands. Short-term decreases in post-fire DOC concentrations in surface water have been attributed to the combustion of soil organic matter[43], decrease of root exudates production after vegetation mortality[38], lower canopy throughfall, and inhibition of soil microbial activity[39]. On the other hand, increases in DOC concentrations in streams and wetlands immediately post-fire have primarily been attributed to erosion[46] of organic carbon and decrease in sorptive ability of soils due to higher pH[47]. Over shorter and longer timescales post-fire, rapid vegetation regeneration[48], and shift in vegetation structure and composition in wetlands and riparian areas will also have an impact on DOC and greenhouse gas fluxes [27 28]. Recent research has indicated that it takes close to nine months for dissolved organic carbon levels in a riverine watershed to recover to pre-fire levels[41] although the post-fire response in DOC concentrations could persist longer, up to 15 years, in smaller streams[39].

Here, we investigated the short-term impact (< 1 year) of forest fires on DOC concentrations and greenhouse gas fluxes in subalpine wetland soils. Given monthly temperature variations in summer, it was also important to investigate this impact across different temperatures. To achieve this, we performed controlled laboratory experiments with systems of increasing complexity (slurry experiments on homogenised soil, and flow-through experiments on intact soil cores) in order to measure potential rates of greenhouse gas production and DOC export using soils sampled shortly (< 1 year) post-fire. The slurry experiments allow for comparison with published literature where these experiments are ubiquitous. We found higher rates of DOC loss and carbon dioxide production from burned wetland sections, and also observed that production of greenhouse gases from burned and unburned wetlands increased with higher temperatures.

2. Methods

2.1 Location

The Mullen fire complex (WY, USA) is an ideal system to study the short-term (<1 year) post-fire biogeochemistry of wetlands and to examine the effects of inputs of pyC on DOC exports and GHG fluxes. The 2020 Mullen fire burned 715 km^2 of lodgepole pine (*Pinus contorta*) on the Colorado-Wyoming border in the Medicine Bow National Forest starting in September, 2020 and was 97% contained as of January, 2021[49], roughly seven months prior to sampling. The burned wetland is located 7 km on Road 517/Dry Park Road on Lake Creek (41.148244, -106.155794) in the Medicine Bow-Routt National Forest (Figures 1, 2). To limit inherent spatial heterogeneity in soil and porewater biogeochemical properties which make comparisons difficult, adjacent burned and unburned sections of the same wetland were sampled in July 2021. Three locations on the burned wetland were sampled to account for differences in post-fire vegetation growth, ranging from reed grass (***Calamagrostis canadensis*)** dominant sampling site #1 (Figure 1), tall cottongrass (***Eriophorum angustifolium***) dominant site 2, and water sedge (***Carex aquatilis***) dominant site #3.

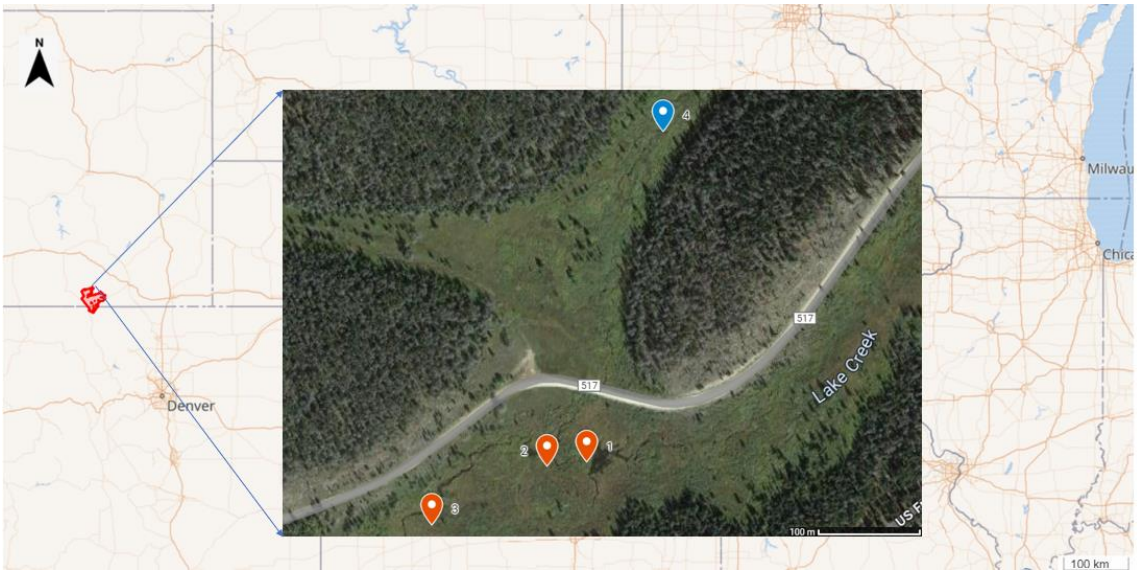

Figure 1. Extent of the 2020 Mullen fire (red outline). The inset shows sampling locations for the burned section of the wetland (sites 1-3, red) and for the unburned section of the wetland (site 4, blue).

Figure 2. Picture of the burned wetland section (Site 1) 9 months after fire (July 8, 2021), showing charred vegetation patches and adjacent burned forest.

2.2 Sampling and soil/water characterization

Porewater diffusion chambers, "peepers"[50,51] were installed in duplicate in each location of the 3 burned and single unburned locations (down to 30 cm) in July 2021, for a total of 8 peepers, and left to equilibrate for 21 days. Pore waters were sampled using dialysis samplers [50,51], also known as 'peepers'. The peepers were 36 cm long, 25 cm wide, and 5 cm thick, and included a removable stainless-steel handle for easy retrieval and a triangular base to facilitate submersion into wet sediments. They were constructed of low-density polyethylene with 22 equally spaced (0.5 cm intervals) 60-mL chambers (1×20×3 cm). The chambers were initially filled with deoxygenated, deionized water and covered with a 0.45 µm nitrocellulose membrane and the peepers were kept in anoxic conditions when transported to the field. At each site, a meter near the shoreline, peepers were quickly inserted into the unvegetated part of the sediment to prevent oxygenation and were left to equilibrate with the surrounding pore water for 8-10 weeks. Upon retrieval, the peepers were immediately placed in a N_2-flushed box and transported to the laboratory where they were transferred in a N_2/H_2 (96-4%) glove bag. Pore waters were extracted from the chambers, filtered, and transferred into vials until processing. The peepers were deployed at the four study sites in During retrieval, peepers were instantly transferred to a large Ziploc bag and flushed with N_2 gas using a small cylinder brought into the field to prevent oxidation of water samples in the peeper chambers. They were then transferred to an ice cooler, along with the soil cores, and subsampled for chemical analyses within 6 hours of being retrieved from the field. Water samples were subsequently acidified with dilute (2% w/v) HNO_3 to preserve chemical speciation of dissolved Fe and N cations/anions. Relevant extractable anions and cations were measured using a Dionex ion chromatograph (IC) (electrochemical detector, ED40; analytical column, AS23/AG23; anion self-regenerating suppressor, ASRS-I, 4 mm; mean detection limit: 30 µg/L, error: 5 µg/L) supplied with a carbonate eluant (7.2 mM Na_2CO_3 and 1.28 mM $NaHCO_3$) at a flow rate of 1.0 mL min^{-1}.

For each peeper location, duplicate soil cores were taken to a depth of 24 cm after removal of the top organic matter layer, which overlaid soils from all three sites. One core was separated in two depth intervals (0-12 cm and 12-24 cm) and each was used for soil physical and chemical characterization, while the second one was used for flow-through reactor experiments (see section 2.4). Soil dry bulk density was determined by drying a known volume of soil for 24 hours at 105^{o}C. Soil pH was measured by suspending 5g of soil in a 10 mM $CaCl_2$ solution[52]. Total organic carbon and nitrogen percent was measured by combusting 30 mg of dried soil using a NC 2100 Elemental Analyzer (CE Instruments, USA). Soil samples were digested in an Environmental Express Digester following the EPA 3050B protocol[53]. . Oxalate-extractable Fe, understood as a proxy for poorly-ordered oxides more likely to participate in redox reactions, was determined using Schwertmann's protocol[54]. The percentage ash in soil was determined by combusting the dried soil to 450^{o}C in a muffle furnace in a ceramic crucible and calculating the reduction in weight following the ASTM (American Society for Testing and Materials) D2794 protocol[55].

2.3 Slurry experiments

Duplicate soil slurry experiments were carried out in 125 mL serum bottles, using a 1:4 (w/w) wet soil: deionized water mixture[56], with pH held constant at 7.5 to mimic field conditions (Appendix 1), in order to get preliminary estimates of potential rates CO_2, CH_4, and N_2O production in each site. Soils from 0-12 cm and 13-24 cm were homogenized prior to incubations. Serum bottles were also evacuated, and the sterile deionized water was flushed with N_2 to maintain oxygen-free experimental conditions. Slurries were sub-sampled every hour for the first six hours, and subsequently daily, for a period of seven days for liquid and gas analyses. An equal amount of $N_2$was injected into the bottles to maintain vapour pressure during gas sampling. Liquid samples were filtered through a 0.22 µm PTFE membrane syringe filter (Whatman; 25 mm filter size) prior to chemical analyses for total Fe, Fe(II), NO_3^-, SO_4^{-2} , NH_4^+ , and DOC. Liquid samples were analysed as described in Section 2.2. Concentrations of CO_2, CH_4, and N_2O in the gaseous sub-samples were analysed on an Agilent 7890B GC (Agilent, Santa Clara, CA) for using thermal conductivity, flame ionization, and nitrogen chemiluminescence detectors (TCD, FID, and NCD) respectively. Concentrations of CO_2, CH_4, and N_2O were then used to calculate potential CO_2, CH_4, and N_2O fluxes according to:

$$F = \frac{V}{A*m} * \frac{\Delta C}{\Delta T} \quad (1)$$

Where *F* is the gas flux (µmol [CO_2 or CH_4] g $soil^{-1}$ m^{-2} s^{-1}), V is the volume of the slurry, A is the area of the serum bottle cross-section, Δ*C* is the gas concentration difference between consecutive time points (mol m^{-3} [CO_2, CH_4, and N_2O]), *m* is the mass of dry soil, and Δ*t* is the time increment. Values were converted from ppm to mol m^{-3} using the ideal gas equation. Gas concentrations from initial kinetic phase were considered for flux calculations due to a stronger linear slope, following best practices from Hutchinson et.al[57]. Due to constant mixing of the slurries leading to a disruption of the soil and microbial community structure, the potential fluxes measured this way reflect the maximum potential of the system to produce those GHGs. In comparison, flow through reactors preserve the pore structure and the spatial distribution of solid-bound constituents, including microorganisms and substrates, thereby providing a simple means of determining reaction rates under conditions that more closely reflect the initial in situ conditions than would well-mixed batch experiments[58].

2.4 Flow-through reactor experiments

Flow-through reactor (FTR) experiments were performed to measure the potential rates of Fe(II), DOC, DIC and methane export under conditions that preserve the pore structure and the spatial distribution of solid-bound constituents, including microorganisms and substrates,

thereby providing a simple means of determining reaction rates under conditions that more closely reflect the initial in situ conditions than would well-mixed slurry experiments[58]. The advantages of the FTR are that reaction rates are determined for near steady-state conditions and dissolved metabolic byproducts do not accumulate in the reactor[58]. The reaction rates, Fe(II), DOC/DIC, and methane rates obtained from our experiments are referred to as ''potential'' rates, as they correspond to conditions where Fe(III) oxides are the dominant terminal acceptor accessible to microbes[59]. Experiments were performed in duplicate using from two depths: 0-2 and 15-17 cms. Each FTR contained an undisturbed soil core within a 2 cm long and 4.2 cm diameter Plexiglass ring, with 0.2 µm pore size nitrocellulose filters and glass fiber filters at each end (Figure 3). The FTR were sealed on either side with Plexiglass caps tightened with screws, with O-rings to prevent leaks. Input/output channels opened at the center of the caps at the contact with the glass fibers filters and create a uniform flow throughout the cross-section of the soils[58]. The experiments were carried out in a glove bag under anoxic conditions (4.5% H_2, 95% N_2) and the FTR were placed in a temperature-controlled water bath to ensure constant temperatures of 9, 18, and 27°C, simulating minimum, mean, and maximum air temperatures for the month of July for this area, using data from the Elk Mountain Weather Station, located at a similar elevation (2,225 m)[60]. An input solution was supplied to the reactors at a constant volumetric flow rate (1.5 ± 0.1 mL hr^{-1}) imposed by a peristaltic pump, corresponding to residence times between 12-14 hours, similar to residence times for wetland geographies at similar elevation and slope[61,62,63]. The input solution was a synthetic porewater that mimicked the chemical composition of porewater samples in the field. It contained an average of 5 mg L^{-1} Na^+, 30 mg L^{-1} Ca^{+2}, 15 mg L^{-1} K^+, and 0.15 mg L^{-1} NH_4^+ And was purged with N_2 to remove any oxygen. Outflow samples were collected every day and analyzed for Fe(II) and DOC/DIC concentrations. Fe(II) was measured spectrophotometrically using the ferrozine method at 562 nm[64]. DOC/DIC was measured using a wet oxidation total inorganic and total organic C analyzer (Model 1010 Wet Oxidation Total Organic/ Total Inorganic Carbon Analyzer OI Analytical) with 50 g L^{-1} H_3PO_4 for total inorganic C and 100 g L^{-1} $Na_2S_2O_8$ for total organic C with heat catalysis at 100 °C (detection limit: 12 µg/L, standard error: 3.5 %). Outflow samples were subsampled and sparged with N_2 gas and the headspace sampled to purge the water of CO_2, CH_4 and N_2O. Gas samples were analysed on an Agilent 7890B GC (Agilent, Santa Clara, CA) for CO_2, CH_4, and N_2O using thermal conductivity, flame ionization, and nitrogen chemiluminescence detectors (TCD, FID, and NCD) respectively.

Potential steady-state rates of Fe(II) export, DOC export, DIC export, CH_4, and N_2O export were calculated according to the equation (2) using 18±3 data points from steady-state conditions when chemical composition of the outflow was no longer fluctuating significantly, according to:

$$R = \frac{\Delta C * Q}{V} \qquad (2)$$

where Q is the volumetric flow rate, V is the reactor volume, and ΔC is the difference in concentration of the solute between the outflow and inflow solutions at steady-state[65]. It took for Fe(II) and DOC concentrations around 12 days after the start of the experiment to reach steady-state. Fe(II) export rates provide a lower limit for Fe(III) reduction rates due to secondary precipitation of Fe(II) to siderite and lepidocrocite[66], sorption onto clay minerals, and/or binding to native organic matter sorbed onto mineral surfaces[67]. These rates were then used to calculate Q_{10} values following Chen et.al[68] as:

$$Q_{10} = \left(\frac{R_2}{R_1}\right)^{\frac{10}{T2 - T1}}$$

where R_2 and R_1 are rates calculated for temperatures T_2 and T_1, where T_2 and T_1 are temperatures tested in the experiment, with $T_2 > T_1$.

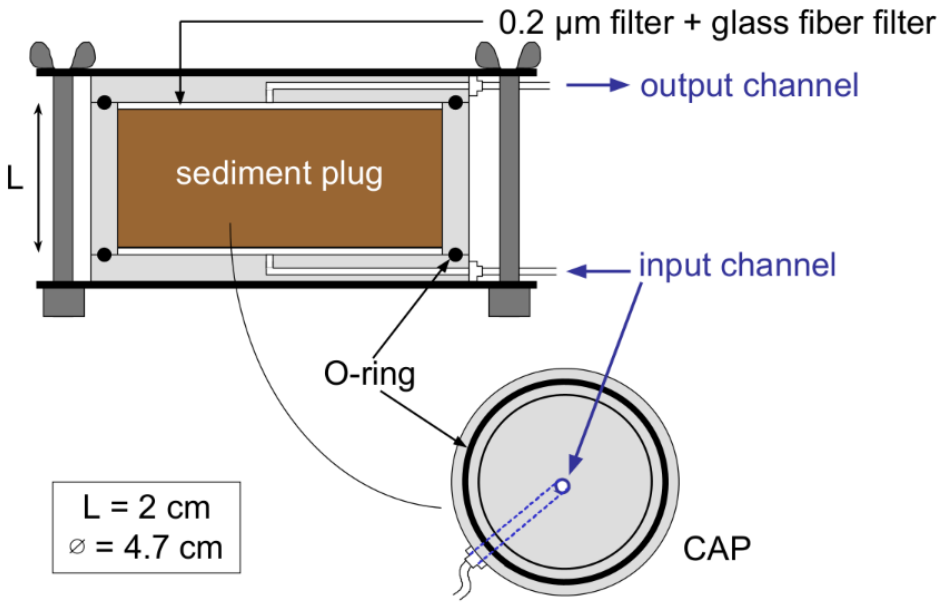

Figure 3. Side and top view of a flow-through reactor, adapted from Pallud and van Cappellen[58].

2.5 Statistical analyses

All statistical analyses were carried out in R[69]. Data was tested for normality using the Shapiro-Wilk test and log-transformed when necessary. Differences between all measured water, soil, and gas variables were determined using a t-test with a threshold of $p <= 0.05$. Tukey's honest significance difference test was used to determine which sites, if found significant ($\alpha = 0.05$),

were different. Pearson's correlation coefficients were calculated between measured water, soil, and gas variables and visualized using the 'corrplot' function in R[70]. Multivariate analyses were performed to evaluate differences in water, soil, and gas concentrations. Given these concentrations vary by orders of magnitude, it was desirable to relativize them by column totals through the 'decostand' function using the 'vegan' package[71]. These were then visualized using Principal Components Analysis (PCA) ordinations. PCA was performed in R using the 'prcomp' function which is a part of the 'stats' package[29]. NMDS, or non-metric dimensional scaling, was used to collapse data from multiple response variables for the purposes of dimension reduction and visualization. The NMDS plot is a useful tool for illustrating overall differences between sites, especially with multivariate response data. NMDS relies on distance matrices, which are computed on the basis of differences between relativized concentrations of all measured response variables The function was performed using "metaMDS" and visualized using "ordiellipse", both included within the 'vegan' package[71].

3. Results

3.1 Soil and porewater characteristics

Table 1. Soil and porewater physical and chemical characteristics for the four study sites and two studied depth intervals (0-12 and 13-24 cm). Values reported are means obtained from triplicate samples. Different superscripted letters indicate significant differences at p<= 0.1 for each row. Standard deviations were <30% of measured values and omitted for brevity.

Soil characteristics **Depth interval (0-12 cm)**	**Burned 1**	**Burned 2**	**Burned 3**	**Unburned**
Sand content (%)	32.1±2.5 ^{a}	29.7±1.5^{a}	24.4±3.7^{b}	12.3±1.9^{c}
Silt content (%)	25.3±2.5^{a}	22±2.5^{a}	30.6±4.1^{b}	36.5±2.7^{c}
Clay content (%)	42.3±6.5^{a}	47±4.6^{b}	44.9±2.5^{a}	50.9±2.5^{b}
Textural class	Clay	Clay	Clay	Clay
Dry bulk density (g cm^{-3})	0.31±.07^{a}	0.30±.05 ^{a}	0.29±.03^{a}	0.34±.08^{b}
pH	6.17±.61^{a}	6.36±.42 ^{a}	6.19±.33^{a}	5.28±.53^{b}
Percent ash (by weight)	8.83±1.71^{a}	7.19±2.51 ^{a}	6.55±1.5^{a}	1.12±.25^{b}
C_{org} content (%)	23.6±2.11^{a}	21.3±3.45 ^{a}	22.5±1.95^{a}	30.7±2.27^{b}
Total N content (%)	1.17±.11^{a}	1.2±.35^{a}	0.97±.25^{a}	2.28±.57^{b}
Molar C_{org}:N ratio	22.54±2.06^{a}	19.73±3.15^{a}	22.6±1.87^{a}	14.39±2.16^{b}
Extractable Fe content (mg g of $soil^{-1}$)	22.57±4.51^{a}	23.89±3.63^{a}	22.86±5.52^{a}	19.37±3.72^{a}
Extractable Ca content (mg g of $soil^{-1}$)	344.7±42.5^{a}	281.5±31.6^{b}	266.7±37.1^{b}	126.3±12.9^{c}
Extractable Mg content (mg g of $soil^{-1}$)	27.12±3.92^{a}	24.80±2.33^{a}	23.9±4.91^{a}	19.86±2.55^{b}

Depth interval (13-24 cm)	**Burned 1**	**Burned 2**	**Burned 3**	**Unburned**
Sand content (%)	12.1±3.6[a]	9.17±2.7[b]	14.24±1.9[a]	7.35±1.15[b]
Silt content (%)	35.32±4.16[a]	32.61±5.19[a]	32.62±4.57[a]	38.57±6.1[a]
Clay content (%)	52.63±4.94[a]	57.63±6.67[a]	54.91±4.77[a]	55.91±7.59[a]
Textural class	Clay	Clay	Clay	Clay
Dry bulk density (g cm^{-3})	0.51±.13[a]	0.48±.11[a]	0.53±.07[a]	0.52±.09[b]
pH	6.28±.35[a]	6.33±.47[a]	6.11±.37[a]	6.09±.42[a]
% ash (by weight)	2.43±.57[a]	3.19±.36[b]	2.55±.44[a]	0.73±.17[b]
C_{org} content (%)	7.56±1.38[a]	9.73±2.51[b]	10.51±1.67[b]	15.67±3.45[c]
Total N content (%)	0.33±.06[a]	0.32±.07[b]	0.34±.09[b]	0.58±.11[c]
Molar C_{org}:N ratio	26.54±1.37[a]	30.31±2.15[a]	30.91±1.16[a]	28.39±3.36[a]
Extractable Fe content (mg g of $soil^{-1}$)	28.17±4.57[a]	24.19±5.51[a]	29.86±6.17[a]	25.37±4.75[a]
Extractable Ca content (mg g of $soil^{-1}$)	284.19±32.77[a]	270.41±42.19[a]	226.69±39.17[a]	116.4±12.71[b]
Extractable Mg content (mg g of $soil^{-1}$)	28.32±2.65[a]	25.98±4.57[a]	27.9±3.97[a]	22.19±1.87[b]
Porewater concentrations				
Depth interval (0-12 cm)				
Porewater DOC (mg/L)	84.15±10.37[a]	103.70±2.5[b]	104.82±2.5 [b]	65.12±2.5 [c]
Porewater sulfate (ppm)	3.33±.55[a]	2.83±.47[a]	3.12±.39[a]	1.38±.33[b]
Porewater nitrate (ppm)	1.88±.36[a]	1.39±.25[b]	1.30±.17[b]	0.47±.08[c]
Porewater Fe(III) (ppm)	2.51±.49[a]	2.83±.38[a]	2.45±.67[a]	1.57±.29[b]
Depth interval (13-24 cm)				
Porewater DOC (mg/L)	90.27±17.15[a]	108.93±22.7[b]	104.23±12.4[b]	60.27±12.33[c]
Porewater sulfate (ppm)	1.11±.27[a]	1.43±.36[a]	1.22±.27[a]	0.78±.15[b]
Porewater nitrate (ppm)	0.12±.02[a]	0.15±2.5 [b]	0.10±.01[b]	0.11±.03[c]
Porewater Fe(III) (ppm)	0.25±.06[a]	0.31±.09[a]	0.31±.05[a]	0.27±.03[a]

Table 1 shows that the sites were statistically similar with regards to their measured physical properties, with similar bulk density and textural class. All sites were characterized by high clay content (>42%), and the unburned site was characterized by a lower sand content but higher silt content than the other sites. The unburned site had significantly less ash ($p = 0.001$) than the burned sites (6.6-8.8%), and ash content across the burned sites was significantly higher in the

top soil (0-12 cm) than for the deeper depth interval (13-24 cm) ($p = 0.064$). The burned sites had significantly lower C content (21.5-23.3%) ($p = 0.025$) and N content (0.97-1.26%) ($p = 0.027$) than the unburned site (30.7% and 2.28%, respectively). The C:N ratios increased significantly by depth for both burned and unburned sites ($p = 0.012$). The soil pH was slightly acidic, and the pH of the topsoil in the burned sites was about one unit higher than for the unburned site (5.28) ($p = 0.027$), although there were no significant differences between sites for the deeper soil. Extractable Fe content did not significantly differ between the burned and unburned soils, but significantly increased with depth ($p = 0.041$). Burned and unburned soils from shallower depths were characterized by significantly higher porewater nitrate concentrations compared to deeper soils ($p = 0.057$). Additionally, they possessed higher porewater sulfate concentrations compared to unburned soils ($p = 0.031$) and higher DOC concentrations compared to unburned soils ($p = 0.05$). For deeper depths, differences for porewater nitrate, sulfate, and dissolved organic carbon were found not to be statistically significant.

3.2 Concentrations and fluxes of greenhouse gases in slurry experiments

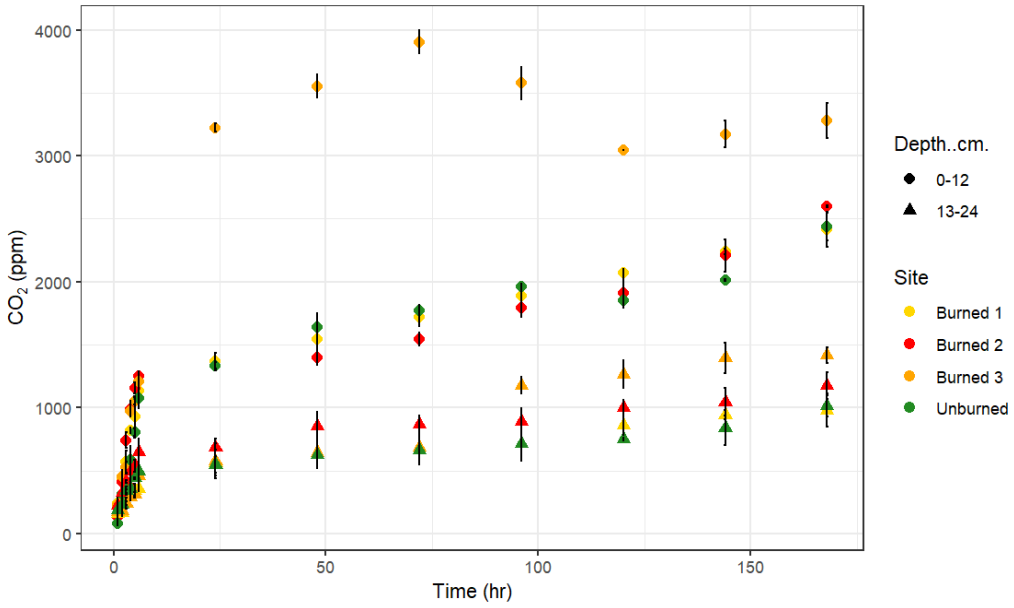

Figure 4. Concentrations of CO_2 produced as a function of time in slurry experiments with soils from two depths (shallow soil: diamonds, deep soil: triangles), and four sampling locations. Error bars represented standard deviations of triplicate measurements, found not to exceed >40% of measured value for any time point.

Figure 4 shows the temporal evolution of CO_2 concentrations in the slurry experiments. Concentrations of CO_2 increased throughout the course of the experiment across 6 of the 8 experimental conditions shown here. Averaged for all time points, burned shallow soils, produced on average as much as 24.7% more CO_2 than unburned soils (Figure 4). This trend was not significant for the deeper soils. Deeper soils, on average across all time points, also produced 52.7% less CO_2 than shallower soils by the end of the experimental period.

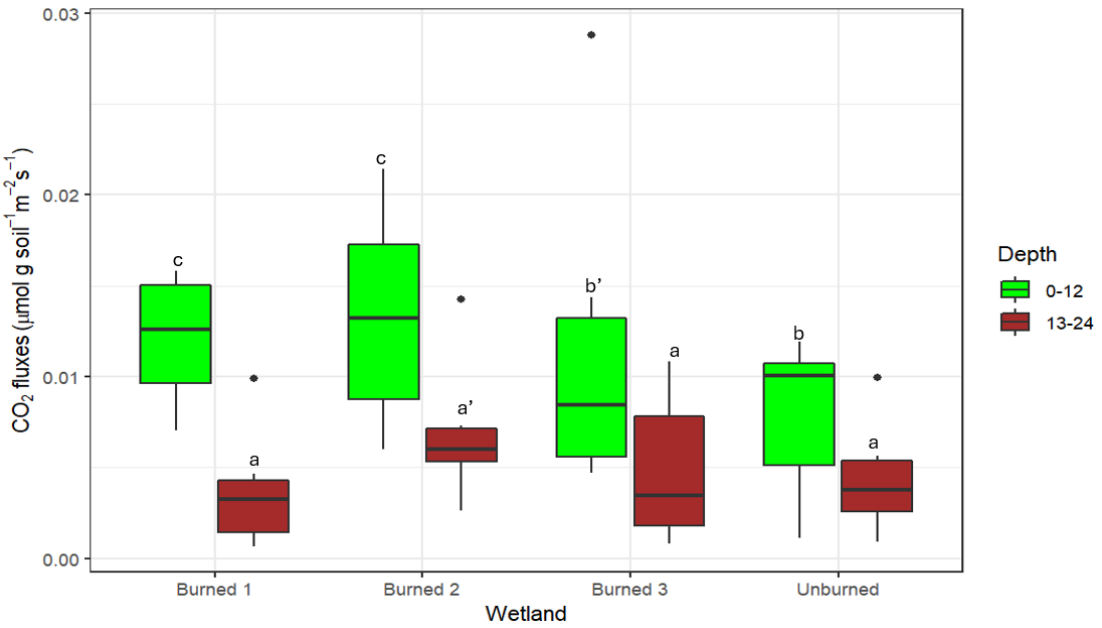

Figure 5. Average CO_2 fluxes calculated for the initial rapid evolution phase of the slurry experiments, spanning measurements taken from 1-24 hours. Green and red bars represent depth interval of 0-12 and 12-24 cm, respectively. Different letters indicate significant differences at p<= 0.05. Letter' represents differences at significance level p <=0.1.

Figure 5 shows initial rapid fluxes of CO_2 calculated for the first 24 hours of the incubation period. Burned sediments, on average, produced significantly higher fluxes, 0.013 µmol g $soil^{-1}m^{-2}s^{-1}$ compared to 0.08 µmol g $soil^{-1}m^{-2}s^{-1}$ for unburned sediments (p << 0.05). Burned topsoil produced significantly higher CO_2 fluxes compared to deeper sediments (0.011 µmol g $soil^{-1}m^{-2}s^{-1}$ v/s 0.049 µmol g $soil^{-1}m^{-2}s^{-1}$). Burned site 3 topsoil had lower fluxes of CO_2 despite higher CO_2 accumulation (Figure 3), however they were still higher than fluxes from unburned topsoils (p = 0.076). There was some statistically significant variation between Burned site 1 and Burned 2 (p = 0.091) despite having similar concentration profiles and accumulation. There were minimal differences between soils from deeper depths between burned and

unburned wetland sections, with only wetland 2 being significantly different from the rest (p = 0.089).

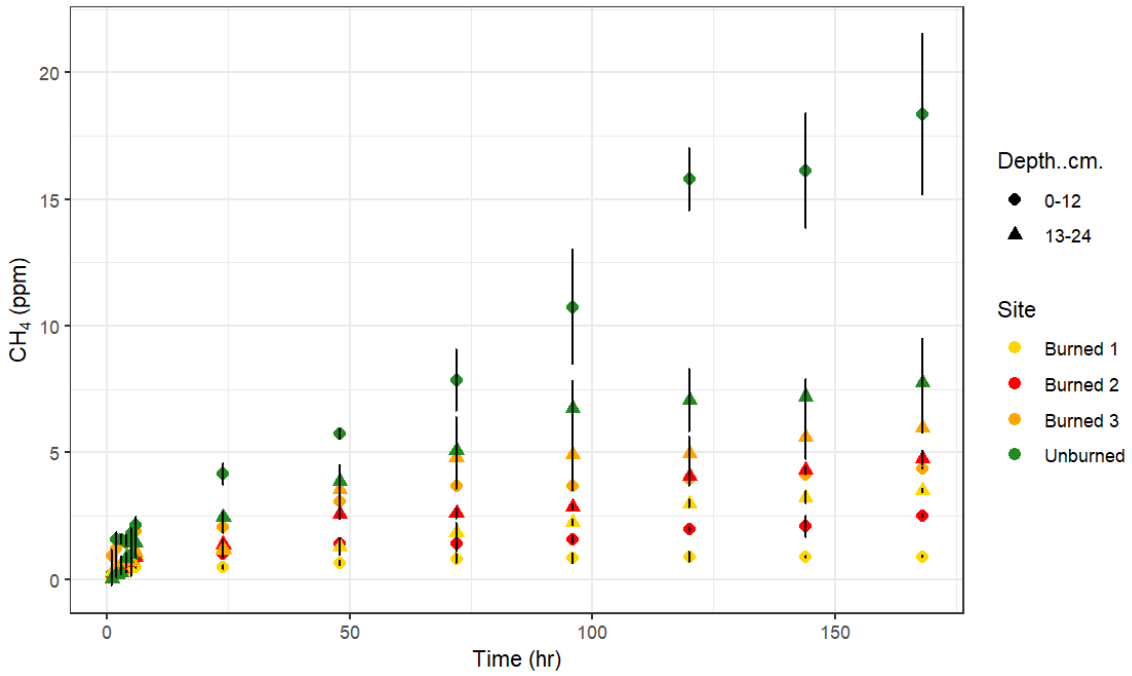

Figure 6. Concentration of CH_4 produced as a function of time in slurry experiments with soils from two depths (shallow soil: diamonds, deep soil: triangles), and four sampling locations. Error bars represented standard deviations of triplicate measurements, found not to exceed >40% of measured value for any time point.

Figure 6 shows the temporal evolution of CH_4 concentrations in the slurry experiments. Concentrations of CH_4 increased over time, but stabilized in the experiments with burned soils sometimes within 1 day (Burned 1), whereas they increased for the whole duration of the experiments for unburned soils. Unburned soils, on average, produced 2.89 times more CH_4 compared to soils from burned areas averaged over all time points. Shallower unburned soils produced significantly more CH_4 concentrations than deeper soils, however this trend was reversed for shallow and deep soils from burned wetland sections.

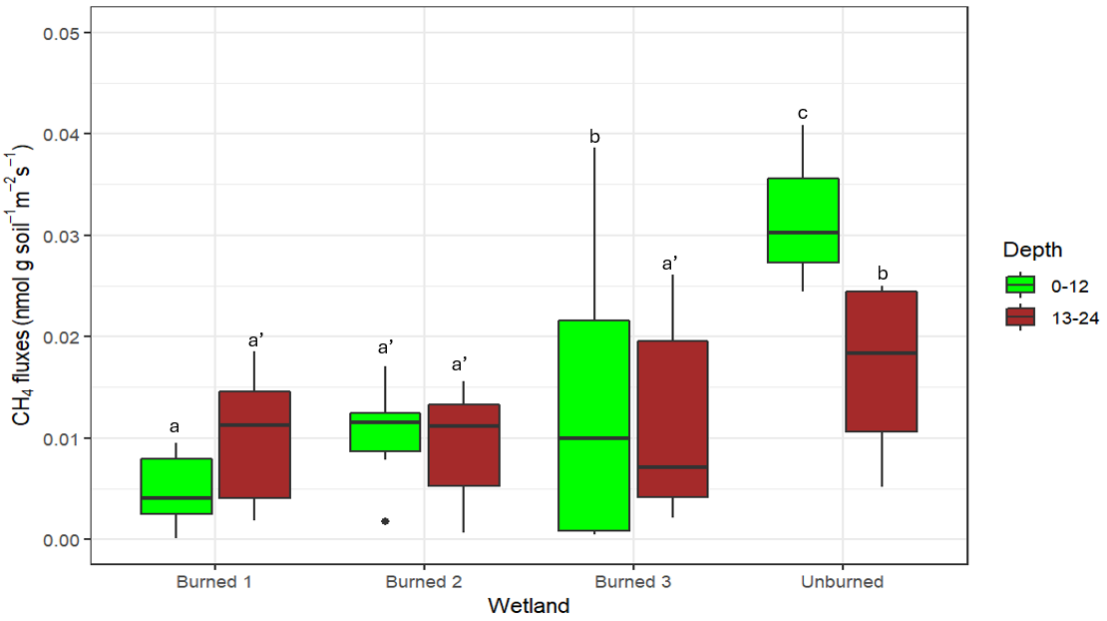

Figure 7. Average CH_4 fluxes calculated for the initial rapid evolution phase of the slurry experiments, spanning measurements taken from 1-24 hours. Green and red bars represent depth intervals of 0-12 and 12-24 cm, respectively. Different letters indicate significant differences at p<= 0.05. Letter' represents differences at significance level p <=0.1.

Figure 7 shows initial rapid fluxes of CH_4 calculated for the first 24 hours of the incubation period. Fluxes shown in Figure 6 highlight the statistically significant differences ($p << 0.05$) between CH_4 fluxes from unburned and burned wetland sections, for shallow and deep soils. Unburned topsoils produced 0.13 nmol g $soil^{-1}$ m^{-2} h^{-1} compared to an average of 0.062 nmol g $soil^{-1}$ m^{-2} h^{-1} for burned topsoils. This trend persisted for deeper soils, with a flux of 0.071 nmol g $soil^{-1}$ m^{-2} h^{-1} for unburned wetland sections compared to an average of 0.032 nmol g $soil^{-1}$ m^{-2} h^{-1} for burned wetland sections. Averaging for shallow and deep soils across burned and unburned sections, there were no statistically significant differences for CH_4 fluxes, however shallow soils from unburned and burned site 3 produced significantly higher fluxes ($p = 0.023, 0.067$) than deeper soils.

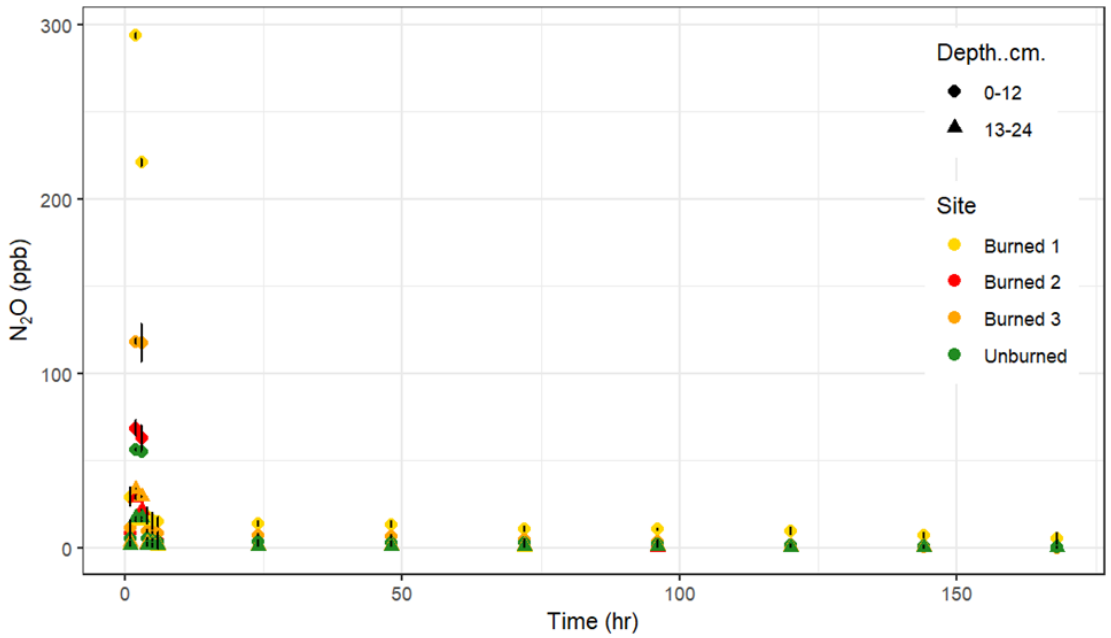

Figure 8. Concentrations of N_2O produced as a function of time in slurry experiments with soils from two depths (shallow soil: diamonds, deep soil: triangles), and four sampling locations. Error bars represented standard deviations of triplicate measurements, found not to exceed >40% of measured value for any time point.

Figure 8 shows the temporal evolution of N_2O concentrations in the slurry experiments. Burned soils produced higher N_2O concentrations compared to burned soils (Figure 7), however the pattern of N_2O concentrations across the sites was a strong initial pulse around 1-2 hours after the start of the experiment, followed by a steep decline for the remainder of the experiment.

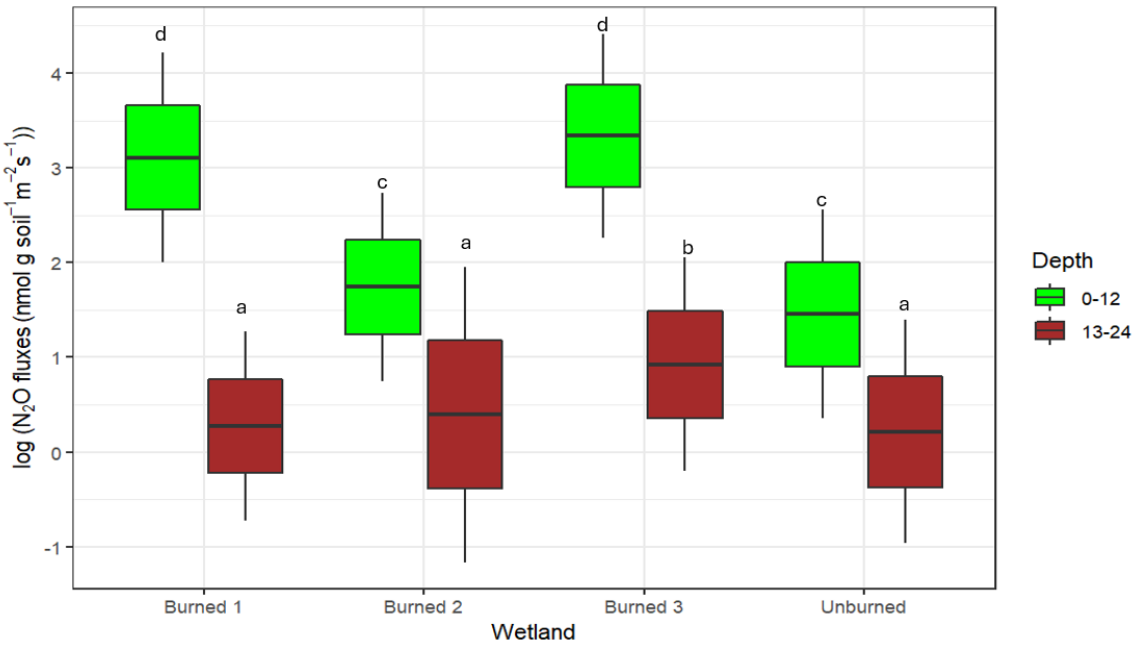

Figure 9. Average log-transformed N_2O fluxes calculated for the initial rapid evolution phase of the slurry experiments, spanning measurements taken from 1-24 hours. Green and red bars represent depth intervals of 0-12 and 12-24 cm, respectively. Different letters indicate significant differences at p<= 0.05. Letter' represents differences at significance level p <=0.1.

Figure 9 shows initial rapid fluxes of N_2O calculated for the first 24 hours of the incubation period, and plotted as log-transformed for ease of visual representation. On average, shallow soils from burned sites significantly higher N_2O fluxes compared to unburned shallow soils ($p << 0.05$). Differences in deeper sediments were less pronounced, with burned site 3 producing the highest N_2O fluxes ($p = 0.035$) with the remaining burned and unburned N_2O fluxes not significantly different from each other.

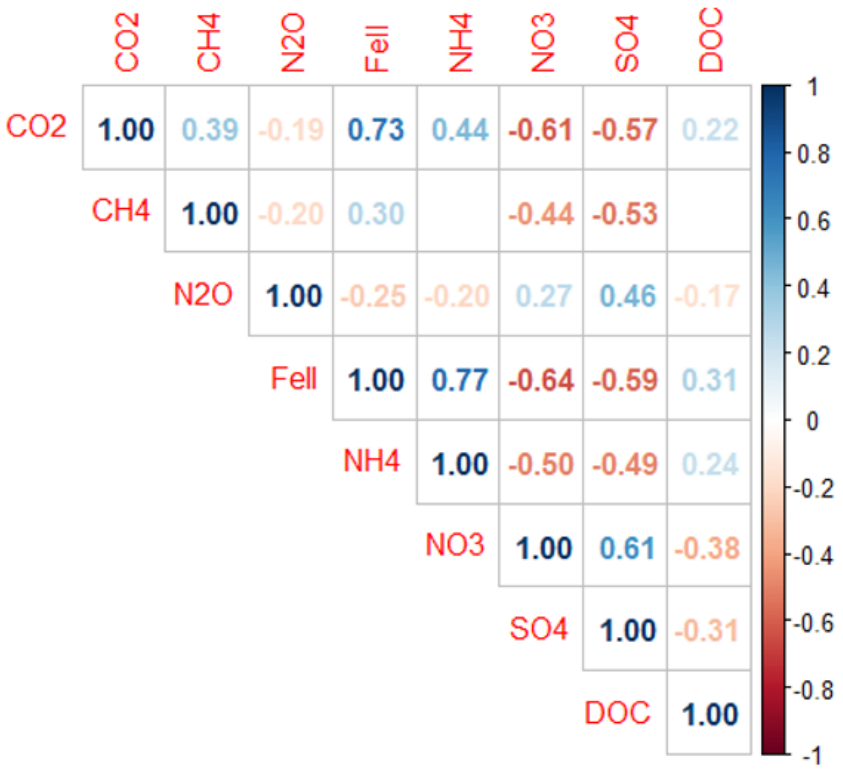

Figure 10. Correlation plot of all measured response variables from the slurry experiments for each time point. Fe(II), NH_4^+, NO_3^-, SO_4^{-2} and DOC were measured from aqueous samples post filtering. Correlation coefficients are reported at a threshold of p <= 0.05.

Correlation plot for measured chemical parameters from the slurry experiments (Figure 10) reveals more associations between gas and aqueous chemical parameters. Carbon dioxide concentrations were strongly positively correlated with porewater reduced iron (Fe(II)), and ammonium concentrations, whereas associations of carbon dioxide with methane and DOC were a bit weaker. Carbon dioxide was also strongly negatively associated with porewater nitrate and sulfate concentrations, and weakly negatively associated with nitrous oxide concentrations. Methane concentrations were negatively associated with porewater nitrate and sulfate concentrations, while being weakly positively correlated with porewater Fe(II) concentrations levels in the bottle reactors. Nitrous oxide concentrations were weakly positively correlated to nitrate and sulfate concentrations in the slurry mix. There were also notable strong associations between redox-relevant ionic species, with porewater nitrate and sulfate concentrations being positively correlated, whilst both were negatively correlated with porewater ammonium and Fe(II) concentrations.

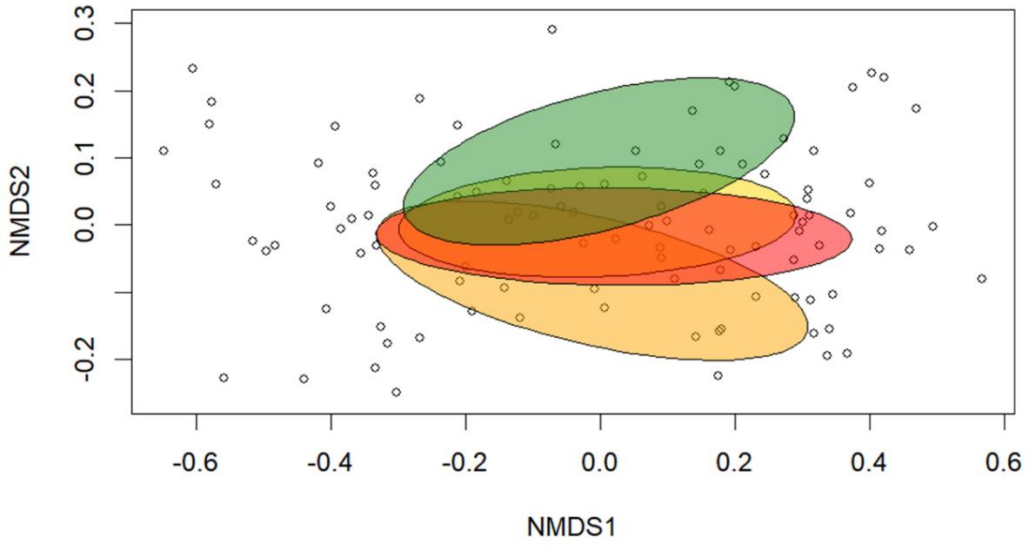

Figure 11. NMDS (non-metric multidimensional scaling) plot of all measured variables from the slurry experiments. Gold, red, orange, and green ellipses represent Burned 1, Burned 2, Burned 3, and Unburned sites' measured variables, respectively.

Figure 11 shows the NMDS plot of all measured variables from the slurry experiments. There is separation between unburned and burned soils, whereas there exists a significant amount of overlap between the three burned soil ellipses. There is higher overlap in the NMDS plot with polygons representing the two depth intervals (not shown here).

3.3 Potential export rates of iron, greenhouse gases, and dissolved carbon measured using FTR experiments.

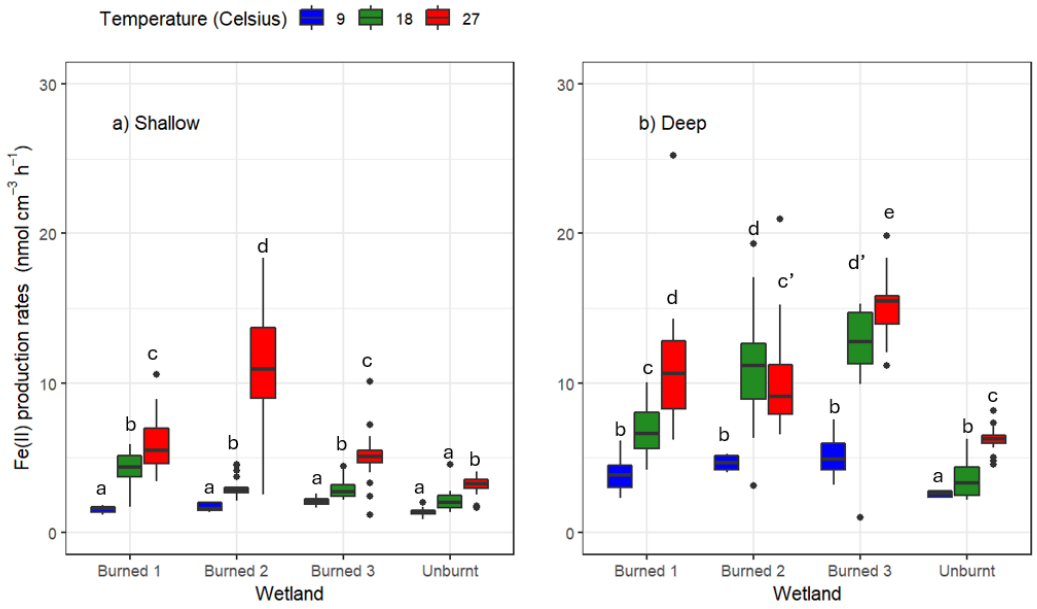

Figure 12 Potential steady-state Fe(II) export rates measured using FTR experiments for the four sampling locations in response to temperatures of 9 (blue), 18 (green), and 27°C (red), for **(a)** the shallow soil interval (0-2 cm) and **(b)** the deeper soil interval (15-17 cm). Different letters denote significant differences at p <= 0.05. Letter' denote significant differences at p <= 0.1.

Table 2. Q_{10} values reported for each site and depth combination for potential Fe(II) production rates. Values are reported pairwise for temperatures at which flow-through reactor columns were incubated.

Site + Depth	Q_{10} (9-18)	Q_{10} (18-27)	Q_{10} (9-27)
Burned 1 (0-2 cm)	3.14	1.42	2.11
Burned 2 (0-2 cm)	1.87	4.31	2.84
Burned 3 (0-2 cm)	1.45	1.86	1.64
Unburned (0-2 cm)	1.62	1.53	1.57
Burned 1 (15-17 cm)	1.91	1.71	1.80
Burned 2 (15-17 cm)	2.59	0.92	1.54
Burned 3 (15-17 cm)	2.73	1.24	1.84
Unburned (15-17 cm)	1.43	1.86	1.63

Figure 12 shows the steady-state potential Fe(II) export rates measured for all sites and depths, and in response to three temperatures, while Table 2 summarizes the Q_{10} calculated from those rates. Fe(II) export rates varied considerably among the wetland sites and across incubation temperatures. The unburned site exhibited the lowest rates, ranging from approximately 3.1 to 4 mmol cm^{-3} h^{-1}, with minimal variation across the temperature treatments. In contrast, the burned sites showed significantly higher Fe(II) export rates, particularly at the higher incubation temperatures. Burned site 2 showed significantly higher Fe(II) export rates at the warmest temperature ($p << 0.05$), with the 27°C incubation yielding a rate of nearly 20.1 mmol cm^{-3} h^{-1}, followed by the 18°C and 9°C incubations at approximately 5.4 and 5.1 mmol cm^{-3} h^{-1}, respectively, which were not significantly different than other burned sites at similar temperatures. Burned sites 1 and 3 also showed elevated Fe(II) export rates compared to the unburned site, with rates ranging from 5 to 10 mmol cm^{-3} h^{-1} across the temperature treatments. On average, burned wetland sites exhibited substantially higher reduced iron export rates compared to the unburned reference site ($p < 0.05$), and increasing incubation temperatures led to higher Fe(II) export rates ($p < 0.05$).

This trend was reflected in Q_{10} values obtained *via* pairwise comparison of rates for our three temperatures for shallow and deep soils from burned and unburned sections. Q_{10} values ranged from 1.45 to 4.31 for shallow soils compared to 0.92 to 2.73 for deeper soils. On average Q_{10} values were found to be higher for shallow soils from burned sections compared to unburned sections. This trend was also observed for deep soils as well with higher Q_{10} for burned sections compared to unburned sections. There was high variation in values obtained for Q_{10} comparing rates between 18 and 27°C, ranging from 0.92 to 4.11

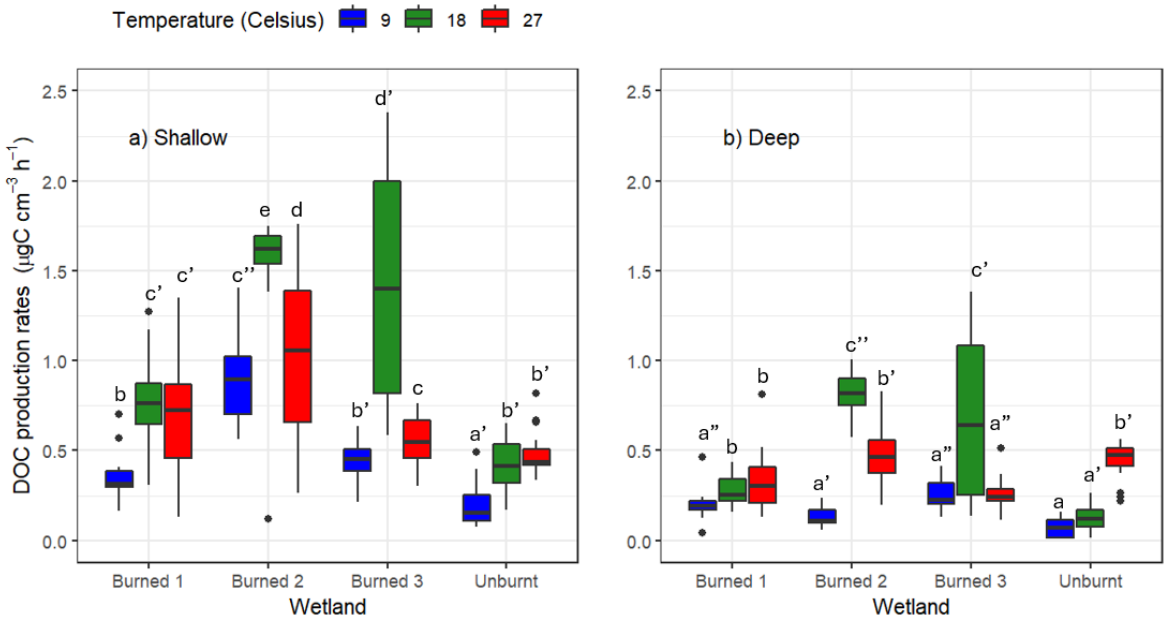

Figure 13. Potential steady-state DOC export rates measured using FTR experiments for the four sampling locations in response to temperatures of 9 (blue), 18 (green), and 27°C (red), for **(a)** the shallow soil interval (0-2 cm) and **(b)** the deeper soil interval (15-17 cm). Different letters denote significant differences at p <= 0.05. Letter' represents differences at p <= 0.1

Table 3. Q_{10} values reported for each site and depth combination for potential DOC production rates. Values are reported pairwise for temperatures at which flow-through reactor columns were incubated.

Site + Depth	Q_{10} (9-18)	Q_{10} (18-27)	Q_{10} (9-27)
Burned 1 (0-2 cm)	2.36	0.88	1.44
Burned 2 (0-2 cm)	1.83	0.64	1.08
Burned 3 (0-2 cm)	3.58	0.36	1.13
Unburned (0-2 cm)	2.13	1.22	1.61
Burned 1 (15-17 cm)	1.46	1.18	1.31
Burned 2 (15-17 cm)	7.59	0.55	2.04
Burned 3 (15-17 cm)	2.96	0.34	1.01
Unburned (15-17 cm)	1.82	3.94	2.68

Figure 13 shows the steady-state potential DOC export rates measured for all sites and depths, and in response to three temperatures, while Table 3 summarizes the Q_{10} calculated from those rates. Burned site 2 exhibited the highest DOC export rates, significantly different ($p = 0.028$) from the others with rates increasing from approximately 1.0 to 2.5 μg C cm^{-3} h^{-1} as temperatures increased from 9°C to 27°C. Burned sites 1 and 3 had lower DOC production rates, ranging from 0.5 to 1.5 μg C cm^{-3} h^{-1}, while the unburned site had the lowest rates (< 0.5 μg C cm^{-3} h^{-1}) across all temperature treatments. Flow through reactor experiments carried out at 18°C produced the highest DOC ($p << 0.05$) compared to experiments at 9 and 27°C. Shallower soils produced significantly higher DOC compared to deeper soils ($p << 0.05$). Deeper soils from burned sections also produced significantly higher DOC compared to unburned sections ($p = 0.012$).

Q_{10} values listed in Table 3 varied widely between 0.34 and 7.59. These values were the lowest when comparing rates between 18 and 27°C compared to the two other pairwise comparisons.

Unburned sediments had all of their Q_{10} values greater than 1 whereas rates obtained from burned wetland soils varied more in comparison.

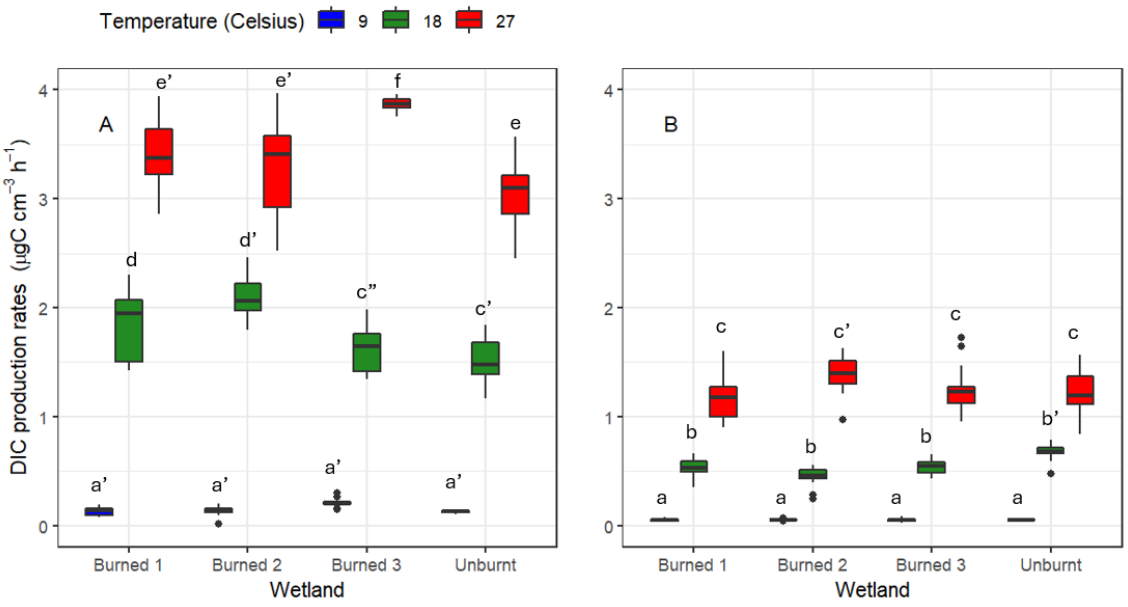

Figure 14. Potential steady-state DIC export rates measured using FTR experiments for the four sampling locations in response to temperatures of 9 (blue), 18 (green), and 27°C (red), for **(a)** the shallow soil interval (0-2 cm) and **(b)** the deeper soil interval (15-17 cm). Different letters denote significant differences at p <= 0.05. Letter' represents differences at p <= 0.1

Table 4. Q_{10} values reported for each site and depth combination for potential DIC production rates. Values are reported pairwise for temperatures at which flow-through reactor columns were incubated.

Site + Depth	Q_{10} (9-18)	Q_{10} (18-27)	Q_{10} (9-27)
Burned 1 (0-2 cm)	18.89	2.02	6.18
Burned 2 (0-2 cm)	21.70	1.68	6.03
Burned 3 (0-2 cm)	9.80	3.02	5.44
Unburned (0-2 cm)	15.43	2.17	5.79
Burned 1 (15-17 cm)	12.50	2.39	5.46
Burned 2 (15-17 cm)	11.82	3.46	6.40

Burned 3 (15-17 cm)	13.57	2.52	5.85
Unburned (15-17 cm)	18.78	1.90	5.97

Figure 14 shows the steady-state potential DIC export rates measured for all sites and depths, and in response to three temperatures, while Table 4 summarizes the Q_{10} calculated from those rates. For each temperature tested, DIC production rates were very similar for the four study sites. Additionally, there was a strong positive effect of temperature, for all sites, with all differences between rates measured at different temperatures being statistically significant ($p <<< 0.05$). Burned site 3 had the highest DIC production rates at 27°C ($p < 0.05$) (approx. 3.5 µg C cm^{-3} h^{-1}), while Burned site 2 had the highest rate at 9 and 18°C (approximately 2.5 µg C cm^{-3} h^{-1}). The unburned site, on average had slightly lower DIC production rates at the highest temperature, but similar and slightly higher rates at the lowest and intermediate temperature respectively. Deep soils from burned site 2 had slightly higher DIC concentrations ($p = 0.87$) compared to the other burned and unburned site. A similar trend of increasing rates concurrent with higher temperatures was also observed for deep soils ($p << 0.05$).

Q_{10} values ranged from 1.68 to 21.7 for DIC rates across burned and unburned shallow and deep soils. The variability was noticeably higher for shallow soils from burned site 2, however there was a general trend of high Q_{10} values comparing DIC production rates between 9 and 18°C. Values were lower when comparing the intermediate and the highest temperature.

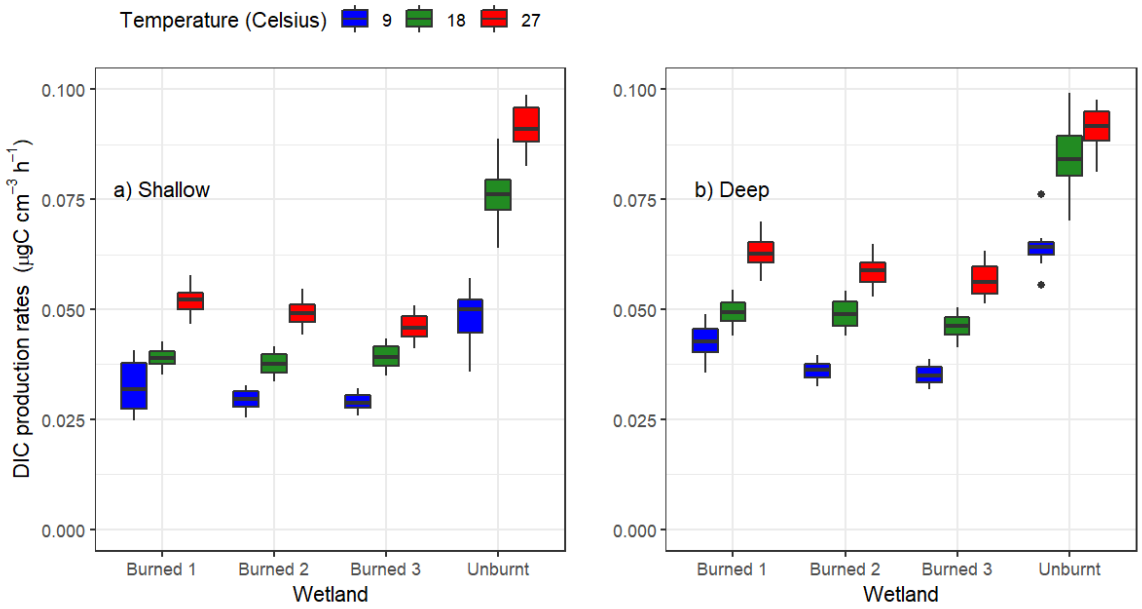

Figure 15. Potential steady-state methane export rates measured using FTR experiments for the four sampling locations in response to temperatures of 9 (blue), 18 (green), and 27°C (red), for **(a)** the shallow soil interval (0-2 cm) and **(b)** the deeper soil interval (15-17 cm). Different letters denote significant differences at p <= 0.05. Letter' represents differences at p <= 0.1

Table 5. Q_{10} values reported for each site and depth combination for potential methane production rates. Values are reported pairwise for temperatures at which flow-through reactor columns were incubated.

Site + Depth	**Q_{10} (9-18)**	**Q_{10} (18-27)**	**Q_{10} (9-27)**
Burned 1 (0-2 cm)	1.23	1.38	1.30
Burned 2 (0-2 cm)	1.31	1.35	1.33
Burned 3 (0-2 cm)	1.40	1.20	1.29
Unburned (0-2 cm)	1.65	1.25	1.44
Burned 1 (15-17 cm)	1.18	1.31	1.24
Burned 2 (15-17 cm)	1.43	1.22	1.51
Burned 3 (15-17 cm)	1.36	1.26	1.62
Unburned (15-17 cm)	1.39	1.11	1.23

Figure 15 shows the steady-state potential CH4 export rates measured for all sites and depths, and in response to three temperatures, while Table 5 summarizes the Q_{10} calculated from those rates. For all temperatures, the burned soil exhibited significantly higher methane production rates for shallow and deep soils, particularly at 27°C (approximately 0.10 µg C cm^{-3} h^{-1}), while the three burned sites had lower rates ranging from 0.04 to 0.08 µg C cm^{-3} h^{-1}, with no significant differences between them for each temperature tested

The effect of temperature on methane production rates varied across the sites, with the unburned site, on average, showing a more pronounced increase at higher temperatures compared to burned sites. Q_{10} values for methane production ranged from 1.11 to 1.65 across the three temperatures tested in flow-through reactor experiments for shallow and deep soils. There was a general trend of gradual increase in methane production rates from 9 to 18 to 27°C, as indicated by the rates listed in Table 5.

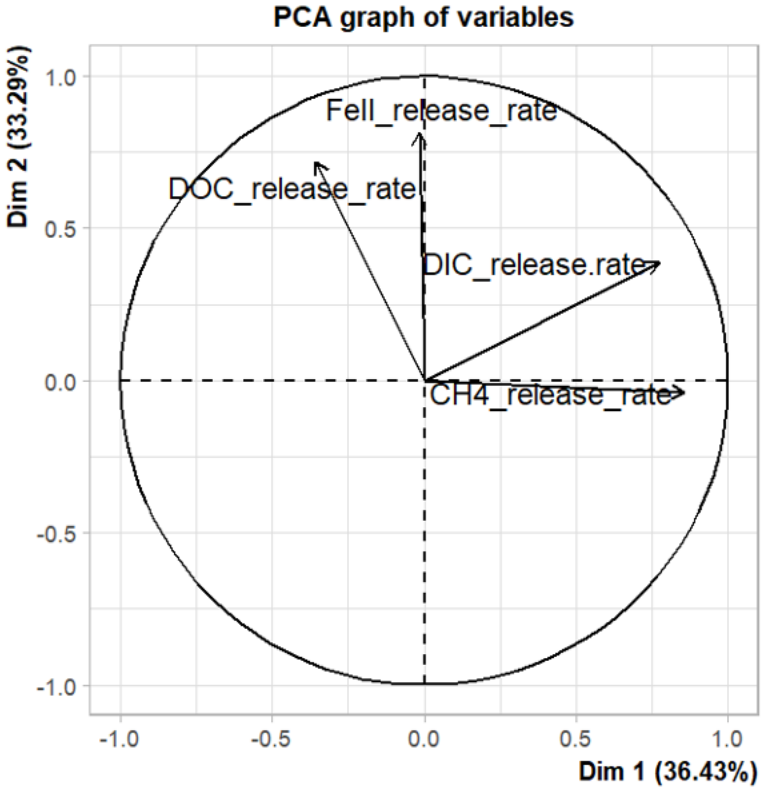

Figure 16. PCA plot of the four measured variables from the FTR experiments.

The PCA plot shown in Figure 16 additionally highlights relationships between all the four potential rates measured from flow-through reactor experiments. There was higher positive association observed between inorganic carbon and methane production rates (Pearson's coefficient $r = 0.37$, $p < 0.05$), whereas methane production rates have little to no association with Fe(II) production rates.

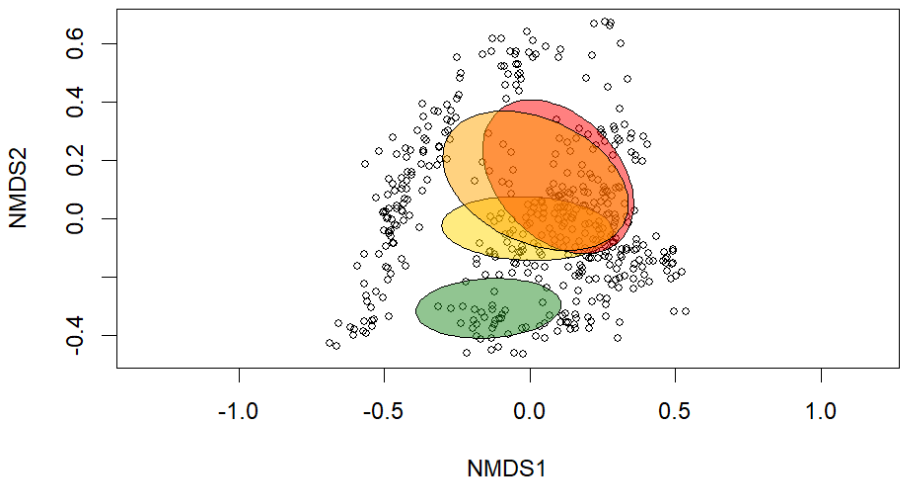

Figure 17. NMDS plot of all measured variables from FTR experiments. Gold, red, orange, and forest green ellipses represent Burned 1, Burned 2, Burned 3, and Unburned measured variables respectively.

Figure 17 shows the NMDS plot of all measured variables from FTR experiments, which highlights a clear separation between combined GHG, DOC/DIC, and Fe(II) production rates from soils from unburned and burned wetland sections. This consolidates the multivariate response variables into two dimensions, which lead to neat separation of the unburned site from the three burned sites in question.

4. Discussion

4.1 Influence of site characteristics on greenhouse gas fluxes and export rates.

Results revealed that soils from the burned wetland sites behaved significantly differently from soils from the unburned site in terms of greenhouse gas fluxes, dissolved carbon and reduced iron export rates from the unburned section, especially within shallow soils.

The production of CO_2 measured in both slurry and FTR experiments were higher in burned soils compared to unburned soils, probably driven by the lower C/N ratios observed in the former. This suggests that fires and subsequent inputs of pyrogenic carbon had a positive stimulating effect on microbial mineralization of organic carbon in the short-term, potentially through priming. Previous research has highlighted the presence of labile or easily mineralizable fractions in pyC, which could lead to enhanced activity of native microbial communities and lead

to higher carbon dioxide fluxes shortly post-fire[72]. Shifts in microbial communities post-fire, favoring Actinobacteria and genes implicated in heat tolerance, rapid growth, and substrate utilization could also explain the higher mineralization rates for burned sites compared to unburned sites observed in our experiments[30,73]. Increased Fe(II) fluxes, positively associated with DOC and carbon dioxide fluxes, have also been shown to be elevated due to the electron-shuttling ability of pyrolic and pyridinic nitrogen which constitutes pyrogenic organic matter (pyOM)[74]. This could explain the higher porewater nitrate concentrations in the burned sites, compared to the unburned site. PyC inputs can also physically alter the structure of wetland soils, by promoting aggregation and preferential flow-paths for the access of microbes to organic carbon[35]. They are also known to promote enhanced microbial activity by increasing the pH, mineralizing organic N and S, which can be readily utilized by microbes[75]. Additionally, they have been known to increase the redox potential inside soils, due to their ability to store electrons[76]. Therefore, they can behave as "electron snorkels", speeding up nitrate and Fe(III) reduction leading to higher carbon dioxide fluxes, most notably at the expense of methane emissions[77]. Higher Fe(II) export rates for burned soils compared to unburned soils also reflect this enhanced redox potential due to the addition of pyrogenic matter. Our results suggest that fires increase reduction of Fe(III) oxides in soils leading to higher fluxes of carbon dioxide and DOC, which was reflected in the strong correlation between DOC and Fe(II) production rates and concentrations in the burned sites observed in the correlation and PCA ordination plots . It was also evident that methane fluxes and production rates were significantly lower for burned sites compared to the unburned site, supporting the theory that pyrogenic matter serves as an electron snorkel and shuttle for electrons stored within reduced organic matter in anoxic systems, increasing the redox potential and thereby decreasing methane production.

Measured fluxes of CO_2, CH_4, and N_2O were lower than values reported for northern wetlands and other wetland geographies [78–80]. A reason for this could be low mean temperatures which would limit microbial mineralization of organic matter due to energetic limitations.

The highest Fe(II) reduction rates, DOC production rates, and CO_2 fluxes from slurry incubations were observed for Burned site 2, which also possessed the highest concentrations of oxalate-extractable iron oxides, a proxy for reactive iron oxides in soils, and the substrate for iron reducing bacteria. These oxides are known to stabilize up to 22% of all carbon in sediments[81,82] which would explain higher rates of reduced iron for this particular site. On close observation of Table 1, it seems clear that the fire event was the dominant driver of differences in chemical properties between the sites, especially since these differences diminished at depth. Given that the percent ash, a proxy for pyrogenically derived carbon, varied significantly between burned and unburned sites, this would suggest that the differences in carbon and iron cycling could be explained by differences in ash content, or inputs of pyrogenic carbon.

4.2 Temperature sensitivity of measured production rates.

Results from Table 2 indicate significantly higher DIC rates observed for the incubations carried out at 27^{o}C which explains lower DOC rates for the same temperatures. In tandem, Figures 12 and 13 suggest that at the highest temperature, the missing DOC might be reflected in the high DIC concentrations observed for the same temperature. At higher temperatures, microbial activity is elevated, therefore the DOC in the output solution would have been mineralized to CO_2 leading to elevated DIC concentrations, a trend observed in a previous study investigating temperature-dependent Fe(III) reduction in subalpine wetland soils[63].

Q_{10} values for DOC production for burned and unburned shallow soils reached as high as 3.58, agreeing with previous estimates made for a spodosol rich forest[83] where values ranged from 1.7-2 for dry to wet soils. A study looking at temperature sensitivity of peatlands in the UK estimated Q_{10} values ranging from 1.84 to 3.53 spanning high and low water table regimes[84], also spanning similar ranges as our study. However, Q_{10} values for deep soils in our experiments went as high as 7.56, indicating higher thermal sensitivity than shallow soils and published estimates.

For DIC production rates, proxy for soil respiration rates, rates were found to be similarly variable for burned and unburned shallow and deep sediments, ranging from 1.68 to 21.7, much higher than estimates from Chari et.al[80] who used soils from the Sacramento-San Joaquin Delta and Puerto Rico. However, measured values are consistent with Q_{10} estimates from modeling approaches on wetlands in Michigan where values as high as 16.4 were measured[85], and a global dataset spanning different ecosystems, where values could go as high as 300 for tundra soils and around 30 for peat and mineral wetlands[86].

Measured Q_{10} values from our experiments fell within a narrow range, 1.11-1.65, which would be on the lower end of values measured from northern Sweden (1.2-3.5)[87]. In fact, adjacent mires from northern Sweden were found to have values as high as 5.8[88]. However, they agreed well with values measured for methanogenesis in paddy soils from China (1.1-2.3)[89] incubated between 5-35°C.

Q_{10} values from our experiments for Fe(II) production rates for burned and unburned sites ranged from 0.92 to 4.31, with higher values on average measured for burned shallow soils. Flow-through reactor experiments from a subalpine wetland in the Rocky Mountain National Forest using an organic Fe complex spanning 6-18°C estimated Q_{10} values spanning 1.5-8.9 for depression and slope wetland soils[59]. A study from the same wetland using a different approach with no supplied Fe estimated values between 0.8 to 5.3[63]. Studies from freshwater lake soils in

China supplemented with biomass and pit lake sediment from Germany[90] supplemented with iron hydroxides estimated values spanning 1.2-3.54[68] and 1.8-2 respectively. Given the limited data on Fe(III) reduction/Fe(II) production, our values are consistent with previous literature.

4.3 Implications for wetland carbon sequestration and water quality.

Given that fires are predicted to increase in frequency and intensity due to warmer temperatures, it is crucial that we understand their effects not just on dryland soils but also in critical high-altitude subalpine wetland systems. Wildfires are known to increase emissions of greenhouse gases and lead to elevated dissolved organic carbon concentrations due to high-temperature oxidation of accumulated organic matter in wetland soils[91]. It is less clear whether these emissions persist post-fire, both on shorter and longer temporal scales. Our experiments fill a critical gap in the literature by shedding light on short-term greenhouse gas dynamics *via* slurry and flow-through reactor soil experiments. Broadly, it appears from these experiments that there is a shift in greenhouse gas emissions and C sequestration in response to fire and subsequent inputs of fire-derived pyrogenic matter in these subalpine wetlands. This underscores the importance of fire-derived organic matter in shaping biogeochemical processes and microbial activity in these ecosystems. Overall, this analysis highlights the intricate coupling between carbon and iron cycling in wetland soils and how this relationship is influenced by fire events. Additionally, high DOC fluxes post-fire pose a challenge to environmental engineers and water filtration systems for cities dependent on subalpine wetlands for their drinking water. It also underscores the importance of post-fire sampling and consideration of short-term GHG fluxes in response to pyrogenic matter additions. Subalpine wetlands have been considered as sinks of carbon, due to their lower temperatures and high gross primary productivity[92,93], which makes this work important both for the continued ability of these systems to sequester carbon, and broadly for the global carbon cycle.

Chapter 2: Assessing the impact of increasing nitrate and salinity levels on dissolved organic carbon and greenhouse gas fluxes spanning a salinity gradient in the Sacramento-San Joaquin Delta

1. Introduction

Wetlands are crucial to the global carbon cycle, acting as exceptional carbon sinks by sequestering atmospheric carbon dioxide through plant photosynthesis and the accretion of organic matter in soils[94]. In fact, despite comprising a small percentage of the global landmass (6-8%), wetlands comprise 20-30% of the global carbon pool[10,95]. They also store carbon at higher densities and rates than any other ecosystem on our planet[96]. However, their capacity to sequester carbon is influenced by a suite of environmental factors, and some wetlands actually act as carbon sources rather than sinks[97]. Disturbance, such as increasing salinization[98] and increasing nitrate loading[99,100] have been shown to compromise wetland carbon sequestration capacity and increase fluxes of nitrous oxide (N_2O), a greenhouse gas with a global warming potential (GWP) 300 times greater than CO_2[101] . This is particularly important in the Sacramento-San Joaquin Delta, a critical wetland ecosystem in California that increasingly faces challenges related to salinization from sea level rise and nitrate loading from agriculture and wastewater effluents[102,103].

The Sacramento-San Joaquin Delta (Figure 18), or the Delta, is an expansive web of rivers, channels, and islands that supports a diverse array of wildlife[104], provides water for millions of Californians[105,106], and plays a crucial role in the state's agricultural economy. The Delta was once an expansive 2,200 km^2 wetland and riparian zone, but has been rapidly shrinking and sinking since drainage beginning in the 1850s[107,108]. The initial land use was primarily agriculture, but it expanded to grazing, salt production, and later urbanization. Due to drainage, the previously inundated accreted peat and organic matter were exposed to oxygen, resulting in a loss of around 200 Tg of carbon over the past century[109] and to dramatic land surface subsidence. Currently, the Delta provides drinking water through a series of canals to more than two-thirds of California's population through the Central Valley and State Water projects[110]. Since the 1970s, the Delta also has been the site for extensive wetland restoration projects to mitigate the surrounding areas from sea level rise and flooding, in addition to providing habitat for birds, fishes, and creation of recreational areas. More recently, attention with respect to the Delta has shifted to reducing GHG emissions and therefore the potential of these restored

wetlands as a natural climate solution for carbon sequestration. However, the Delta is also highly vulnerable to the impacts of salinization[111]. Sea-level rise, coupled with reduced freshwater inflows due to upstream diversions and climate change, has led to increased salinity intrusion in the Delta[112,113]. Furthermore with climate change and changing patterns of precipitation and evaporation, decrease river discharge due to shrinking of glacial cover in the Sierra Nevada will lead to the upriver migration of the saltwater-freshwater mixing zone[114]. This salinization can shift wetland plant communities, reduce gross primary productivity and decrease carbon inputs, and affect soil microbial processes, all of which can impact the carbon balance of these ecosystems[17,115,116]. Increasing salinization has been known to increase[115,117], decrease[118], or not impact carbon dioxide emissions[119,120] from wetland soils. Saltwater has higher concentrations of sulfate (SO_4^{-2}), which can also shift wetland function from methanogenesis to sulfate reduction due to thermodynamic favorability, known to increase organic matter mineralization and decrease production of methane[121]. Increasing salinization has also been linked to reduced denitrification rates[122,123], decreasing nitrous oxide emissions. However, increase in nitrate concentrations due to higher organic matter mineralization rates has been known to lead to higher nitrous oxide emissions[124]. In any case, site specific processes have been agreed upon as important predictors of wetland nitrous oxide response to salinization[125,126]. This necessitates further experimental study from different wetland geographies and site characteristics, the Delta being a prime candidate in this regard.

Additionally, the Delta has historically received higher nitrate inputs from agricultural runoff and wastewater discharge[112], also coinciding with soils rich in nitrogen[127], and this trend is projected to intensify in the future [128,129]. While nitrate enrichment can lead to higher plant growth and gross primary productivity (GPP) in the short term leading to higher carbon sequestration[130], excessive nitrate levels can lead to eutrophication, causing algal blooms, oxygen depletion, and shifts in plant communities. In fact, wetlands receiving elevated nutrient (nitrogen and phosphorus) loads have shown responses ranging from release of sequestered carbon to an increase in carbon sequestration and N_2O fluxes by orders of magnitude[131 132]. Global modeling of greenhouse gases has indicated that agricultural activities, including nitrogen fertilization has increased N_2O emissions by 13% in wetlands in the Northern Hemisphere. Fertilization also led to higher carbon emissions, however it also sequestered an equal amount of carbon and nitrogen through elevated gross primary productivity (GPP)[132].

Conversely, in wetlands experiencing sustained elevated nutrient loading, especially adjacent to agricultural systems, a reduction in nitrate removal efficiency has also been observed[133]. This can be explained by the fact that wetlands, similar to other ecosystems, also possess intrinsic

nutrient processing/carrying capacities and are already working at their maximum limit to metabolize excess nutrient loads[134].

Given the ecological, economic, and social importance of the Sacramento-San Joaquin Delta, it is essential we understand how salinization and nitrate loading will influence carbon sequestration and GHG emissions. This becomes especially important considering the trend of converting agricultural land to wetlands for carbon storage in the Delta and instrumentalization through carbon crediting and offsets[135]. Here, we assessed the potential of wetland soils from sites spanning a salinity gradient in the Sacramento-San Joaquin Delta to produce greenhouse gas and export dissolved organic carbon, and how those would respond to increasing salinity and nitrate loading.

2. Methods

2.1 Study sites

Our study focused on three sites in the Sacramento-San Joaquin Delta that are located within a narrow geographic zone (Figure 17) and constitute sites characterized by different salinities. The sites on Twitchell Island (West Pond and East End) are non-tidal and therefore have a low salinity (0.19 and 0.22 ppt respectively), whereas Dutch Slough is tidally connected and has a higher salinity (0.48 ppt). Salinity measurements were taken from water samples collected in July 2022. All three sites have similar mean annual precipitation (338 mm) and air temperature (around 16^{o}C). West Pond and East End have been extensively studied in the past for their carbon fluxes on larger spatial scales[97,136], with eddy covariance (EC) towers established in 2012 and 2014 respectively, whereas Dutch Slough is a relatively new site with its EC tower established in 2021[137]. The dominant vegetation across the sites is cattail and tule grasses, as they were brought in to stabilize berms from persistent wind and water-mediated soil erosion.

Soils on Twitchell Island feature a complex patchwork of alluvium Mollisols adjacent to peat Histosols which were separated from main river channels, which accumulated organic matter over the last hundred or so years[138]. The East End site was established on alluvium soils whereas West Pond was established on peat-rich Histosols. The three sites were sampled in June 2022. Triplicate topsoil cores were taken to a depth of 5 cm of mineral soil at each site within the flux footprint of the EC tower and immediately transferred to a cooler with ice to prevent biogeochemical changes. Shallow depths were sampled as soil cores contained peat-like organic matter at the top which was discarded, and we were more interested in incubating mineral soils underneath that contain higher concentrations of native electron acceptors known to influence greenhouse gas production. Grab water samples totaling 50 mL were taken in triplicate at each

location nearby plants adjacent to the EC tower and instantly acidified with 2% HNO_3 to prevent oxidation of redox-relevant dissolved ions.

Figure 18: Location of the three study sites. US-Tw1 corresponds to West Pond, US-Tw4 corresponds to East End, and US-Dmg corresponds to Dutch Slough.

2.2 Sediment and surface water characterization

Water samples were acidified with dilute (2% w/v) HNO_3 to preserve chemical speciation of dissolved Fe and N cations/anions. Relevant extractable anions and cations were measured using a Dionex ion chromatograph (IC) (electrochemical detector, ED40; analytical column,

AS23/AG23; anion self-regenerating suppressor, ASRS-I, 4 mm; mean detection limit: 30 µg/L, error: 5 µg/L) supplied with a carbonate eluant (7.2 mM Na_2CO_3 and 1.28 mM $NaHCO_3$) at a flow rate of 1.0 mL min^{-1}.

Our study focused on mineral soil, which was collected and analyzed after discarding the O horizon, which overlaid soils from all three sites. Soil dry bulk density was determined by drying a known volume of soil for 24 hours at 105°C. Soil pH was measured in a soil slurry after suspending 5g of soil in a 10 mM $CaCl_2$ solution[52]. Total % organic carbon and nitrogen was measured by combusting 30 mg of dried soil using a NC 2100 Elemental Analyzer (CE Instruments, USA). Oxalate-extractable Fe, used as a proxy for poorly-ordered oxides more likely to participate in redox reactions, was determined using Schwertmann's protocol[54].

2.3 Slurry experiments

Slurry experiments were performed in order to quantify the effect of nitrate concentrations and salinity on potential greenhouse gas (CO_2, CH_4 and N_2O) production in soils from our three study sites (section 2.1). These experiments allow for direct comparison with literature from similar slurry experiments from soils in published literature. Anoxic slurry experiments were conducted in 125 mL serum bottles, using a 1:4 (w/w) wet soil: deionized water mixture. Soils from 0-5 cm were homogenized prior to the incubation. The slurries were incubated under gentle orbital shaking to maintain the soil in suspension, and experiments lasted 7 days with temperature maintained at 25°C. Prior to the incubation, the serum bottles were evacuated, and the deionized water was flushed with N_2 to remove most O_2 from both systems. Slurries were sampled for water and gas samples. This was performed with higher frequency for the first six hours, and subsequently daily lasting 7 days, for water and gas samples. This was done to capture the gas fluxes from the initial kinetic phase of reactions implicated in greenhouse gas production, especially N_2O, known to be driven by 'hot spots and hot moments' in the soil continuum[139]. An equal amount of N_2 was injected into the bottles to maintain vapour pressure during gas sampling.

In a first series of experiments, nitrate concentrations were varied (0, 1, 2 and 3 ppm, as KNO_3) while salinity remained constant (0 ppt), in order to test a range of concentrations covering values similar to what has been reported, ~1.5 ppm[140,141], but also values that represent scenarios in which nutrient loading from agriculture and effluents increase. In a second series of experiments, salinity was varied (0, 1, 2 and 3 ppt using NaCl) while nitrate remained constant (0 ppm), in order to test scenarios where saltwater intrusion affects freshwater wetlands due to sea level rise[98,102].

Liquid samples were filtered through a 0.22 µm PTFE membrane syringe filter (Whatman; 25 mm filter size) prior to chemical analyses. Liquid samples were analysed as described in Section 2.2. Gas samples were analysed on an Agilent 7890B GC (Agilent, Santa Clara, CA) for CO_2, CH_4, and N_2O using thermal conductivity, flame ionization, and nitrogen chemiluminescence detectors (TCD, FID, and NCD) respectively. Concentrations of CO_2, CH_4, and N_2O were then used to calculate potential CO_2, CH_4, and N_2O fluxes according to:

$$F = \frac{V}{A*m} * \frac{\Delta C}{\Delta T} \quad (1)$$

Where *F* is the gas flux (µmol [CO_2 or CH_4] g soil^{-1} m^{-2} s^{-1}), V is the volume of the slurry, A is the area of the serum bottle cross-section, Δ*C* is the gas concentration difference between consecutive time points (mol m^{-3} [CO_2, CH_4, and N_2O]), *m* is the mass of dry soil, and Δ*t* is the time increment. Values were converted from ppm to mol m^{-3} using the ideal gas equation.

.

Two potential fluxes of CO_2, CH_4 and N_2O production were calculated from the initial linear increases (0-24 hr) in CO_2, CH_4, and N_2O concentration, respectively and final stable values (> 96 hr)

2.4 Statistical analyses

All statistical analyses were carried out in R[69]. Differences between all measured water, soil, and gas variables were determined using a t-test with a threshold of p <= 0.05. Tukey's honest significance difference test was used to determine which sites, if found significant (α = 0.05), were different. Pearson's correlation coefficients were calculated between measured water, soil, and gas variables and visualized using the 'corrplot' function in R[70]. Multivariate analyses were performed to evaluate differences in water, soil, and gas concentrations. Given these concentrations vary by orders of magnitude, it was desirable to relativize them by column totals through the 'decostand' function using the 'vegan' package[71]. These were then visualized using Principal Components Analysis (PCA) ordinations. PCA was performed in R using the 'prcomp' function which is a part of the 'stats' package[29].

3. Results

3.1 Soil characteristics

Table 6. Physical and chemical characteristics of surface mineral soils (depth interval 0-5 cm) and selected chemical characteristics of surface waters from the three study sites. Values are reported as mean obtained from triplicate samples. Different superscripted letters indicate significant differences at p<= 0.1. Standard deviations were <30% of measured values.

Site characteristics	Dutch Slough	East End	West Pond
Soil (0-5 cm)			
Sand	79.6±13.5^{a}	55.2±11.2^{b}	59.3±7.75^{b}
Silt	10.1±2.3^{a}	33.2±6.7^{b}	21.2±3.4^{c}
Clay	11.1±3.1^{a}	12.4±2.6^{a}	20.1±4.7^{b}
Textural class	Loamy sand	Loam	Sandy clay loam
Dry bulk density	1.22±.29^{a}	1.07±.18^{b}	1.16±.25^{a}
pH	7.57±.36^{a}	5.96±.44^{b}	6.49±.29^{c}
C_{org} content (%)	7.89±1.19^{a}	15.32±3.65^{b}	18.95±2.77^{c}
Total N content (%)	0.47±.06^{a}	0.91±.14^{b}	0.93±.22^{b}
Molar C_{org}:N ratio	17.54±1.15^{a}	16.38±3.11^{a}	19.17±2.79^{a}
Extractable Fe content (mg g of soil^{-1})	2.17±.33^{a}	11.89±2.96^{b}	8.16±1.47^{c}
Extractable Mn content (mg g of soil^{-1})	0.12±.03^{a}	0.78±.17^{b}	0.31±0.06^{c}
Extractable Al content (mg g of soil^{-1})	1.41±.23^{a}	5.59±1.14^{b}	3.27±0.55^{c}
Extractable Ca content (mg g of soil^{-1})	44.32±10.71^{a}	121.42±20.39^{b}	78.13±15.52^{c}
Surface water			
Salinity (ppt)	0.48±.06	0.22±.03	0.19±.02
NH_4^+ concentrations (ppm)	1.67±.44^{a}	1.19±.16^{b}	2.12±.079^{c}
NO_3^- concentrations (ppm)	0.27±.03^{a}	0.86±.17^{b}	0.13±.03^{c}
Cl^- concentrations (ppm)	267.81±15.39^{a}	122.31±15.32^{b}	110.57±20.91^{b}
SO_4^{-2} concentrations (ppm)	20.87±4.11^{a}	0.78±.11^{b}	0.56±.09^{c}

Dutch Slough was characterized by soils that had significantly lower C_{org} and N contents (p = 0.008, 0.01), as well as significantly lower contents of extractable Fe, Mn, Al and Ca and a higher pH (7.9 versus <6.5 for the other two sites). The Dutch Slough site was also characterized by statistically significantly higher SO_4^{2-} and Cl^- concentrations in surface water, by factors of 27-37 and 2.1-2.4, respectively. East End soils had significantly higher contents of Fe, Mn, Al and Ca

than those of West Pond, but lower C_{org} and N content and a more acidic pH. Its surface water was characterized by slightly higher NO_3^-, Cl^- and SO_4^{2-} concentrations than the one of West End. All of the sites had similar C_{org}/N ratios. Most of our measured physical and chemical parameters for West Pond and East End agree well with previous measurements made for the two sites[142,143].

3.2 Greenhouse gas emissions in response to nitrate addition

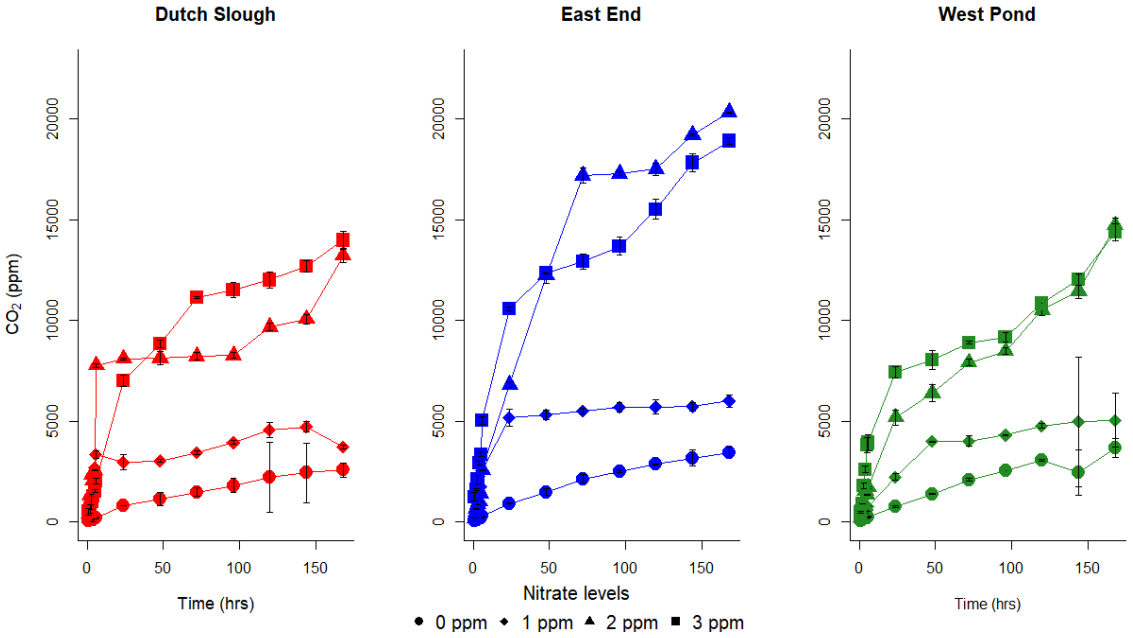

Figure 19. Effect of nitrate concentrations on CO_2 concentrations produced over time in slurry experiments with top soil (0-5 cm) from the sampled Delta sites. Salinity was set at 0 ppt. Error bars represent standard deviations from triplicate experiments for each time point found not to exceed >40% of measured value for individual time points.

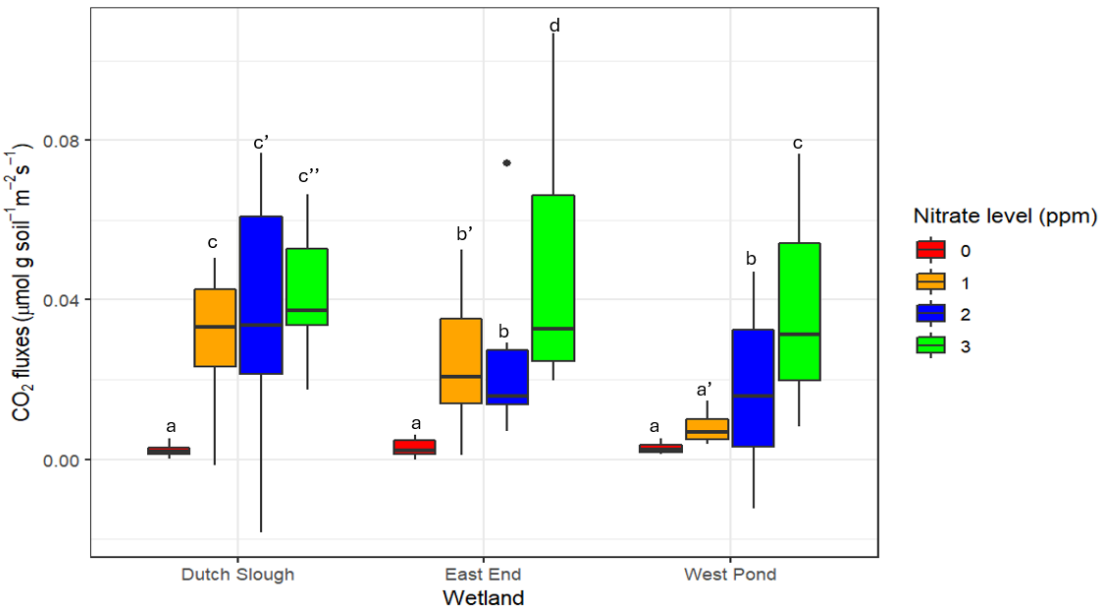

Figure 20. Average CO_2 fluxes calculated for the initial rapid evolution phase of the slurry experiments, spanning measurements taken from 1-24 hours in conditions with 0 (red), 1 (orange), 2 (blue) and 3 (green) ppm of nitrate. Different letters indicate significant differences at p<= 0.05. Letter' represents differences at significance level p <=0.1.

Figure 19 shows the temporal evolution in CO_2 concentrations in slurry experiments in response to various nitrate concentrations, while Figure 19 shows the corresponding initial (first 24h) CO_2 fluxes. For control experiments with no nitrate amendments, CO_2 concentrations and their evolution (Figure 19) as well as initial CO_2 fluxes (Figure 20) were not found to be significantly different between the sites. in response to various concentrations of nitrate, both average cumulative CO_2 concentrations (Figure 19) and CO_2 fluxes (Figure 20) were significantly different between sites ($p < 0.05$). On average, East End slurry incubations produced the highest cumulative CO_2 concentrations from slurry experiments compared to West Pond and Dutch Slough. CO_2 concentrations tend to level off for lower-nitrate treatment levels but keep increasing for higher nitrate treatment (Figure 18). East End was also characterized by the highest initial CO_2 fluxes in response to 3ppm of nitrate, however, the highest initial CO_2 fluxes in response to 1 and 2ppm concentrations of nitrate were reported for Dutch Slough (Figure 20).

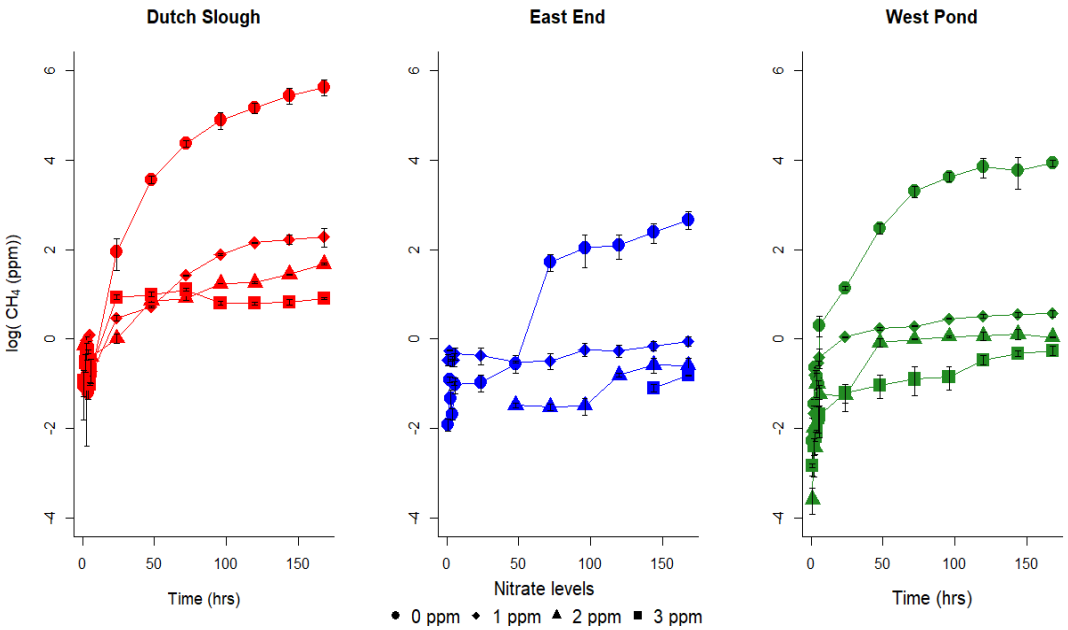

Figure 21. Effect of nitrate concentrations on log transformed methane concentrations produced over time in slurry experiments with top soil (0-5 cm) from the three study sites. Salinity was set at 0 ppt. Error bars represent standard deviations for triplicate experiments for each time point.

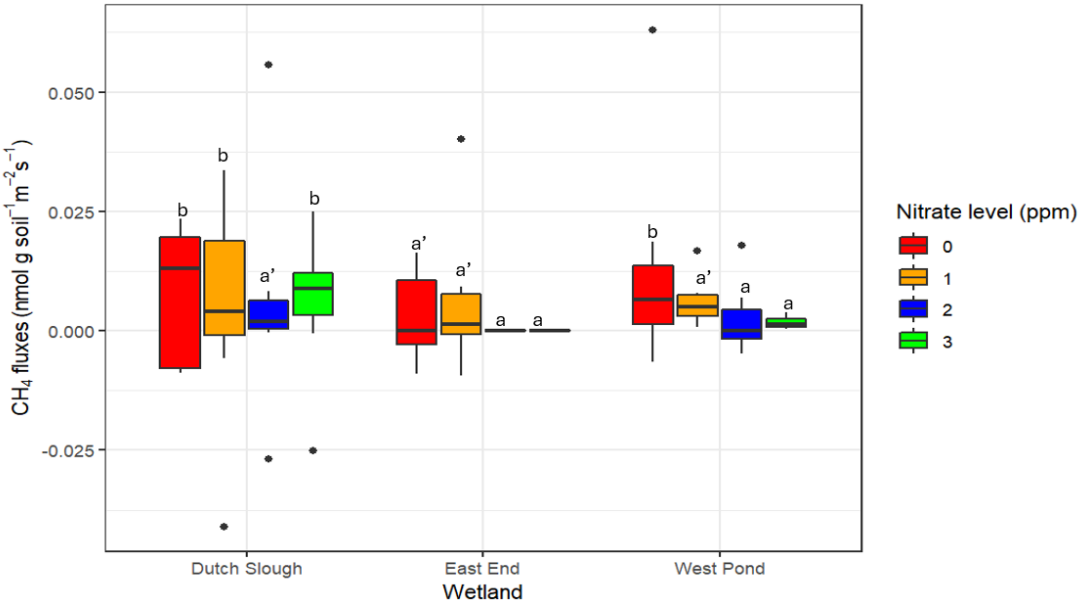

Figure 22. Average CH_4 fluxes calculated for the initial rapid evolution phase of the slurry experiments, spanning measurements taken from 1-24 hours in conditions with 0 (red), 1 (orange), 2 (blue) and 3 (green) ppm of nitrate. Different letters indicate significant differences at p<= 0.05. Letter' represents differences at significance level p <=0.1.

Figure 21 shows the temporal evolution in CH_4 concentrations in slurry experiments in response to various nitrate concentrations, while Figure 22 shows the corresponding initial (first 24h) CH_4 fluxes. For control experiments with no nitrate, Dutch Slough exhibited the highest CH_4 concentrations across the three sites (Figure 21), followed by West Pond and East End, whereas CH_4 fluxes were similar for Dutch Slough and West Pond, and lower for East End soils ($p = 0.032$). Incubations carried out with no pre-existing nitrate in the solution produced the highest concentrations across all three sites. In response to addition of 1 ppm nitrate, CH_4concentrations decreased steeply for Dutch Slough, followed by West Pond and East End. However, CH_4 fluxes were not found to be significantly lower for Dutch Slough and East End, but significantly lower for West Pond ($p = 0.067$). In response to addition of 2 ppm nitrate, there was no detectable methane produced in the slurry experiments for East End until the latter half of the experiment for the higher nitrate treatments (Figure 21). West Pond also had low CH_4 fluxes for 2 ppm nitrate amendments, significantly lower than the 1 ppm incubation ($p = 0.077$). Dutch Slough's CH_4 fluxes were also significantly lower for 2 ppm compared to 1 ppm ($p = 0.021$). Finally for 3 ppm concentrations, we measured higher CH_4 fluxes from Dutch Slough soils ($p = 0.018$), however no CH_4 was detected for experiments with East End soils. Fluxes from West Pond soils were not found to be significantly different between 2 and 3 ppm nitrate amendments, however they were not significantly different from zero.

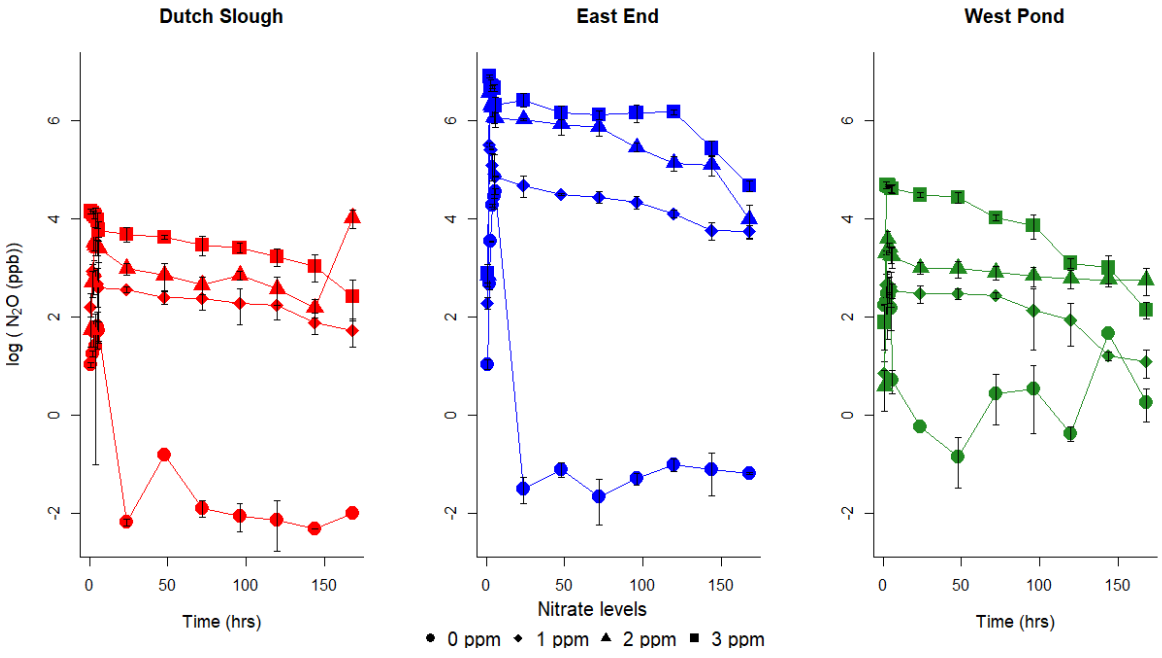

Figure 23. Effect of nitrate concentrations on log transformed nitrous oxide concentrations produced over time in slurry experiments with top soil (0-5 cm) from our three study sites.

Salinity was set at 0 ppt. Error bars represent standard deviations from triplicate experiments for each time point, found not to exceed >40% of measured value.

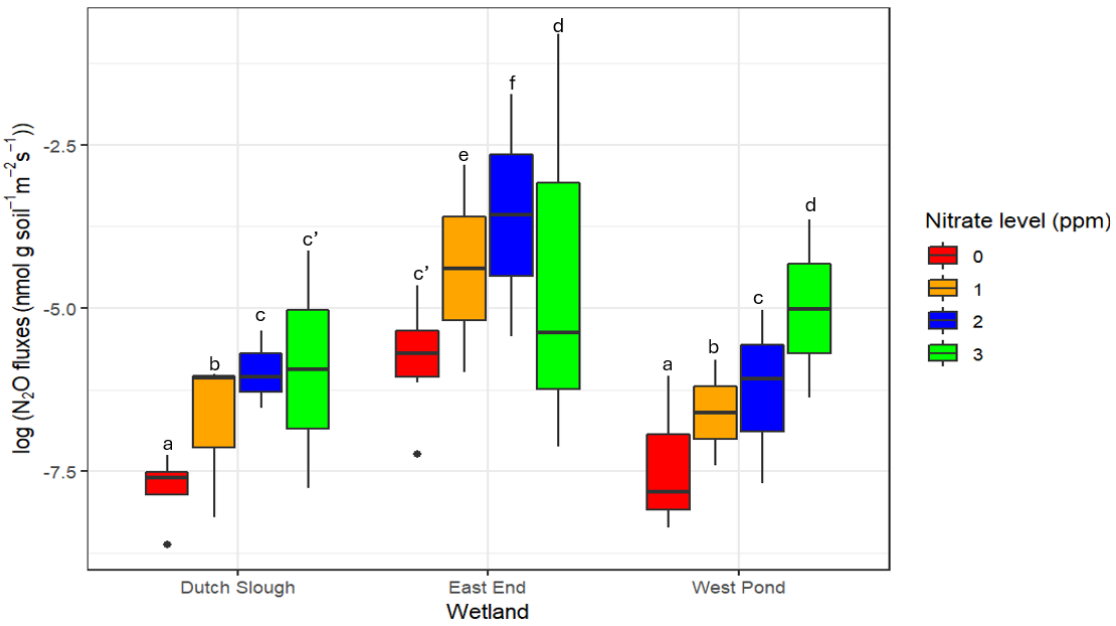

Figure 24. Average log-transformed N_2O fluxes calculated for the initial rapid evolution phase of the slurry experiments with top soil (0-5 cm), spanning measurements taken from 1-24 hours in conditions with 0 (red), 1 (orange), 2 (blue) and 3 (green) ppm of nitrate. Different letters indicate significant differences at p<= 0.05. Letter' represents differences at significance level p <=0.1.

Figure 23 shows the temporal evolution in N_2O concentrations in slurry experiments in response to various nitrate concentrations, while Figure 24 shows the corresponding initial (first 24h) N_2O fluxes. Log transformation was performed for ease of visual representation. For control experiments with no nitrate, we observed significantly higher N_2O fluxes for East End ($p << 0.05$), with no differences observed between West Pond and Dutch Slough (Figure 24). Each increase in nitrate concentrations led to increases in N_2O concentrations for time points after 50h, for all sites (Figure 23), with higher N_2O concentrations observed for East End. Similarly, N_2O fluxes increased significantly ($p << 0.05$) over control for 1 ppm nitrate experiments for all three sites, and also increased significantly in response to increase in nitrate concentrations from 1 to 2ppm for all sites (Figure 24). Similarly, N_2O fluxes tended to increase significantly ($p << 0.05$) over control for 1 ppm nitrate incubations for all three sites For 3 ppm nitrate incubations, there was a statistically significant decline in N_2O fluxes for East End ($p = 0.028$), whereas Additionally, N_2O fluxes increased significantly for West Pond and Dutch Slough in response to increase in nitrate concentrations from 2 to 3 ppm($p = 0.59$ and 0.021 respectively), but decreased significantly for East End ($p = 0.028$).

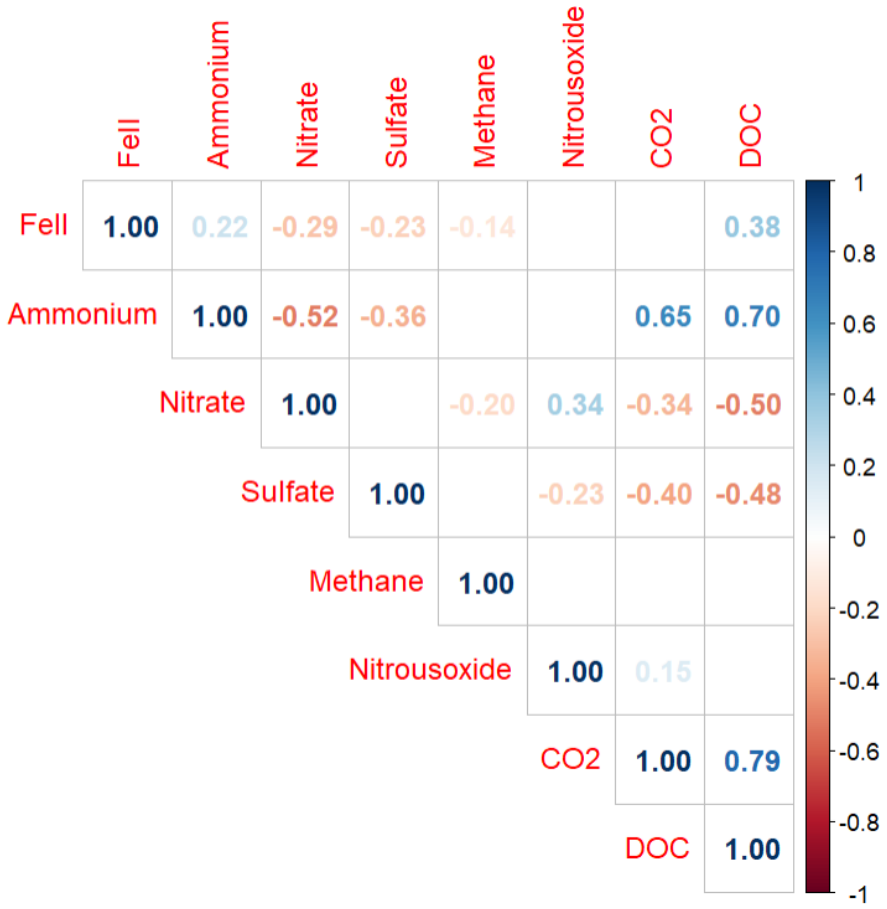

Figure 25. Correlation plot of all measured response variables from the slurry experiments. Fe(II), NH_4^+, NO_3^-, SO_4^{-2} and DOC were measured from aqueous samples post filtering. Correlation coefficients are reported at a threshold of p <= 0.05.

The correlation plot in Figure 25 details all relevant associations between measured chemical parameters in the slurry experiment. DOC and CO_2 were found to be strongly positively correlated to each other. They were also both significantly negatively correlated with nitrate and sulfate concentrations in solution. This means that as nitrate and sulfate declined, CO_2 and DOC fluxes increased throughout the experiments. There were also significant associations between different nitrogen compounds and ions measured in the experiment. NH_4^+ concentrations were strongly negatively correlated with NO_3^- concentrations, while N_2O fluxes were positively correlated with NO_3^- concentrations. Fe^{+2} concentrations were also found to be negatively correlated with NO_3^- and SO_4^{-2} concentrations, whilst being positively associated with DOC fluxes from these experiments.

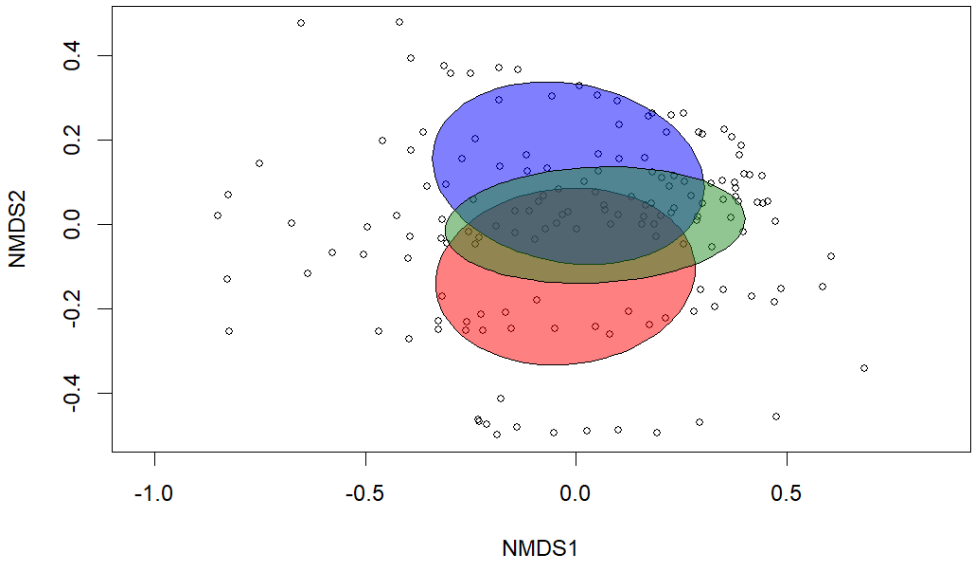

Figure 26. NMDS plot of all measured variables from the slurry experiments. Red, blue, and forest green ellipses represent measured variables from Dutch Slough, East End, and West Pond soils respectively.

NMDS ordination, shown in Figure 26, highlights the degree of similarity or differences between the three wetland sites with respect to all measured parameters. There was higher degree of overlap between East End and West Pond wetland soils compared to Dutch Slough and East End.

3.3 Greenhouse gas emissions in response to salinity

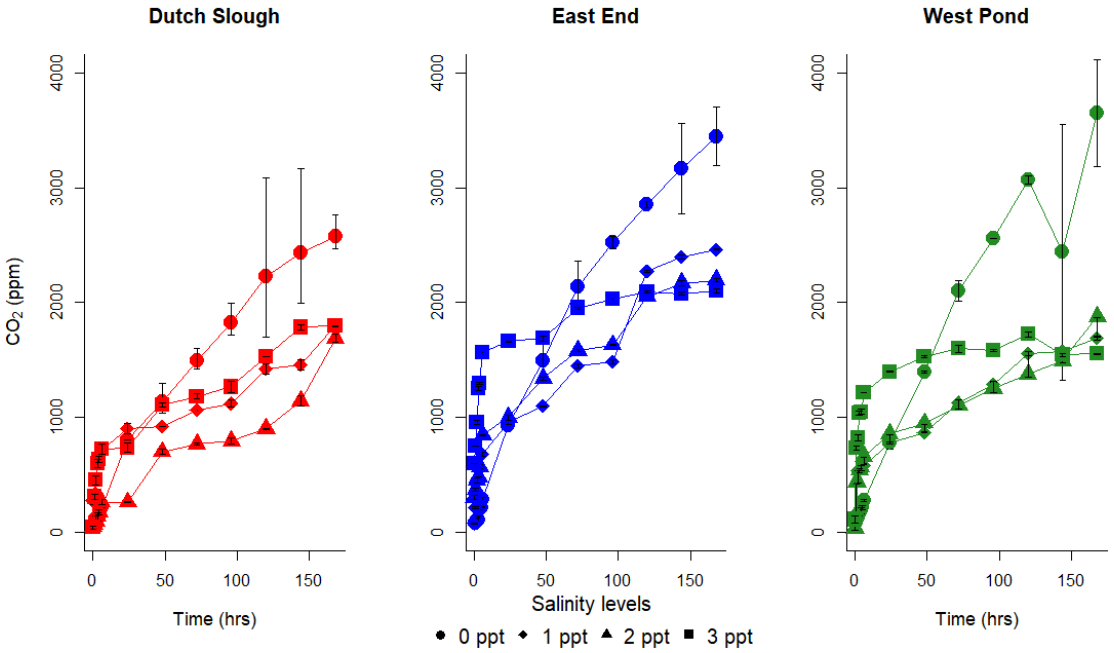

Figure 27. Effect of salinity on CO_2 concentrations produced over time in slurry experiments with top soil (0-5 cm) from our three study sites. Nitrate concentration was set at 0 ppm. Error bars represent standard deviations from triplicate experiments found not to exceed >40% of the value at a particular time point.

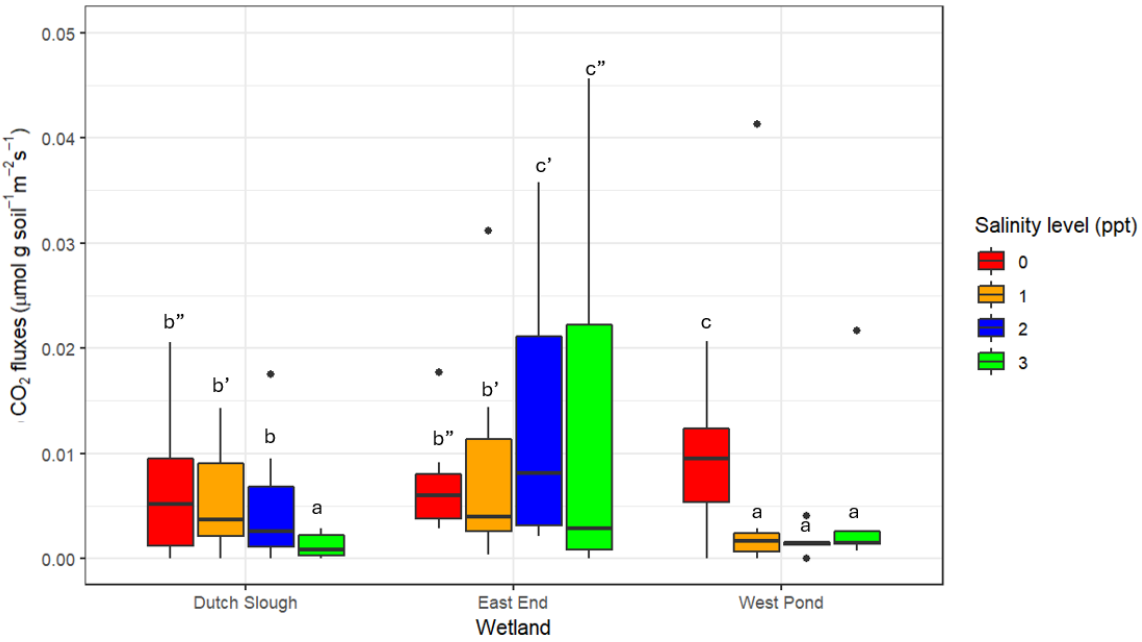

Figure 28. Average CO_2 fluxes calculated for the initial rapid evolution phase of the slurry experiments with top soil (0-5 cm), spanning measurements taken from 1-24 hours in

conditions with 0 (red), 1 (orange), 2 (blue) and 3 (green) ppm salinity level. Different letters indicate significant differences at p<= 0.05. Letter' represents differences at significance level p <=0.1.

Figure 27 shows the temporal evolution in CO_2 concentrations in slurry experiments in response to various salinity, while Figure 28 shows the corresponding initial (first 24h) CO_2 fluxes. The absolute CO_2 concentrations and their temporal evolution were affected by salinity for all sites (Figure 27). For the three sites, higher salinity led to a faster production of CO_2 and higher concentrations for early time points, but also to lower concentrations for the later part of the experiments (>70h). The highest CO_2 concentrations were reported for the control slurry experiments with 0 salinity. At higher salinity levels, CO_2 fluxes seemed to asymptote at West Pond and East End, but not for Dutch Slough where concentrations kept increasing, even if they are lower in magnitude compared to control incubations. For fluxes calculated for control experiments, West Pond exhibited statistically higher fluxes compared to East End and Dutch Slough ($p = 0.47$) (Figure 28), however, this site was characterized by the lowest CO_2 fluxes for all other salinity values. For 1 ppt incubations, East End exhibited the highest CO_2 concentration decline out of the three sites, followed by West Pond and Dutch Slough. There were also statistically significant declines in CO_2 fluxes for all three sites, with West Pond showing the steepest decline ($p = 0.011$) followed by Dutch Slough and East End ($p = 0.062$ and 0.057 respectively). 2 ppt incubations produced the steepest declines in Dutch Slough and West Pond soil CO_2 concentrations, with East End concentrations slightly higher than 1 ppt incubations. However, fluxes for East End soils increased significantly ($p = 0.036$), although this trend was not seen for the other two sites, with statistically significant decline in fluxes for Dutch Slough ($p = 0.062$ and 0.031 respectively). Finally, for 3 ppt incubations, we saw declines in concentrations for all three sites compared to the control, however higher concentrations were observed for Dutch Slough compared to 1 and 2 ppt incubations. There were also statistically significant declines seen in the flux data for East End ($p = 0.073$) and Dutch Slough ($p = 0.022$), but not found to be statistically significant for West Pond CO_2 fluxes, which were already not significantly different from zero.

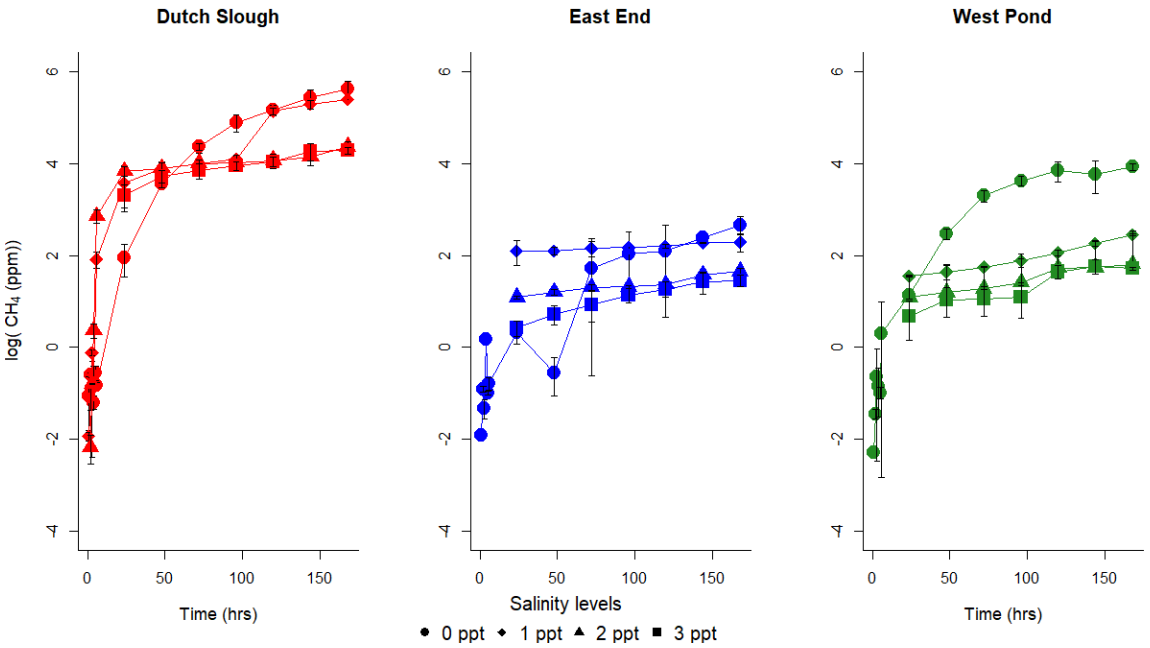

Figure 29. Effect of salinity on log transformed methane concentrations produced over time in slurry experiments with topsoil (0-5 cm) from our three study sites. Nitrate concentration was set at 0 ppm. Error bars represent standard deviations from triplicate experiments, which for most points were found not to exceed >30% of the measured value.

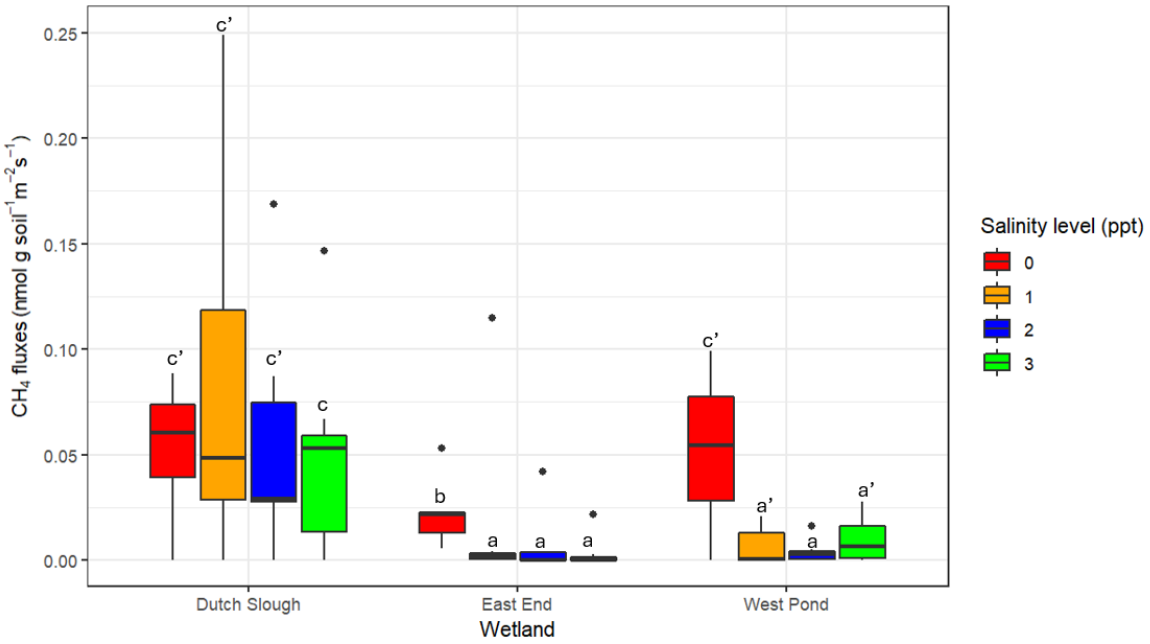

Figure 30. Average CH_4 fluxes calculated for the initial rapid evolution phase of the slurry experiments with top soil (0-5 cm), spanning measurements taken from 1-24 hours in

conditions with 0 (red), 1 (orange), 2 (blue) and 3 (green) ppm of nitrate. Different letters indicate significant differences at p<= 0.05. Letter' represents differences at significance level p <=0.1

Figure 29 shows the temporal evolution in CH_4 concentrations in slurry experiments in response to various salinity, while Figure 30 shows the corresponding initial (first 24h) CH_4 fluxes. For control experiments, CH_4 concentrations were found to be the highest for all three sites compared to higher salinity treatments, with Dutch Slough producing the most CH_4followed by West Pond and East End (Figure 29). Methane production also started in East End soils 48 hours after the start of the experiment. Stabilization of methane concentrations was observed across all three sites and salinity treatments, which was preceded by a steep increase in concentrations initially after the start of experiments. Dutch Slough and West Pond soils exhibited the highest CH_4fluxes for control incubations ($p = 0.042$) compared to East End, however there were no differences between Dutch Slough and West Pond (Figure 30). For East End and West Pond, CH_4 fluxes were lower when salinity was increased, with no significant differences between fluxes measured in experiments with a, 2 or 3ppt salinity levels (Figure 30).

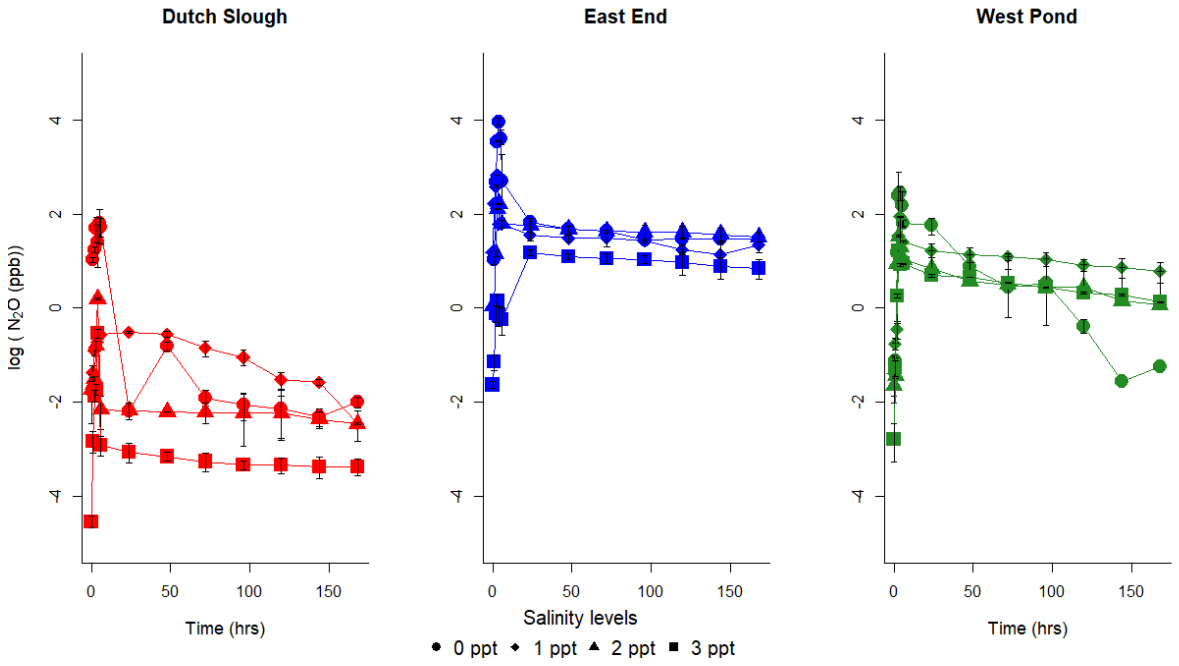

Figure 31. Effect of salinity on log transformed nitrous oxide concentrations produced over time in slurry experiments with top soil (0-5 cm) from our three study sites. Nitrate concentration was set at 0 ppm. Error bars represent standard deviations from triplicate experiments found not to exceed >40% of the measured value at any time point.

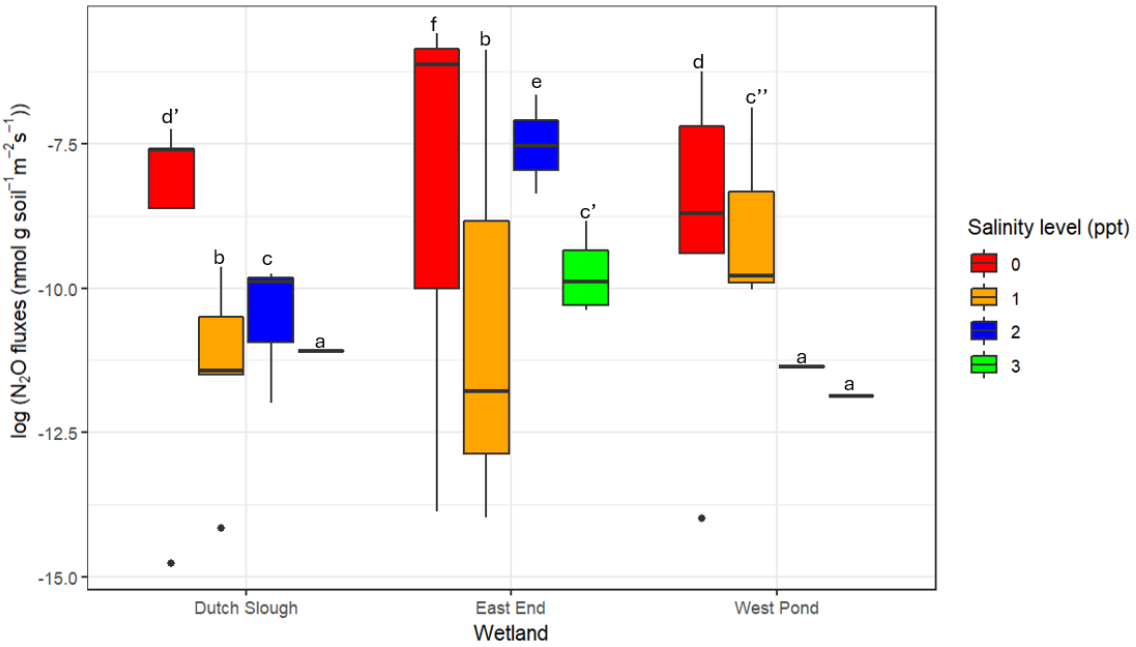

Figure 32. Average log-transformed N_2O fluxes calculated for the initial rapid evolution phase of the slurry experiments with top soil (0-5 cm), spanning measurements taken from 1-24 hours of the experiment in conditions with 0 (red), 1 (orange), 2 (blue) and 3 (green) ppm salinity level. Different letters indicate significant differences at p<= 0.05. Letter' represents differences at significance level p <=0.1. Lack of boxplots for Dutch Slough 3 ppt treatment and West Pond 2 and 3 ppt incubations are due to negative flux values, which cannot be log transformed.

Figure 31 shows the temporal evolution in N_2O concentrations in slurry experiments in response to various salinity, while Figure 32 shows the corresponding initial (first 24h) N_2O fluxes. Significantly higher N_2O fluxes for East End ($p << 0.05$) were observed for control treatments with no added salts and nitrate, with no differences observed between West Pond and Dutch Slough (Figure 31 and Figure 32). West Pond did produce higher cumulative N_2O concentrations than Dutch Slough. For 1 ppt incubations, lower N_2O concentrations were observed across the three sites, with the exception of later time points for West Pond. Fluxes decreased significantly in response to a 1 ppt increment in salinity over control for all three sites ($p << 0.05$). However, fluxes increased significantly for Dutch Slough and East End for 2 ppt incubations ($p = 0.039$ and 0.011), whereas they decreased significantly for West Pond soils ($p << 0.05$). Concentration profiles for 2 and 3 ppt converged to similar values for all three sites. However, fluxes did decrease for the highest salinity treatment. Negative fluxes were observed for West Pond soils for 2 and 3 ppt incubations, and Dutch Slough soils for 3 ppt incubations. East End soils exhibited significantly lower fluxes at the 3 ppt treatment ($p = 0.012$). Log transformed N_2O

concentrations tended to stabilize at lower values for all sites and treatments with the sole exception of control incubations with West Pond soils.

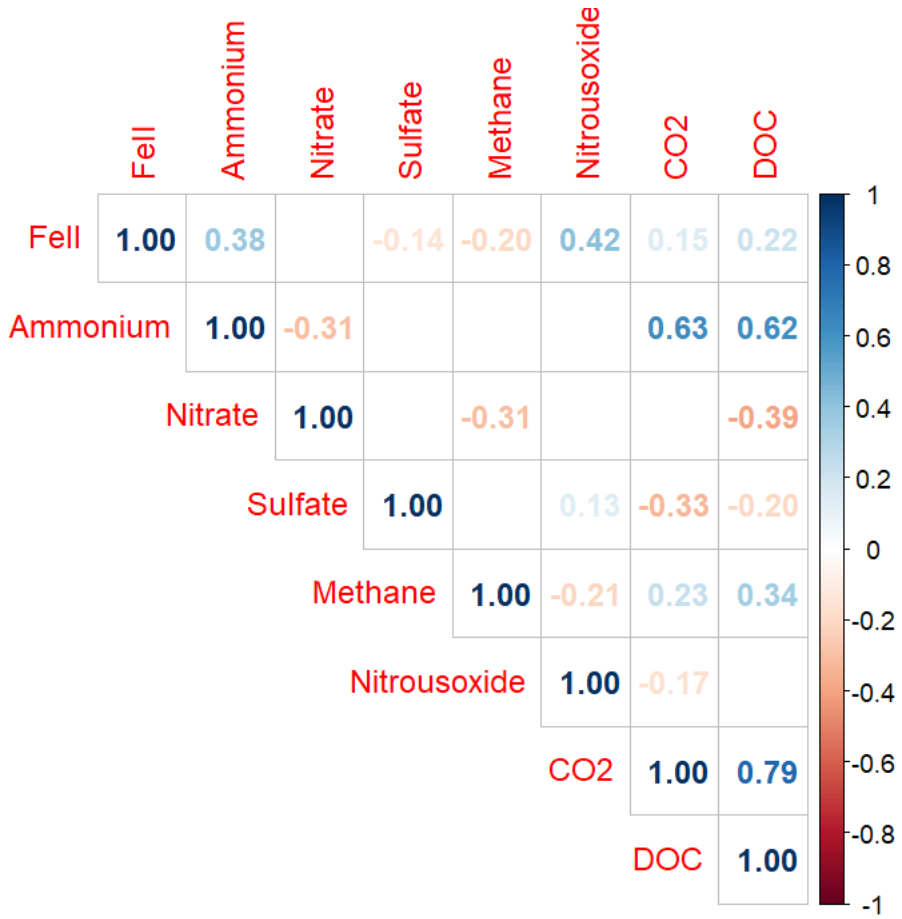

Figure 33. Correlation plot of all measured response variables from the slurry experiments. Fe(II), NH_4^+, NO_3^-, SO_4^{-2} and DOC were measured from aqueous samples post filtering. Correlation coefficients are reported at a threshold of p <= 0.05.

Similar to statistical analyses visually represented in Figure 33, this plot allows us to investigate key associations between measured variables. CO_2 and DOC concentrations were found to strongly positively associated, indicating enhanced mineralization of dissolved organic carbon and conversion to CO_2 or dissolved inorganic carbon (DIC). CO_2 was also positively related with NH_4^+. Fe^{+2} is also correlated with NH_4^+, pointing at a complicated system of substrate utilization and linked redox processes, which will be discussed later in section 4. Additionally, Fe^{+2} was also positively associated with N_2O fluxes, and weakly associated with DOC in solution.

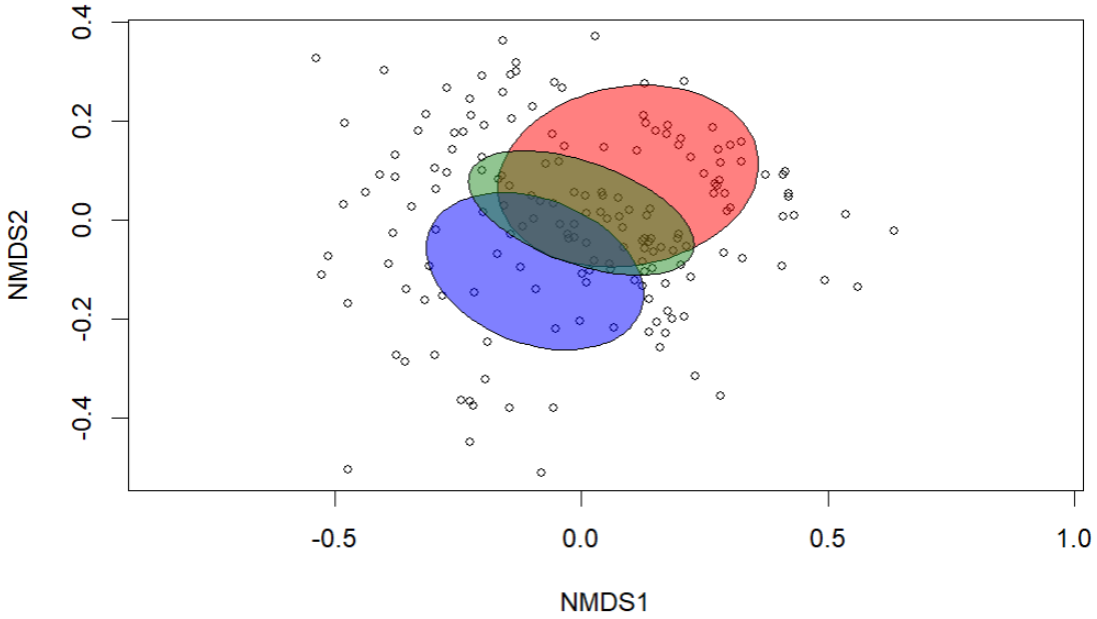

Figure 34. NMDS plot of all measured variables from the salinity experiments. Red, blue, and forest green ellipses represent measured variables from Dutch Slough, East End, and West Pond soil incubations respectively.

The NMDS ordination shown in Figure 34 is similar to the one in Figure 26, with the prime exception being that the order of polygons is reversed. Here, Dutch Slough is on top compared to East End being on the top in Figure 26.

4. Discussion

4.1 Site characteristics

Of the three sites, East End had the highest native nitrate, extractable Fe(III) and Mn oxides concentrations, and the lowest C:N ratio (Table 2), indicating a higher potential to support alternative respiration pathways leading to higher carbon dioxide fluxes compared to Dutch Slough and West Pond. Given the relatively high C:N ratios in Dutch Slough and West Pond soils and low nitrate in surface waters, there was also a high response to nitrate additions in both incubations. The initial pulse and stabilization patterns observed in carbon dioxide profiles across soils and treatment levels matches well with the initial mineralization of labile carbon followed by slower decomposition of more chemically resistant carbon pool[144 145]. There were also strong associations between DOC and carbon dioxide concentrations, indicating higher vertical and horizontal losses of carbon in response to additions of nitrate. Salinity treatments

led to lower carbon dioxide fluxes across all treatment sites. The lowest negative effect of salinity on CO_2 fluxes was observed for Dutch Slough, which could be explained by Dutch Slough being a tidally-connected saline wetland site acclimated to higher salt concentrations. The higher salinity could also be a consequence of summer sampling during a period of low-rainfall. The decrease in CO_2 fluxes with increasing salinity suggests that higher salinity levels inhibit microbial activity and organic matter decomposition, particularly in the more freshwater wetlands. This inhibition may be due to osmotic stress and the energetic costs associated with maintaining cellular functions under high salinity conditions.

Despite the clear salinity gradient based on Cl^- and SO_4^{2-} concentrations from Dutch Slough to West Pond, the gradient from NMDS ordinations in Figures 26 and 34 suggests that Dutch Slough and East End comprise the two ends of composited chemical parameters measured from soil incubations. This is broadly a reflection of a change in environmental parameters tested in the slurry experiments. East End appeared to be better adapted to metabolizing and processing NO_3^- whereas Dutch Slough seemed better adapted to handling higher salinity treatments. This would indicate a higher degree of salt tolerance for Dutch Slough compared to the other two relatively freshwater system.

For the nitrate treatments, East End exhibited the highest CO_2 accumulation across the three sites, followed closely by West Pond and Dutch Slough, which reflects shifts in net ecosystem exchange of carbon (NEE) reported from 2015-2017 in previous studies[146,147].

4.2 Factors driving differences in carbon dioxide fluxes

Fluxes measured during nitrate amendments were an order of magnitude higher than ones measured for the salinity treatments. These fluxes were also an order of magnitude higher than those measured for subalpine wetlands (Chapter 1, Figure 5). This could be explained by the higher temperature of the incubation of Delta soils, and the higher organic matter content of these soils. The observation that East End exhibited the highest CO_2 accumulation across the three sites for the nitrate treatments could be explained by the higher presence of native alternative electron acceptors, such as mineral oxides, which delay methane production under prolonged anoxia and produce more CO_2 instead as long as nitrate persists in the system[148,149]. CO_2 fluxes tend to level off for lower-nitrate treatment levels but keep increasing for higher nitrate treatment. potentially due to excess nitrate in solution at 168 hours after the start of the experiment (Figure 65 Appendix 1). Convergence of CO_2 concentrations across the three salinity levels were also observed across the sites, indicating potential limits on mineralization of

organic matter combined with gradual adaptation to saline conditions[150]. CO_2 fluxes from these sites correspond well with eddy covariance measurements made of net ecosystem exchange (NEE) from these sites[97,143,151].

4.3 Methane dynamics across sites

Methane emissions were significantly reduced for nitrate treatments across all three sites, especially at East End. This can be explained by the presence of native alternative electron acceptors in East End soils. Higher emissions from Dutch Slough could be explained by the higher abundance of sulfate-reducing fermenter and syntrophic microbes in saline soils, which are known to produce substrates utilized by methanogens[152]. Reductions in emissions in response to increasing nitrate levels can be explained by the preferential reduction of nitrate over organic carbon driven by higher energy yields obtained via respiration. For salinity treatments, lowest reduction in CH4 emissions was observed for Dutch Slough compared to the other two sites. Similar to CO_2 fluxes, this is presumably due to higher salt tolerance among microbial communities present in Dutch Slough soils. Expected reductions in CH_4 production results from the suppression of methanogens due to osmotic stress caused by higher salt concentrations and being subsequently outcompeted by halophiles[152–154]. Lower CH_4 fluxes in response to higher nitrate loading, mostly driven by agricultural and population pressures, highlight a critical biogeochemical compromise in these systems, with higher fluxes of CO_2 and N_2O increasing total greenhouse gas warming potential (GWP) from these wetland sites[128,130].

4.4 Factors driving N_2O dynamics across sites.

This spike pattern seen in batch experiment seemed indicative of the native soil nitrate being exhausted instantly and subsequent temporally-limited production of N_2O, a trend observed for incubations with subalpine wetland soils as well. Despite lower pH values observed throughout the slurry incubations with nitrate additions, which are known to inhibit denitrification, East End exhibited the highest nitrous oxide fluxes, with a significant increase in response to increasing nitrate levels. This response was observed across the three sites, indicating higher denitrification rates. East End had the lowest ammonium concentrations across the three sites (Table 6) and these were also found to be negatively correlated with nitrate concentrations, with higher nitrate concentrations preferring denitrification whereas ammonium was produced mostly at lower concentrations. This supports the idea that dissimilatory nitrate reduction to ammonium (DNRA) is relevant mostly at high C/N ratios whereas denitrification dominates at lower C/N ratios[155,156], leading to higher nitrous oxide fluxes for the latter[157]. Given that East End soils possessed sufficient amounts of mineral and organic nitrogen, denitrification was the dominant nitrate removal mechanism compared to DNRA at the other two sites, especially for lower nitrate treatments.

4.5 Implications

Overall, our observed trends agree with eddy-covariance flux measurements made over these wetland sites[97,146,158]. The results highlight the importance of considering site-specific characteristics of wetlands when assessing their response to increasing nitrate and salinity levels among other anthropogenic disturbances[97]. They also complement measurements made from eddy covariance towers which cover larger land area/footprints. Broadly, site history (mineral v/s organic soil plus time of establishment), proximity to nitrate sources, and tidal connectivity seem to be important controls on greenhouse gas fluxes measured across soils. For our experiments, East End possessed higher mineral oxides, was proximally located to an active agricultural site, and therefore better adapted to nitrate loading and subsequent mineralization of organic compared to the other two sites. Broadly, sites or wetlands with proximity to sources of nitrate (i.e. agriculture), seem better at reducing nitrate. Wetlands that are already adapted to higher salinity, such as Dutch Slough, may be more resilient to further increases in salinity, while freshwater wetlands, like East End and West Pond, may be more vulnerable to the impacts of saltwater intrusion and sea-level rise on greenhouse gas production.

Through research on these processes, scientists and stewards need to develop management strategies that optimize carbon storage, protect the Delta's biodiversity, and ensure the sustainability of the region's water resources. This knowledge is essential for guiding restoration efforts, land-use planning, and water management decisions in the face of climate change and other environmental stressors. Moreover, insights gained from studying salinization and nitrate loading in the Sacramento-San Joaquin Delta can inform our general understanding of wetland carbon sequestration in other estuarine systems worldwide. As coastal wetlands around the globe face similar challenges, lessons learned from the Delta can contribute to the development of more effective conservation and adaptation strategies on a broader scale.

Chapter 3: Estimating wetland resilience to nitrate loading across two geographies.

1. Introduction

Wetlands are crucial carbon sinks, sequestering carbon through photosynthetic inputs and accretion of organic matter in soils. Despite comprising a small and ever-shrinking percentage of global land area, they sequester carbon at higher densities compared to other natural ecosystems and account for 20-30% of the terrestrial carbon pool[10,14,94]. Additionally, a critical but underappreciated ecosystem service provided by wetlands is nutrient removal from agriculture and domestic uses, especially nitrate which has been known to lead to eutrophication and hypoxia[159,160]. Given that we have produced unprecedented amounts of reactive nitrogen on our planet using the Haber-Bosch process over the past 150 years, wetlands have been instrumental in cycling that reactive nitrogen back to the atmosphere, or filtering and assimilating ever-increasing nutrient loads.

In comparison to a range of interventions such as wastewater treatment plant upgrades to on-farm reductions in fertilizer application, construction of riparian buffers and use of cover crops, wetlands have known to be more effective against increased nitrate loading with respect to costs and nitrate removal[161,162]. This nitrate loading has intensified as a consequence of increasing populations and agricultural intensification on individual and watershed scales[163,164]. Wetlands remove nitrate primarily through the microbial process of nitrate reduction, including denitrification[157,164],. Denitrifiers convert reactive nitrogen to N_2 gas, whilst also producing nitrous oxide gas (N_2O), a greenhouse gas, as a byproduct. This has been described via the leaky pipe paradigm explained in the seminal paper by Firestone and Davidson[165]. Another nitrate removal process referred to as dissimilatory nitrate reduction to ammonium or DNRA involves the reduction of nitrate to ammonium. The DNRA process prevents loss of nitrogen from soils and leads to higher retention of as dissolved and/or sorbed ammonium on negatively charged clays, which is a crucial source of mineral nitrogen for all living organisms.

In nutrient-rich eutrophic environments, denitrification tends to be the main nitrate removal process. For example, denitrification has been shown to be responsible for the removal of around 80% of dissolved nitrates in the Mississippi Delta[157]. In organic matter rich sediments poor in nitrate, the predominant pathway for nitrate removal tends to be DNRA[166]. For instance, in oligotrophic systems such as subalpine wetlands, mountain lakes, and systems dominated by inputs of freshwater (i.e. high mean annual precipitation), DNRA has been found to be a major component of the nitrogen cycle[155,167]. This ability has been extensively studied and instrumentalized *via* constructed wetlands, a relatively low-cost technology delivering

considerable water quality benefits, with between 40-55% of incoming nitrate loading being removed[168]. .

Increased nitrate loading is an issue that wetlands in diverse geographies have to deal with, for a variety of reasons. The Sacramento-San Joaquin Delta, thereafter referred to as the Delta, is a critical wetland in northern California that supplies drinking water to millions of people[106,112] for domestic and agricultural purposes. As it has shrunk by over 70% in the past century due to land-use change for urban development and agriculture[108] nitrate loading in the Delta has intensified, with concentrations increasing from 0.2-0.6 ppm in the 1950s to 2-5 ppm by the 1980s [128,169,170]. Subalpine wetlands have also experienced increased nitrate loadings, but primarily due to atmospheric deposition and fires. Fires lead to an increase in nitrate in the short-term due to the combustion and subsequent mineralization of organic matter in wetland soils[39,171]. Fires can also have legacy effects lasting up to 90 years post-fire[31,143], due to increased nitrification[143]. This has been attributed to the adsorption of organic compounds known to inhibit nitrification[22,172] or reduction of carbon compounds such as tannins that stimulate nitrogen immobilization[173]. Studying nitrate removal in wetland systems is complicated, with a wider suite of environmental variables, inputs, and fluxes making quantification harder to pin down and associate with variables of interest associated with anthropogenic or natural disturbances[174].

Here, we assessed the potential of wetland soils from the Delta and a burned subalpine wetland to remove nitrate in response to nitrate loading from agricultural and domestic uses. To achieve this, we subjected sediments to incubations with increasing nitrate concentrations and measured rates of nitrate removal, and additionally production of ammonium, nitrous oxide, and dissolved organic carbon. These rates would provide a better understanding of coupled nitrogen and carbon cycling in these systems in response to anthropogenically induced loading of nitrate. We found higher nitrate reduction rates for site with prior or current exposure to higher nitrate concentrations in pore and surface waters. Nitrate reduction rates were found to decrease with increasing depth for burned and unburned subalpine wetland sections. These rates were also diminished in the presence of higher salinity for freshwater sites, and similar for the saline site. These results highlight the role of site characteristics and disturbance history for predicting response to increased nitrate loading.

2. Methods

2.1 Study sites

The Mullen fire complex (WY, USA) is an ideal system to study the short-term (<1 year) post-fire biogeochemistry of wetlands and to examine the effects of inputs of pyC on DOC exports and

GHG fluxes. The 2020 Mullen fire burned 715 km^2 of lodgepole pine (*Pinus contorta*) on the Colorado-Wyoming border in the Medicine Bow National Forest starting in September, 2020 and was 97% contained as of January, 2021[49], roughly seven months prior to sampling. The burned wetland is located 7 km on Road 517/Dry Park Road on Lake Creek (41.148244, -106.155794) in the Medicine Bow-Routt National Forest (Figures 1, 2). To limit inherent spatial heterogeneity in soil and porewater biogeochemical properties which make comparisons difficult, adjacent burned and unburned sections of the same wetland were sampled in July 2021. Three locations on the burned wetland were sampled to account for differences in post-fire vegetation growth, ranging from reed grass (***Calamagrostis canadensis*)** dominant sampling site #1 (Figure 1), tall cottongrass (***Eriophorum angustifolium***) dominant site 2, and water sedge (***Carex aquatilis***) dominant site #3.

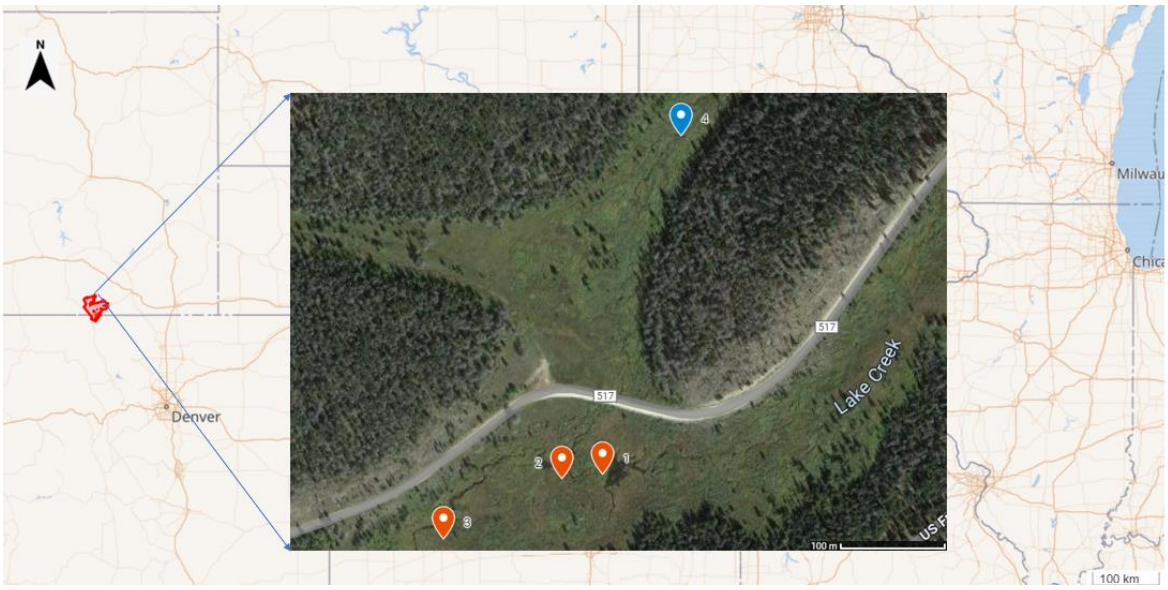

Figure 34. Extent of the 2020 Mullen fire (red outline). The inset shows sampling locations for the burned section of the wetland (sites 1-3, red) and for the unburned section of the wetland (site 4, blue).

Figure 35. Picture of the burned wetland section (Site 1) 9 months after fire (July 8, 2021), showing charred vegetation patches and adjacent burned forest.

Our second geography was constituted by three sites in the Sacramento-San Joaquin Delta that are located within a narrow geographic zone (Figure 17) and constitute sites characterized by different salinities. The sites on Twitchell Island (West Pond and East End) are non-tidal and therefore have a low salinity (0.19 and 0.22 ppt respectively), whereas Dutch Slough is tidally connected and has a higher salinity (0.48 ppt). All three sites have similar mean annual precipitation (338 mm) and air temperature (around 16^{o}C). West Pond and East End have been extensively studied in the past for their carbon fluxes on larger spatial scales[97,136], with eddy covariance (EC) towers established in 2012 and 2014 respectively, whereas Dutch Slough is a relatively new site with its EC tower established in 2021[137]. The dominant vegetation across the sites is cattail and tule grasses, as they were brought in to stabilize berms from persistent wind and water-mediated soil erosion.

Soils on Twitchell Island feature a complex patchwork of alluvium Mollisols adjacent to peat Histosols which were separated from main river channels, which accumulated organic matter

over the last hundred or so years[138]. The East End site was established on alluvium soils whereas West Pond was established on peat-rich Histosols.

Figure 36: Location of the three study sites. US-Tw1 corresponds to West Pond, US-Tw4 corresponds to East End, and US-Dmg corresponds to Dutch Slough.

2.2 Sampling

Wetland soil cores were sampled using a shuttle corer (Figure 26), similar to the one described in Laverman et. al[175]. The shuttle corer was fitted with 2 cm long Plexiglass rings of diameter 4.2

cm. The corer was designed and operated as such to minimize sediment compaction and maintain depth differentiation. The Plexiglass rings were instantly fastened to Plexiglass caps and then steel plates with O rings fastened with screws and stored at 4°C prior to flow-through experiments. Two depths were sampled for subalpine wetland soils; 0-2 and 15-17 cm; and one depth (0-2 cm) was sampled for Delta wetland sites. O horizon was removed and focus was on response from mineral soil, possessing mineral oxides which could participate in redox reactions

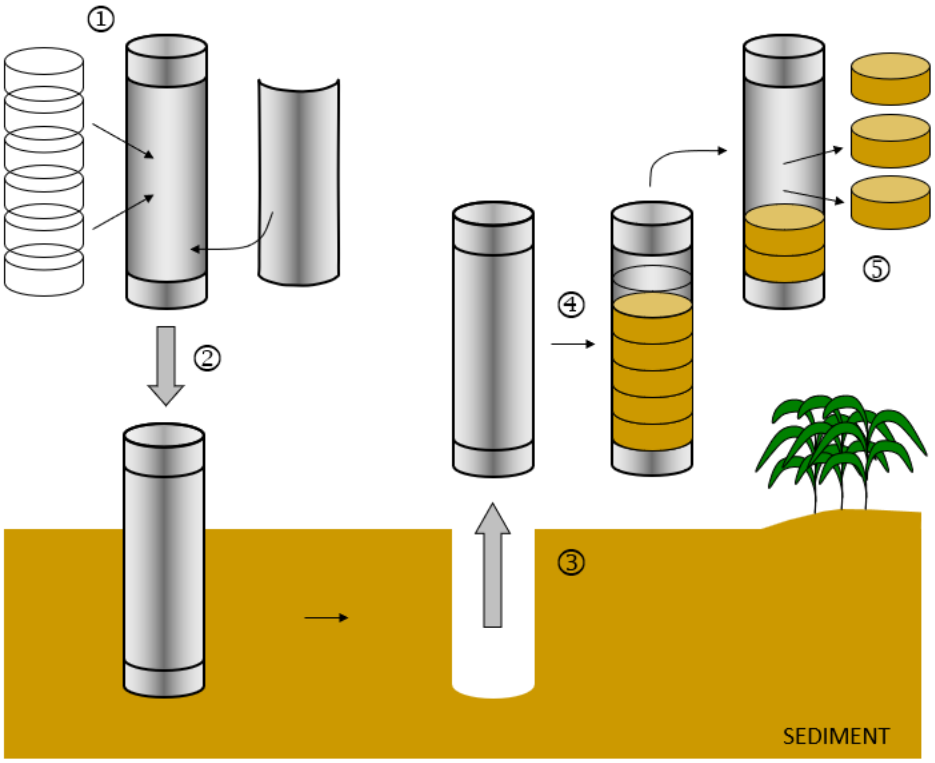

Figure 37. Sampling protocol for sediment-slices used in flow-through reactor experiments[176]. Step 1 refers to the fitting of Plexiglass rings in shuttle corers, Steps 2 and 3 refer the insertion and extraction of sediment from wetland soils, Step 4 highlights the intact sediment slices within Plexiglass rings inside the corer, and Step 5 illustrates the final sediment slices fitted neatly inside Plexiglass rings that were used for flow-through reactor experiments.

2.3 Flow-through reactor experiments

Intact sediment cores from sites sampled from three wetlands in the Sacramento-San Joaquin Delta, namely West Pond, East End, and Dutch Slough were subjected to 6 levels nitrate treatments in flow-through reactor experiments. Subsequently, sediment slices from adjacent burned and unburned subalpine wetland sites in the Medicine Bow Routt National Forest (chapter 1) were also subjected to the same level of nitrate treatments in flow-through reactor

experiments. In addition to nitrate levels, we also subjected the Delta soils to two levels of salinity; 0 and 3 ppt; to simulate freshwater and saltwater scenarios in addition to nitrate loading. These experiments were carried out inside an anoxic glove bag at 18 and 25^{o}C respectively, same as the mean annual average air temperature of both wetland geographies during July.

An input solution was supplied to the reactors at a constant volumetric flow rate (1.5 $\pm$ 0.1 mL hr^{-1}). The solution consisted of DI water amended with appropriate concentrations of $NaNO_3^-$ (0,0.25,0.5,1,2, and 3 mM), and NaBr (2 mM). Additionally, for Delta sediment slices, the input solution was amended with NaCl to simulate salinity treatments of 0 and 3 ppt. Br^- functioned as the flow-tracer for these experiments, and to check for non-ideal flow conditions inside the reactors[177]. NO_3^-, NH_4^+, Br^- were measured using a Dionex ion chromatograph (IC) (electrochemical detector, ED40; analytical column, AS23/AG23; anion self-regenerating suppressor, ASRS-I, 4 mm; mean detection limit: 30 µg/L, error: 5 µg/L) supplied with a carbonate eluant (7.2 mM Na_2CO_3 and 1.28 mM $NaHCO_3$) at a flow rate of 1.0 mL min^{-1}. DOC/DIC were measured via wet oxidation using a total inorganic and total organic C analyzer (Model 1010 Wet Oxidation Total Organic/ Total Inorganic Carbon Analyzer OI Analytical) with 50 g L^{-1} H_3PO_4 for total inorganic C and 100 g L^{-1} $Na_2S_2O_8$ for total organic C with heat catalysis at 100 °C. Outflow samples were subsampled and sparged with N_2 gas and then sampled and measured for CO_2, CH_4, and N_2O using gas chromatography.

2.4 Rates and kinetic parameter estimation

A big advantage of using flow-through reactors over soil slurry incubations is the estimation of nitrate removal and greenhouse gas production rates closer to in-situ microbial activity compared to slurry experiments due to the preservation of pore-structure and spatial distribution of nutrients and microbial populations. These reaction rates obtained from our experiments are referred to as ‘‘potential’’ rates, as they correspond to NO_3^- reduction activity when nitrate is the predominant terminal electron acceptor available to the soil microbial community[175]. Given the supplied concentrations are an order of magnitude higher than values observed in aquatic and wetland systems and no other electron acceptors are provided, they simulate conditions where the availability of nitrate is non-limiting, allowing us to estimate the nitrate processing potential of native microbial populations involved in nitrate removal. Nitrate reduction rates, and production rates of nitrite, ammonium, nitrous oxide, carbon dioxide, and dissolved organic carbon, and kinetic parameters for nitrate reduction reported here in flow-through reactor experiments are derived from steady-state conditions, when the chemical species of interest in the outflow had stabilized and was no longer changing significantly. Potential steady-state rates were calculated according to the equation (1)[176]:

$$R = \frac{\Delta C * Q}{V}$$

where Q is the volumetric flow rate (ml hr^{-1}), V is the reactor volume (cm), and ΔC is the difference in concentration of the solute between the outflow and inflow solutions at steady state (unit). This equation was used to calculate nitrate reduction rates (NRR), where the decrease in nitrate concentrations at the outflow was substituted in this reaction. For species that were not supplied in the inlet solution, such as DOC, CH_4, CO_2, NH_4^+, and N_2O, steady state concentrations at the outflow for these species were used to calculate "export/production rates" (e.g. ammonium export rates (APR)). A distinction was made due to sorption of ammonium and DOC on clay particles, which would make production a misleading term.

The utilization of a substrate by a microbial population is widely described by the so-called Michaelis–Menten, or Monod, rate equation (Eq. 2):

$$R = R_{max} * \frac{C}{K_m + C} \quad (2)$$

where R is the reaction rate, or NRR for this work, R_{max} the maximum reaction rate, C the average nitrate concentration in the reactor, calculated as the midpoint between inflow and outflow concentrations, and K_m is the half-saturation constant. We fitted this equation to the measured NRR/nitrate concentrations data and to obtain the parameters R_{max} and K_m for each of the experimental conditions tested.

2.5 Statistical analysis

All statistical analyses were carried out in R[69]. Differences between all measured water, sediment, and gas variables were determined using a t-test with a threshold of p <= 0.05. Tukey's honest significance difference test was used to determine which sites, if found significant (α = 0.05), were different. Pearson's correlation coefficients were calculated between measured water, sediment, and gas variables and visualized using the 'corrplot' function in R[70]. The Michaelis-Menten function was fitted using the "nls" function in R to steady state NRRs. Model output gave us the parameters R_{max} and K_m. Multivariate analyses were performed to evaluate differences in water, sediment, and gas concentrations. Given these concentrations vary by orders of magnitude, it was desirable to relativize them by column totals through the 'decostand' function using the 'vegan' package[71]. These were then visualized using Principal Components Analysis (PCA) ordinations. PCA was performed in R using the 'prcomp' function which is a part of the 'stats' package[29].

3. Results

3.1 Site characteristics

Table 7. Soil and porewater physical and chemical characteristics for the four study sites and two studied depth intervals (0-12 and 13-24 cm). Values reported are means obtained from triplicate samples. Different superscripted letters indicate significant differences at p<= 0.1 for each row. Standard deviations were <30% of measured values.

Soil characteristics **Depth interval (0-12 cm)**	**Burned 1**	**Burned 2**	**Burned 3**	**Unburned**
Sand content (%)	32.1±2.5 ^{a}	29.7±1.5^{a}	24.4±3.7^{b}	12.3±1.9^{c}
Silt content (%)	25.3±2.5^{a}	22±2.5^{a}	30.6±4.1^{b}	36.5±2.7^{c}
Clay content (%)	42.3±6.5^{a}	47±4.6^{b}	44.9±2.5^{a}	50.9±2.5^{b}
Textural class	Clay	Clay	Clay	Clay
Dry bulk density (g cm^{-3})	0.31±.07^{a}	0.30±.05 ^{a}	0.29±.03^{a}	0.34±.08^{b}
pH	6.17±.61^{a}	6.36±.42 ^{a}	6.19±.33^{a}	5.28±.53^{b}
Percent ash (by weight)	8.83±1.71^{a}	7.19±2.51 ^{a}	6.55±1.5^{a}	1.12±.25^{b}
C_{org} content (%)	23.6±2.11^{a}	21.3±3.45 ^{a}	22.5±1.95^{a}	30.7±2.27^{b}
Total N content (%)	1.17±.11^{a}	1.2±.35^{a}	0.97±.25^{a}	2.28±.57^{b}
Molar C_{org}:N ratio	22.54±2.06^{a}	19.73±3.15^{a}	22.6±1.87^{a}	14.39±2.16^{b}
Extractable Fe content (mg g of soil^{-1})	22.57±4.51^{a}	23.89±3.63^{a}	22.86±5.52^{a}	19.37±3.72^{a}
Extractable Ca content (mg g of soil^{-1})	344.7±42.5^{a}	281.5±31.6^{b}	266.7±37.1^{b}	126.3±12.9^{c}
Extractable Mg content (mg g of soil^{-1})	27.12±3.92^{a}	24.80±2.33^{a}	23.9±4.91^{a}	19.86±2.55^{b}
Depth interval (13-24 cm)	**Burned 1**	**Burned 2**	**Burned 3**	**Unburned**
Sand content (%)	12.1±3.6^{a}	9.17±2.7^{b}	14.24±1.9^{a}	7.35±1.15^{b}
Silt content (%)	35.32±4.16^{a}	32.61±5.19^{a}	32.62±4.57^{a}	38.57±6.1^{a}
Clay content (%)	52.63±4.94^{a}	57.63±6.67^{a}	54.91±4.77^{a}	55.91±7.59^{a}
Textural class	Clay	Clay	Clay	Clay
Dry bulk density (g cm^{-3})	0.51±.13^{a}	0.48±.11^{a}	0.53±.07^{a}	0.52±.09^{b}
pH	6.28±.35^{a}	6.33±.47^{a}	6.11±.37^{a}	6.09±.42^{a}
% ash (by weight)	2.43±.57^{a}	3.19±.36^{b}	2.55±.44^{a}	0.73±.17^{b}
C_{org} content (%)	7.56±1.38^{a}	9.73±2.51^{b}	10.51±1.67^{b}	15.67±3.45^{c}
Total N content (%)	0.33±.06^{a}	0.32±.07^{b}	0.34±.09^{b}	0.58±.11^{c}
Molar C_{org}:N ratio	26.54±1.37^{a}	30.31±2.15^{a}	30.91±1.16^{a}	28.39±3.36^{a}

Extractable Fe content (mg g of soil^{-1})	28.17±4.57^{a}	24.19±5.51^{a}	29.86±6.17^{a}	25.37±4.75^{a}
Extractable Ca content (mg g of soil^{-1})	284.19±32.77^{a}	270.41±42.19^{a}	226.69±39.17^{a}	116.4±12.71^{b}
Extractable Mg content (mg g of soil^{-1})	28.32±2.65^{a}	25.98±4.57^{a}	27.9±3.97^{a}	22.19±1.87^{b}
Porewater concentrations				
Depth interval (0-12 cm)				
Porewater DOC (mg/L)	84.15±10.37^{a}	103.70±2.5^{b}	104.82±2.5 ^{b}	65.12±2.5 ^{c}
Porewater sulfate (ppm)	3.33±.55^{a}	2.83±.47^{a}	3.12±.39^{a}	1.38±.33^{b}
Porewater nitrate (ppm)	1.88±.36^{a}	1.39±.25^{b}	1.30±.17^{b}	0.47±.08^{c}
Porewater Fe(III) (ppm)	2.51±.49^{a}	2.83±.38^{a}	2.45±.67^{a}	1.57±.29^{b}
Depth interval (13-24 cm)				
Porewater DOC (mg/L)	90.27±17.15^{a}	108.93±22.7^{b}	104.23±12.4^{b}	60.27±12.33^{c}
Porewater sulfate (ppm)	1.11±.27^{a}	1.43±.36^{a}	1.22±.27^{a}	0.78±.15^{b}
Porewater nitrate (ppm)	0.12±.02^{a}	0.15±2.5 ^{b}	0.10±.01^{b}	0.11±.03^{c}
Porewater Fe(III) (ppm)	0.25±.06^{a}	0.31±.09^{a}	0.31±.05^{a}	0.27±.03^{a}

Table 8. Mean Physical and chemical characteristics of surface soils (depth interval 0-5 cm) and surface waters from the three study sites obtained from triplicate samples. Different letters indicate significant differences at p <= 0.05. Standard errors were found to be less than 30% of measured parameter values.

Site characteristics	Dutch Slough	East End	West Pond
Soil (0-5 cm)			
Sand	79.6±13.5[a]	55.2±11.2[b]	59.3±7.75[b]
Silt	10.1±2.3[a]	33.2±6.7[b]	21.2±3.4[c]
Clay	11.1±3.1[a]	12.4±2.6[a]	20.1±4.7[b]
Textural class	Loamy sand	Loam	Sandy clay loam
Dry bulk density	1.22±.29[a]	1.07±.18[b]	1.16±.25[a]
pH	7.57±.36[a]	5.96±.44[b]	6.49±.29[c]
C_{org} content (%)	7.89±1.19[a]	15.32±3.65[b]	18.95±2.77[c]
Total N content (%)	0.47±.06[a]	0.91±.14[b]	0.93±.22[b]
Molar C_{org}:N ratio	17.54±1.15[a]	16.38±3.11[a]	19.17±2.79[a]
Extractable Fe content (mg g of $soil^{-1}$)	2.17±.33[a]	11.89±2.96[b]	8.16±1.47[c]
Extractable Mn content (mg g of $soil^{-1}$)	0.12±.03[a]	0.78±.17[b]	0.31±0.06[c]
Extractable Al content (mg g of $soil^{-1}$)	1.41±.23[a]	5.59±1.14[b]	3.27±0.55[c]
Extractable Ca content (mg g of $soil^{-1}$)	44.32±10.71[a]	121.42±20.39[b]	78.13±15.52[c]
Surface water			
Salinity (ppt)	0.48±.06	0.22±.03	0.19±.02
NH_4^+ concentrations (ppm)	1.67±.44[a]	1.19±.16[b]	2.12±.079[c]
NO_3^- concentrations (ppm)	0.27±.03[a]	0.86±.17[b]	0.13±.03[c]
Cl^- concentrations (ppm)	267.81±15.39[a]	122.31±15.32[b]	110.57±20.91[b]
SO_4^{-2} concentrations (ppm)	20.87±4.11[a]	0.78±.11[b]	0.56±.09[c]

Table 7 shows that the sites were statistically similar with regards to their measured physical properties, with similar bulk density and textural class. All sites were characterized by high clay content (>42%), and the unburned site was characterized by a lower sand content but higher silt content than the other sites. The unburned site had significantly less ash ($p = 0.001$) than the burned sites (6.6-8.8%), and ash content across the burned sites was significantly higher in the top soil (0-12 cm) than for the deeper depth interval (13-24 cm) ($p = 0.064$). The burned sites had significantly lower C content (21.5-23.3%) ($p = 0.025$) and N content (0.97-1.26%) ($p = 0.027$) than the unburned site (30.7% and 2.28%, respectively). The C:N ratios increased significantly by depth for both burned and unburned sites ($p = 0.012$). The soil pH was slightly acidic, and the pH of the topsoil in the burned sites was about one unit higher than for the

unburned site (5.28) ($p = 0.027$), although there were no significant differences between sites for the deeper soil. Extractable Fe content did not significantly differ between the burned and unburned soils, but significantly increased with depth ($p = 0.041$). Burned and unburned soils from shallower depths were characterized by significantly higher porewater nitrate concentrations compared to deeper soils ($p = 0.057$). Additionally, they possessed higher porewater sulfate concentrations compared to unburned soils ($p = 0.031$) and higher DOC concentrations compared to unburned soils ($p = 0.05$). For deeper depths, differences for porewater nitrate, sulfate, and dissolved organic carbon were found not to be statistically significant.

Dutch Slough was characterized by soils that had significantly lower C_{org} and N contents ($p = 0.008, 0.01$), as well as significantly lower contents of extractable Fe, Mn, Al and Ca and a higher pH (7.9 versus <6.5 for the other two sites). Both SO_4^{2-} and Cl^- concentrations in surface water were statistically significantly higher in Dutch Slough than in the other sites, by factors of 27-37 and 2.1-2.4, respectively. East End soils had significantly higher contents of Fe, Mn, Al and Ca than those of West Pond, but lower C_{org} and N content and a more acidic pH. Its surface water was characterized by slightly higher NO_3^-, Cl^- and SO_4^{2-} concentrations than the one of West End. All of the sites had similar C_{org}/N ratios. The surface water concentrations make the freshwater/salinity gradient clear, with Dutch Slough having the highest chloride and sulfate concentrations (267.81 and 20.87 ppm) ($p <<< 0.05$), followed by East End and West Pond. The sulfate concentrations were found to be greater by an order of magnitude; 20.87 ppm compared to <1 ppm for the other two sites.
Since you used the depth 0-2 cm for the Delta and Mullen soils, then maybe add some text that specifically compare those.

3.2 Nitrate and nitrite breakthrough curves

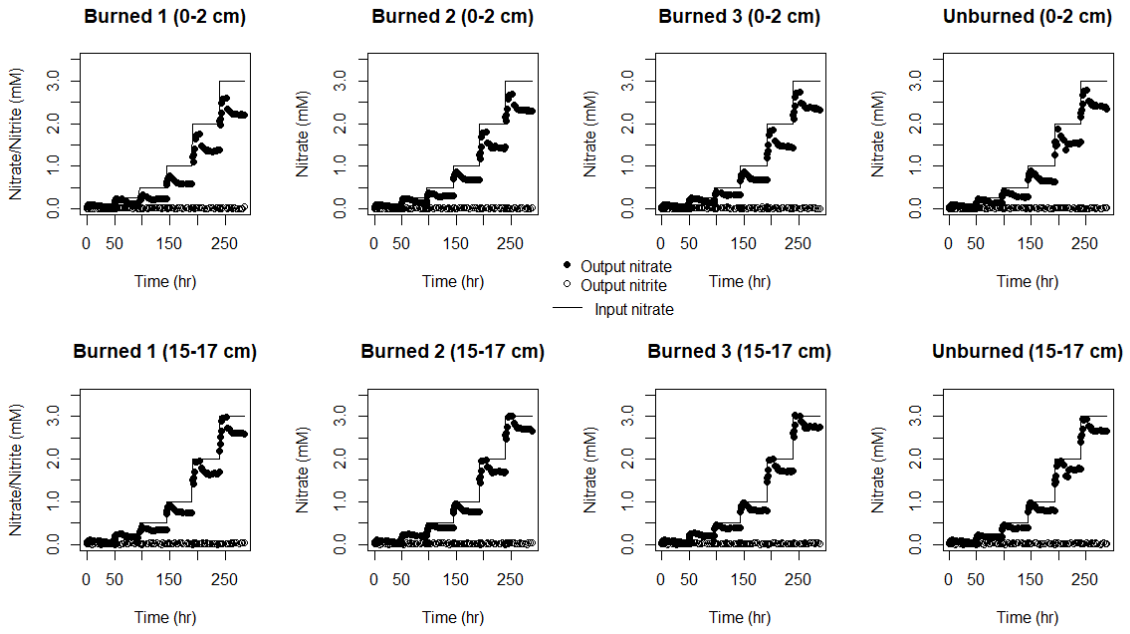

Figure 38. Evolution of nitrate (black circles) and nitrite (white circles) concentrations in the FTR output solution in response to increasing nitrate additions (solid black line). from the four study sites in the subalpine wetland. Experiments were performed with soils from the 0-2 depth interval (top panels) and the 15-17 cm depth interval (bottom panels), with a salinity of 0 ppt.

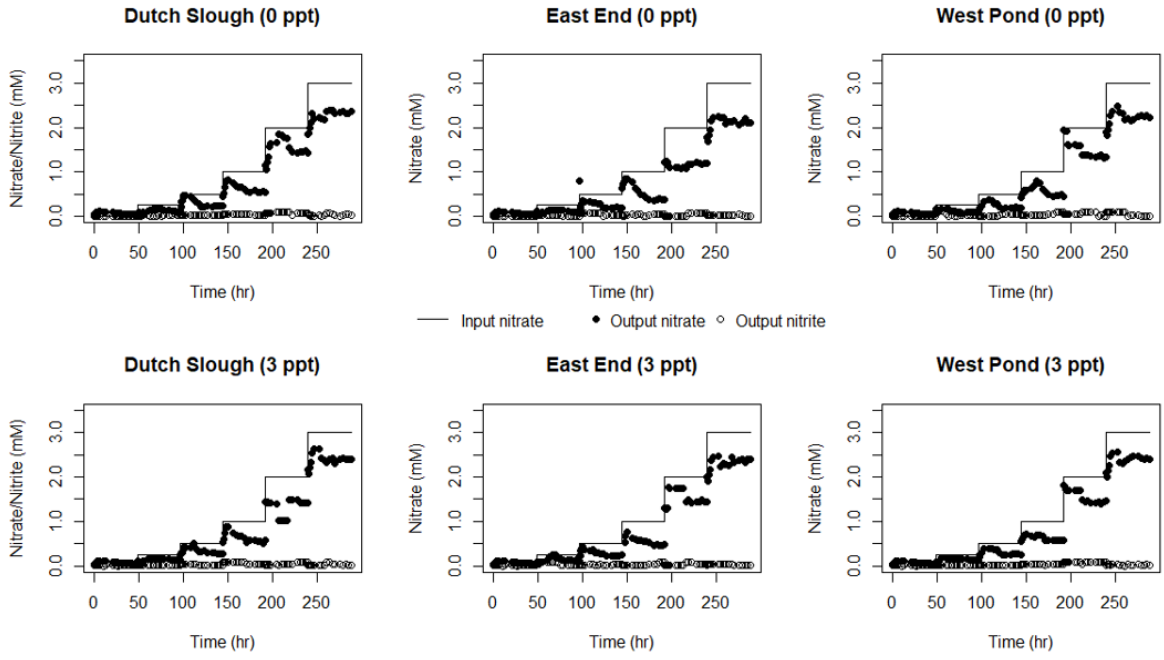

Figure 39. Evolution of nitrate (black circles) and nitrite (white circles) concentrations in the FTR output solution from the three study sites from the Delta wetland in response to increasing

nitrate additions (solid black line). Experiments were performed with soils from the 0-2 depth interval with a salinity of 0 (top panels) and 3 ppt (bottom panels).

Nitrate and nitrite breakthrough curves in response to increasing nitrate concentrations are shown in Figures 38 and 39 for all the FTR experiments. The breakthrough curves indicate that nitrate-reducing activity is taking place in all the study soils, and nitrite does not accumulate in any of the conditions and soils tested. The point after each step up at which output nitrate stabilizes (~78, 120, 180, 220, and 260 hours) is what we refer to as the steady-state, and values post those time points were used for the calculation of nitrate-reduction rates. Concentrations of input nitrate were increased steadily, and the difference in concentrations between the input and the output are the smallest for the lowest input nitrate concentration. Bromide breakthrough curves for the two sites (data not shown) were consistent with solutions for 1D advective-dispersive flow through homogeneous media[176], indicating a uniform, radial flow of solution through the soil core and the absence of any preferential flow.

3.3 Michaelis-Menten kinetics and comparison of R_{max} and K_m values.

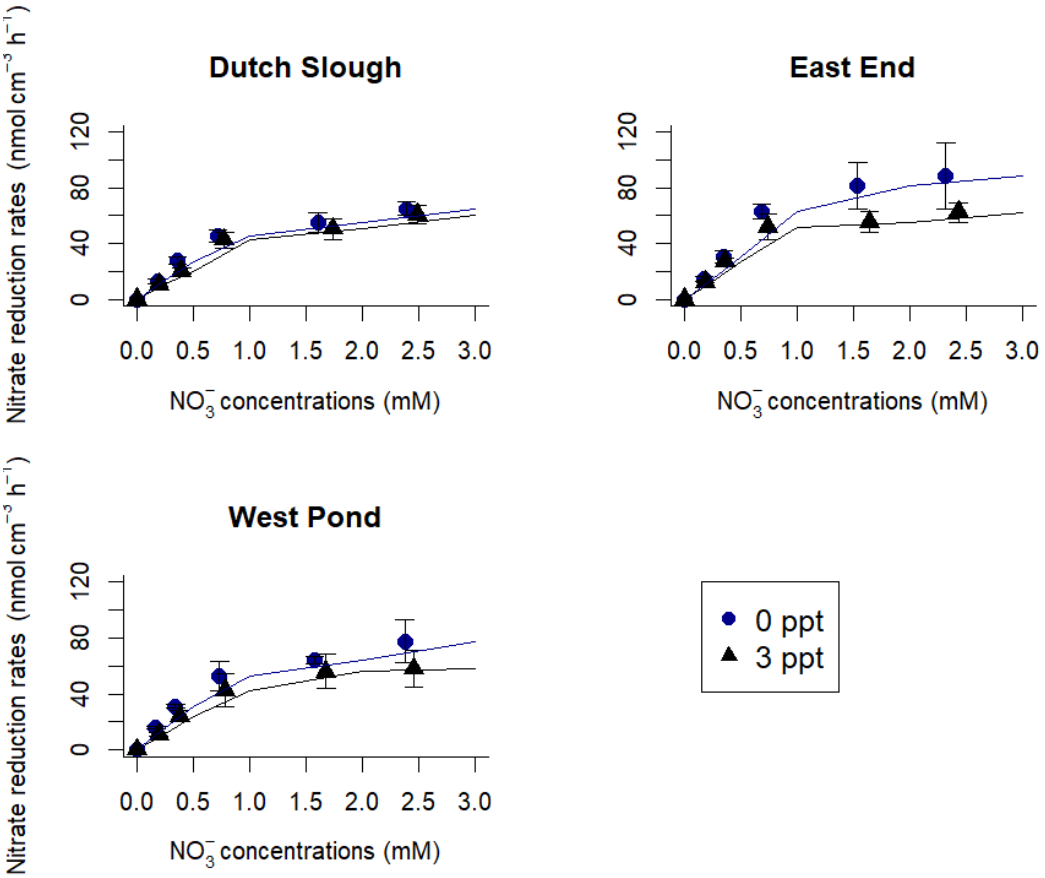

Figure 41. Steady-state nitrate reduction rates (NRRs) measured at 25°C in continuous flow-through reactors (Q = 1.5 ± 0.1 mL hr^{-1}) in conditions with a salinity of 0 (blue circles) and 3 ppt (black triangles) as a function of the average nitrate concentrations in the reactor for the three study sites in the Delta. The lines correspond to the best fit of the Michaelis-Menten rate expression, using the R_{max} and K_m, summarized in Table 9. Error bars indicate confidence intervals at p = 0.95.

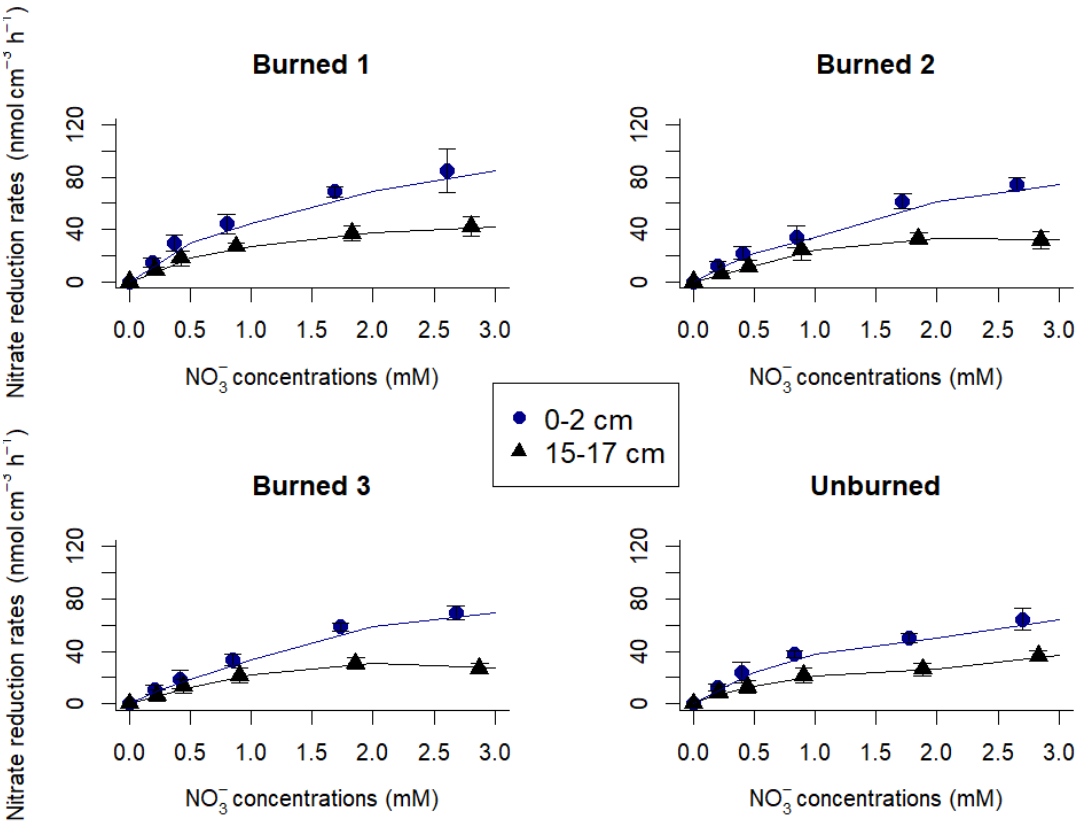

Figure 42. Steady-state nitrate reduction rates (NRRs) measured at 18°C in continuous flow-through reactors (Q = 1.5 ± 0.1 mL hr^{-1}) for soils from the 0-2 cm depth interval (blue circles) and the 15-17 cm depth interval (black triangles) as a function of average nitrate concentrations in the reactor. The lines correspond to the best fit of the Michaelis-Menten rate expression, using the R_{max} and K_m, summarized in Table 9. Error bars indicate confidence intervals at p = 0.95.

Table 9. Kinetic parameters for nitrate reduction, maximum reduction rate (R_{max}) and half-saturation constant (K_m), for all study soils. Values were estimated using the 'nls' function in R. ± refers to standard error during estimation of parameters indicating confidence intervals at p = 0.95.

Site + conditions	Average R_{max} (nmol cm^{-3} h^{-1})	Average K_m (mM)
Delta sampling sites		
Dutch Slough (0 ppt)	84.9 ± 6.6	0.64 ± 0.15
Dutch Slough (3 ppt)	85.3 ± 11.3	1.06 ± 0.32
East End (0 ppt)	127.9 ± 15.9	0.93 ± 0.27
East End (3 ppt)	79.8 ± 10.1	0.63 ± 0.22
West Pond (0 ppt)	100.8 ± 6.	0.77 ± 0.13
West Pond (3 ppt)	81.6 ± 7.6	0.85 ± 0.20
Subalpine wetland sampling locations		
Burned 1 (0-2 cm)	129 ± 8	1.42 ± 0.19
Burned 1 (15-17 cm)	56.79 ± 1.8	0.97 ± 0.08
Burned 2 (0-2 cm)	143.8 ± 14.3	2.43 ± 0.42
Burned 2 (15-17 cm)	47.4 ± 7.4	1.07 ± 0.4
Burned 3 (0-2 cm)	134.7 ± 11.2	2.44 ± 0.3
Burned 3 (15-17 cm)	38.4 ± 5.5	0.79 ± 0.3
Unburned (0-2 cm)	88.0 ± 6.5	1.13 ± 0.19
Unburned (15-17 cm)	38.4 ± 5.2	0.78 ± 0.29

The steady-state nitrate reduction rates as a function of average nitrate concentrations (Michaelis-Menten plots) for the subalpine wetland soils and Delta soils are shown in Figures 41 and 42, respectively, and the corresponding R_{max} and K_m are summarized in Table 9.

In the Delta soils, R_{max} ranged from 79.8 to 134.0 nmol cm^{-3} h^{-1}, with significantly lower values for the higher salinity treatment in the East End and West Pond sites ($p < 0.05$). For the same soils, K_m ranged from 0.63 to 1.05 mM, with no consistent effect of salinity. In the subalpine

wetland soils, R_{max} varied minimally between the three burned sites, with values ranging from 124.7 to 134.0 nmol cm^{-3} h^{-1} in the shallow soils, and from 37.4 to 39.8 nmol cm^{-3} h^{-1} in the deeper soils. R_{max} had lower values in the unburned site, with values of 88.0 nmol cm^{-3} h^{-1} in the shallow soils, and 38.4 nmol cm^{-3} h^{-1} in the deeper soils ($p << 0.05$). For the same soils, K_m ranged from 1.42 to 2.44 mM in the shallow burned soils, and from 0.79 to 1.42 mM in the deep burned soils. Values were slightly lower in the unburned soils ($p < 0.1$).

3.4 Nitrogen and carbon production rates across salinity treatments for Delta soils

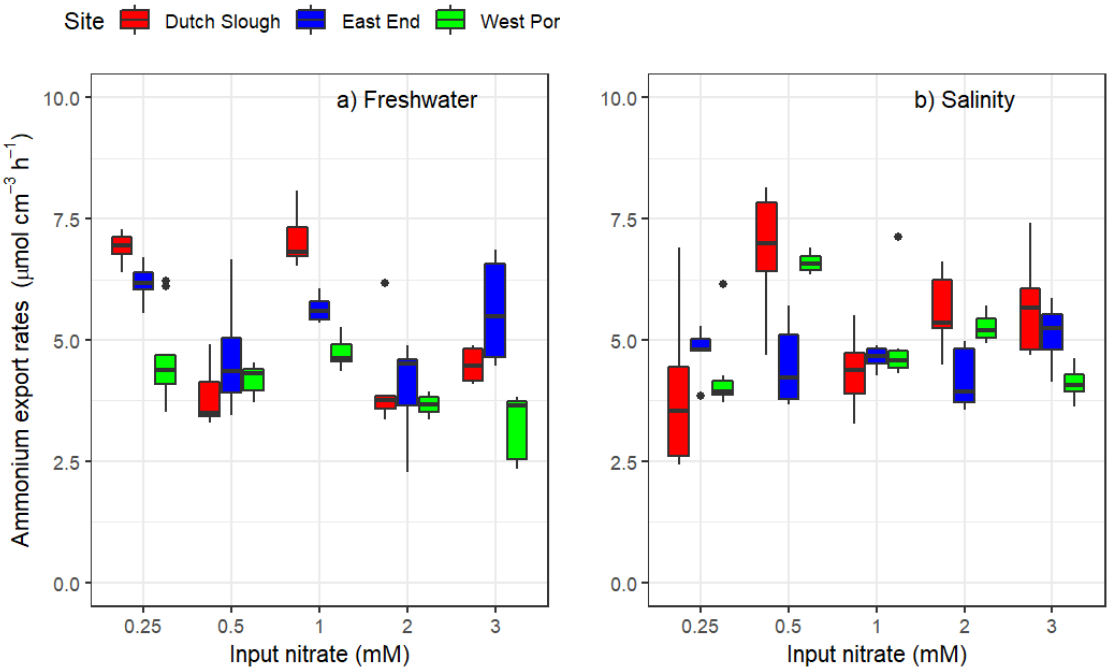

Figure 42. Effect of salinity on potential steady-state ammonium export rates as a function of input nitrate concentrations in the three study sites in the Delta (red: Dutch Slough, blue: East End, green: West Pond). Panel **(a)** shows rates for experiments with a salinity of 0 (freshwater), and **(b)** shows rates for experiments with a salinity of 3 ppt (saline). Rates were calculated after subtracting production rates from control treatments. Error bars were found not to exceed >30% of measured values in flow-through experiments.

The effect of salinity on potential steady-state ammonium export rates in response to increase input nitrate concentrations is shown in Figure 42 for the Delta soils. There were no clear trends observed for the ammonium export rates as a function of nitrate additions across sites and salinity treatments. On average, ammonium production rates declined significantly with increasing nitrate additions ($p < 0.05$) for the low salinity experiments, with the exception of East End soils. For the high salinity experiments, higher ammonium export rates were observed with increasing nitrate additions ($p < 0.05$) for Dutch Slough and West Pond, but not for East End

soils. Ammonium export rates were not found to be significantly different between 0 and 3 ppt experiments.

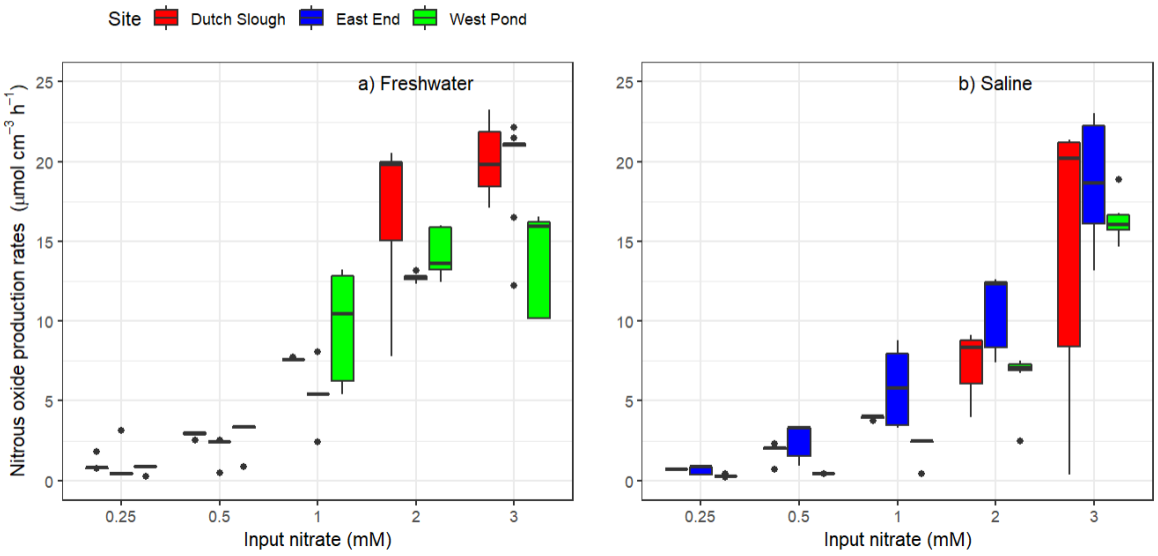

Figure 43. Effect of salinity on potential steady-state nitrous oxide rates as a function of input nitrate concentrations in the three study sites in the Delta (red: Dutch Slough, blue: East End, green: West Pond) in . Panel **(a)** shows rates for experiments with a salinity of 0 (freshwater), and **(b)** shows rates for experiments with a salinity of 3 ppt (saline). Rates were calculated after subtracting production rates from control treatments. Error bars were found not to exceed >30% of measured values in flow-through experiments.

The effect of salinity on potential steady-state N_2O export rates in response to increase input nitrate concentrations is shown in Figure 43 for the Delta soils. Nitrous oxide production rates increased significantly with increasing nitrate concentrations for all three sites ($p < 0.05$) an the two salinity treatments. For freshwater (0 ppt) incubations, highest production rates were observed for West Pond at 1 mM, however East End had the highest nitrous oxide production rates by the end of the experiment. East End production rates were consistently significantly higher for all nitrate additions ($p << 0.05$).

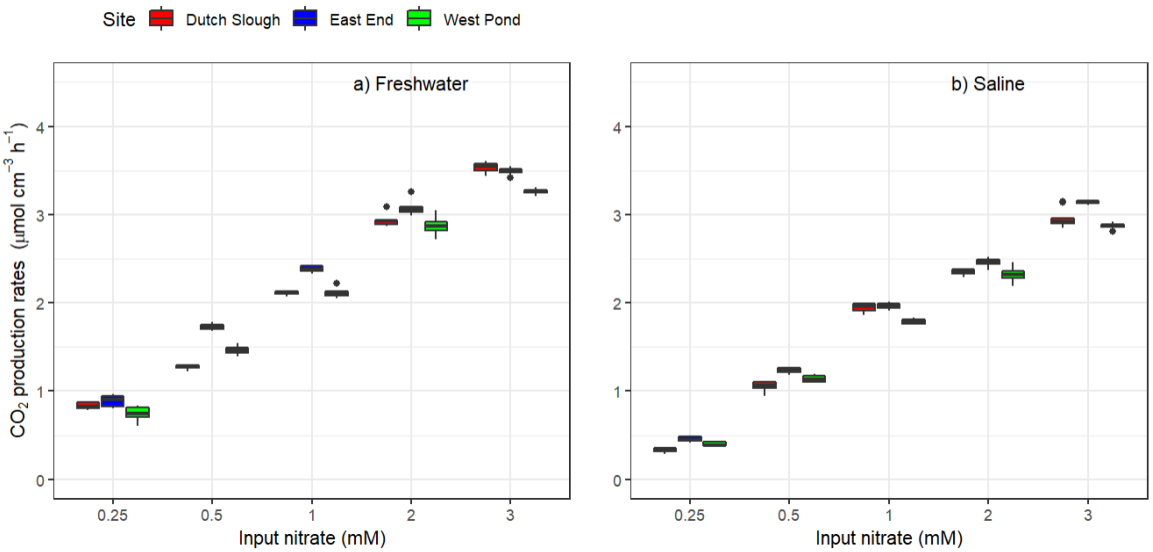

Figure 44. Effect of salinity on potential steady-state carbon dioxide production rates as a function of input nitrate concentrations in the three study sites in the Delta (red: Dutch Slough, blue: East End, green: West Pond). Panel **(a)** shows rates for experiments with a salinity of 0 (freshwater), and **(b)** shows rates for experiments with a salinity of 3 ppt (saline). Rates were calculated after subtracting production rates from control treatments. Error bars were found not to exceed >30% of measured values in flow-through experiments.

The effect of salinity on potential steady-state CO_2 production rates in response to increase input nitrate concentrations are shown in Figure 44 for the Delta soils. Carbon dioxide production rates significantly increased for nitrate additions for the three study sites and the two salinity treatments. East End exhibited the highest CO_2 production rates across the experiments for both freshwater and saline incubations ($p < 0.1$), with no significant differences between Dutch Slough and West Pond production rates. Variance for CO_2 production rates for steady-state conditions was low, which were reflected in the narrow boxplots.

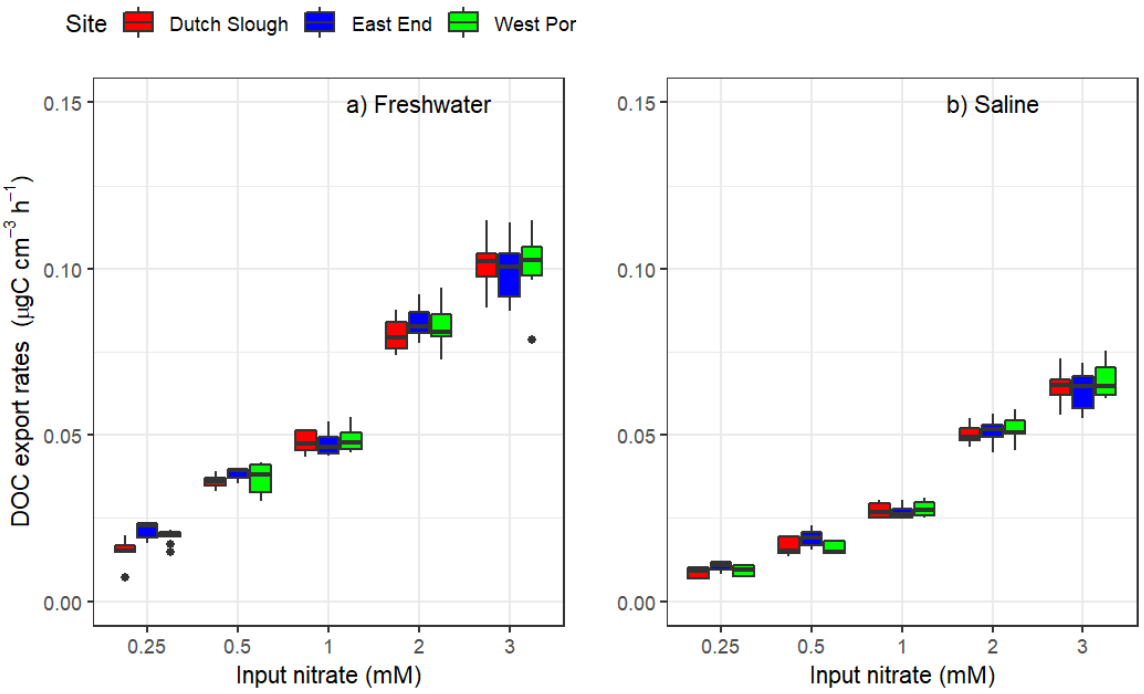

Figure 45. Effect of salinity on potential steady-state DOC export rates as a function of input nitrate concentrations in the three study sites in the Delta (red: Dutch Slough, blue: East End, green: West Pond). Panel **(a)** shows rates for experiments with a salinity of 0 (freshwater), and **(b)** shows rates for experiments with a salinity of 3 ppt (saline). Rates were calculated after subtracting export rates from control treatments. Error bars were found not to exceed >30% of measured values in flow-through experiments.

The effect of salinity on potential steady-state DOC export rates in response to increase input nitrate concentrations are shown in Figure 45 for the Delta soils. DOC export rates increased significantly in response to nitrate increases ($p << 0.05$) for all three study sites and the two salinity treatments. There were no significant differences between the sites at any nitrate increment for the two salinity experiments, however DOC export rates were significantly higher for the low salinity experiment compared to the high salinity ones. No methane was produced during the course of the experiments.

3.5 Nitrogen and carbon production rates for shallow and deep subalpine wetland soils

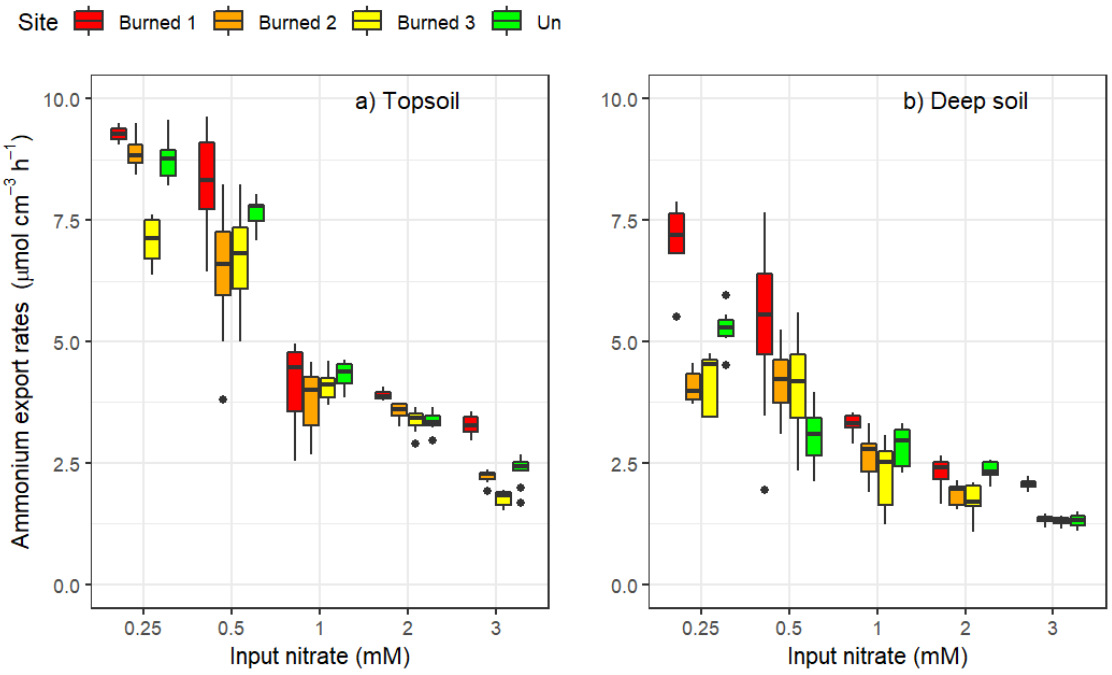

Figure 46. Effect of increasing input nitrate concentrations on potential steady-state ammonium export rates as a function of input nitrate concentrations in the four study sites in the subalpine wetland (red: Burned site 1, orange: Burned site 2, yellow: Burned site 3, green: Unburned site). Panel **(a)** shows rates for experiments topsoils (0-2 cm) and **(b)** shows rates for experiments with a salinity of deep soils (15-17 cm). Rates were calculated after subtracting production rates from control treatments. Error bars were found not to exceed >30% of measured values in flow-through experiments.

The effect of soil depth on potential steady-state ammonium export rates in response to increase input nitrate concentrations are shown in Figure 46 for the subalpine wetland soils. Ammonium export rates followed a significant downward trend with increasing nitrate concentrations in the input for both the topsoil and deeper soils ($p << 0.05$). On average, unburned soils were found to possess lower ammonium export rates compared to burned sites ($p = 0.032$), however those differences were mostly driven by burned site 1, with burned sites 2 and 3 found not to be significantly different, on average, over the duration of the experiments ($p = 0.16$)

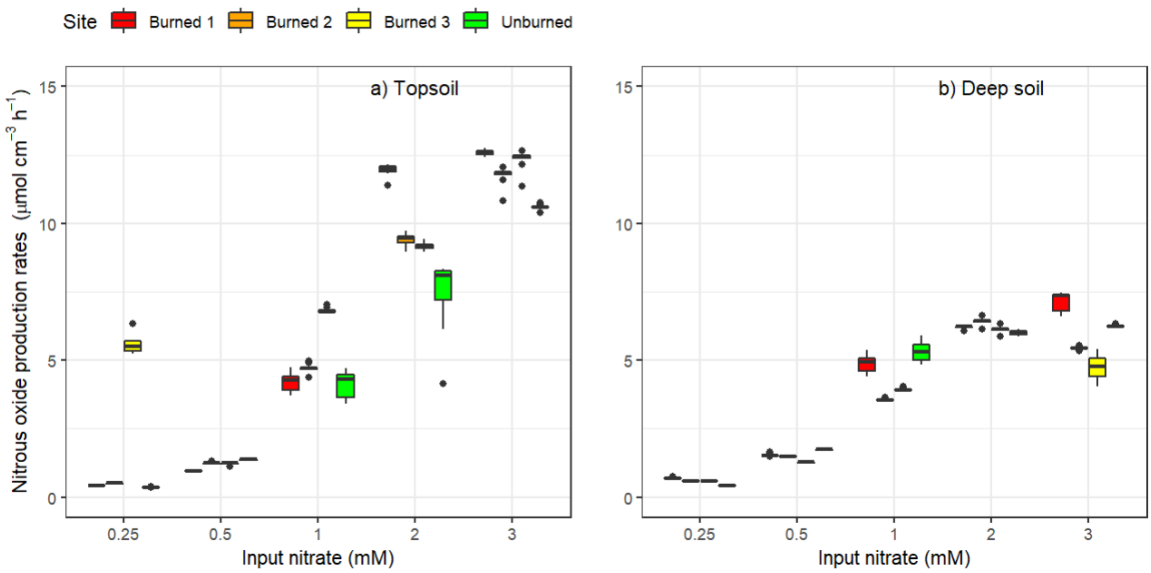

Figure 47. Effect of increasing input nitrate concentrations on potential steady-state nitrous oxide production rates as a function of input nitrate concentrations in the four study sites in the subalpine wetland (red: Burned site 1, orange: Burned site 2, yellow: Burned site 3, green: Unburned site). Panel **(a)** shows rates for experiments topsoils (0-2 cm) and **(b)** shows rates for experiments with a salinity of deep soils (15-17 cm). Rates were calculated after subtracting production rates from control treatments. Error bars were found not to exceed >30% of measured values in flow-through experiments.

The effect of soil depth on potential steady-state N_2O production rates in response to increase input nitrate concentrations are shown in Figure 47 for the subalpine wetland soils. For all sites and soil depth tested, N_2O export rates tend to increase with increased nitrate concentrations. N_2O export rates for the highest nitrate concentrations were higher for the topsoil compared to the deeper one. On average, burned sites were characterized by higher N_2O export rates than the unburned site ($p << 0.05$). For topsoils, unburned soils produced significantly lower nitrous oxide compared to the three burned wetland soils ($p << 0.05$), however this trend did not hold for deep soils.

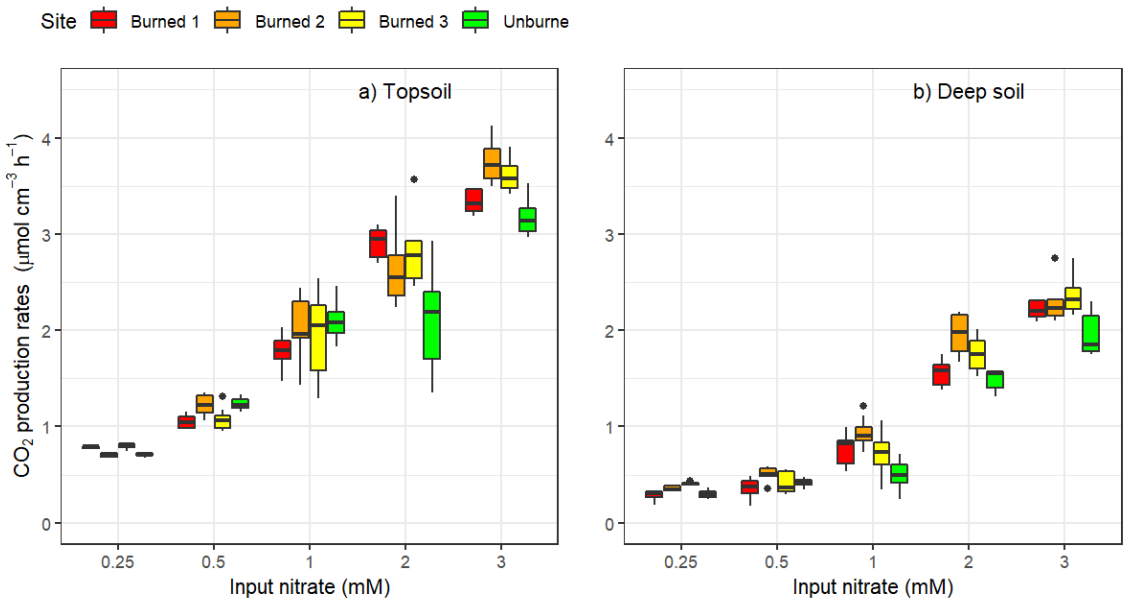

Figure 48. Effect of increasing input nitrate concentrations on potential steady-state carbon dioxide production rates as a function of input nitrate concentrations in the four study sites in the subalpine wetland (red: Burned site 1, orange: Burned site 2, yellow: Burned site 3, green: Unburned site). Panel **(a)** shows rates for experiments topsoils (0-2 cm) and **(b)** shows rates for experiments with a salinity of deep soils (15-17 cm). Rates were calculated after subtracting production rates from control treatments. Error bars were found not to exceed >30% of measured values in flow-through experiments.

The effect of soil depth on potential steady-state CO_2 production rates in response to increase input nitrate concentrations are shown in Figure 48 for the subalpine wetland soils. Overall, CO_2 production from deeper soils was significantly lower than topsoils ($p << 0.05$). Unburned sediments produced the lowest carbon dioxide in response to nitrate treatments for shallow and deep soils ($p << 0.05$). These differences were pronounced with increasing nitrate concentrations for both deep and shallow soils.

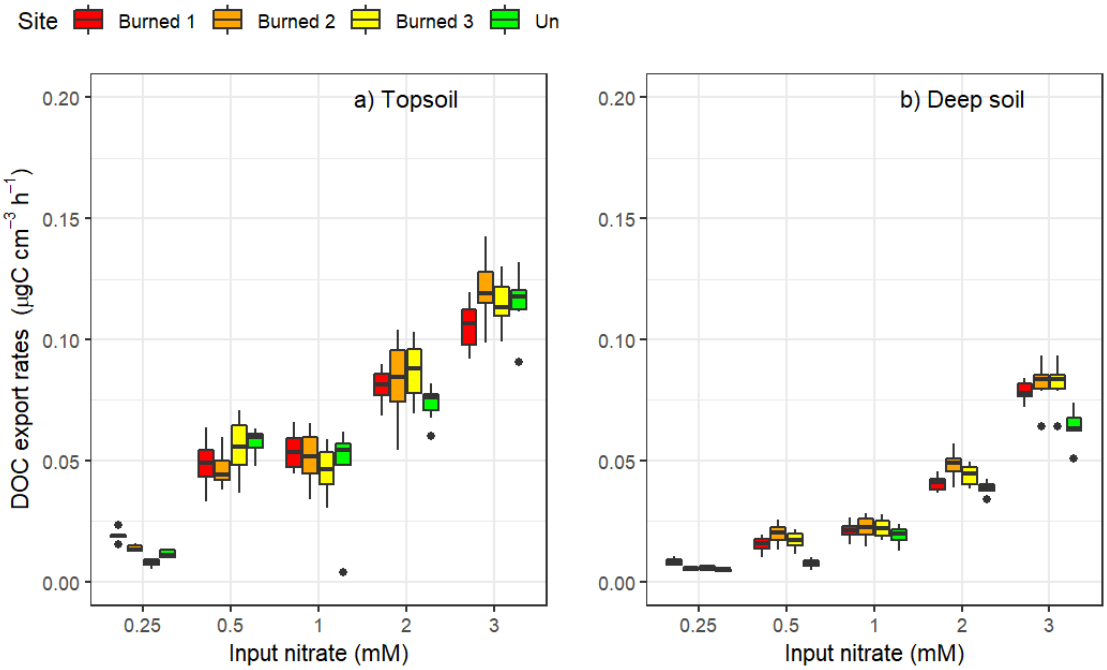

Figure 49. Effect of increasing input nitrate concentrations on potential steady-state dissolved organic carbon export rates as a function of input nitrate concentrations in the four study sites in the subalpine wetland (red: Burned site 1, orange: Burned site 2, yellow: Burned site 3, green: Unburned site). Panel **(a)** shows rates for experiments topsoils (0-2 cm) and **(b)** shows rates for experiments with a salinity of deep soils (15-17 cm). Rates were calculated after subtracting production rates from control treatments. Error bars were found not to exceed >30% of measured values in flow-through experiments.

The effect of soil depth on potential steady-state DOC export rates in response to increase input nitrate concentrations are shown in Figure 49 for the subalpine wetland soils. Overall, CO_2 export from deeper soils was significantly lower than topsoils ($p << 0.05$). For the two soil depth intervals investigated, DOC export rates were higher for unburned wetland site compared to burned sites ($p << 0.05$). With the exception of 0.25 and 2 mM nitrate additions, unburned sediments produced more dissolved organic carbon for each nitrate step compared to unburned sediments ($p < 0.05$). This trend was found to diminish for deeper soils, with no clear trend observed between burned and unburned production rates across nitrate additions.

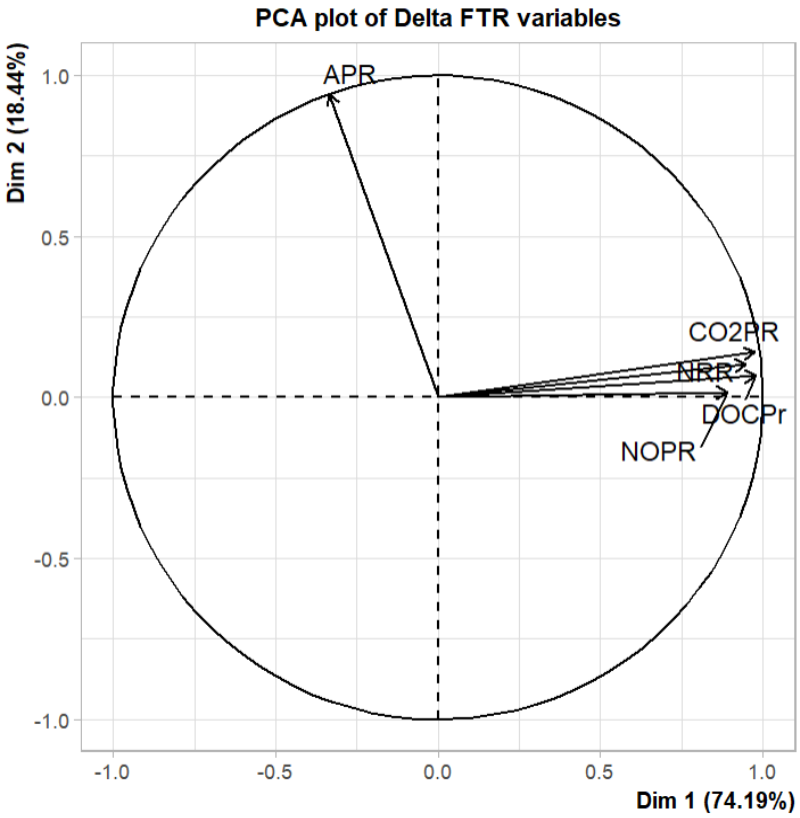

Figure 50. PCA plot for all measured variables from FTR experiments with the Delta soils. APR, CO2PR, NOPR, NRR, and DOCPr stand for ammonium export rate, CO_2 production rate, N_2O production rate, nitrate reduction rate, and DOC export rate, respectively.

The PCA plot in Figure 50 highlighted a strong positive associations between greenhouse gas production rates from Delta sediments. These trends also held for soils from the burned and unburned subalpine wetlands in subalpine wetlands (Figure 51). Nitrate reduction rates across both geographies were found to be strongly positively associated with CO_2 production rates, DOC export rates, and N_2O production rates. Ammonium export rates were found to possess no (Delta) to little correlation (subalpine wetland soils) with any other measured greenhouse gas production rates. Nitrite production rates, not reported here, were extremely minimal given that little nitrite was measured in the outflow from Delta and subalpine wetland sediments.

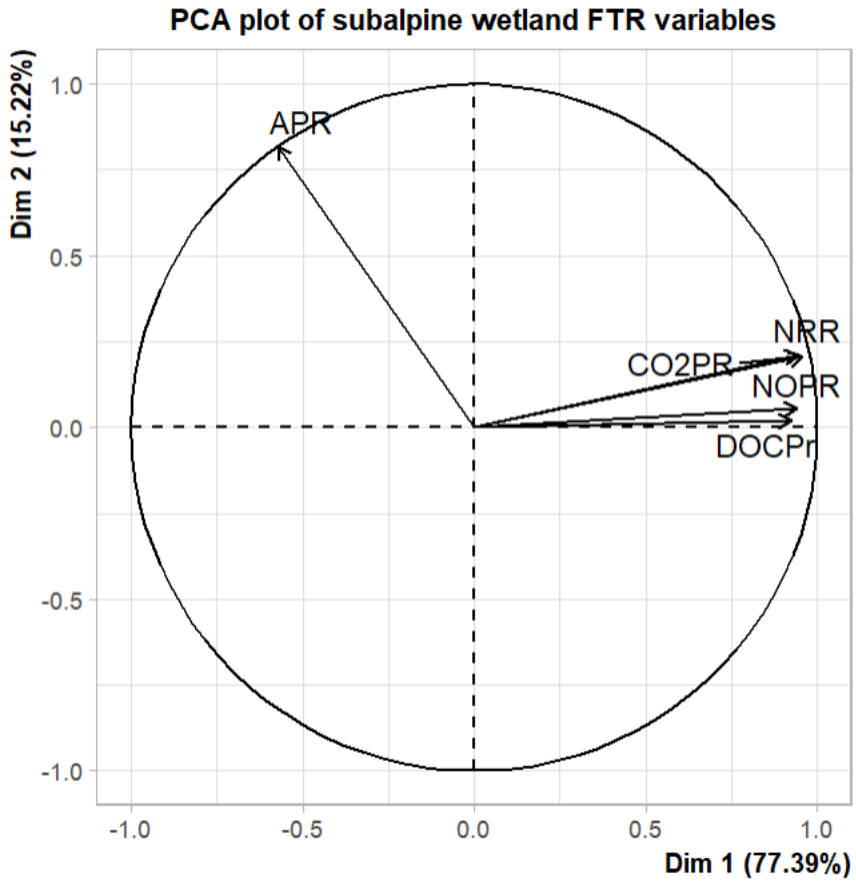

Figure 51. PCA plot for all measured variables from FTR experiments with the subalpine wetland soils. APR, CO2PR, NOPR, NRR, and DOCPr stand for ammonium export rate, CO_2 production rate, N_2O production rate, nitrate reduction rate, and DOC export rate, respectively.

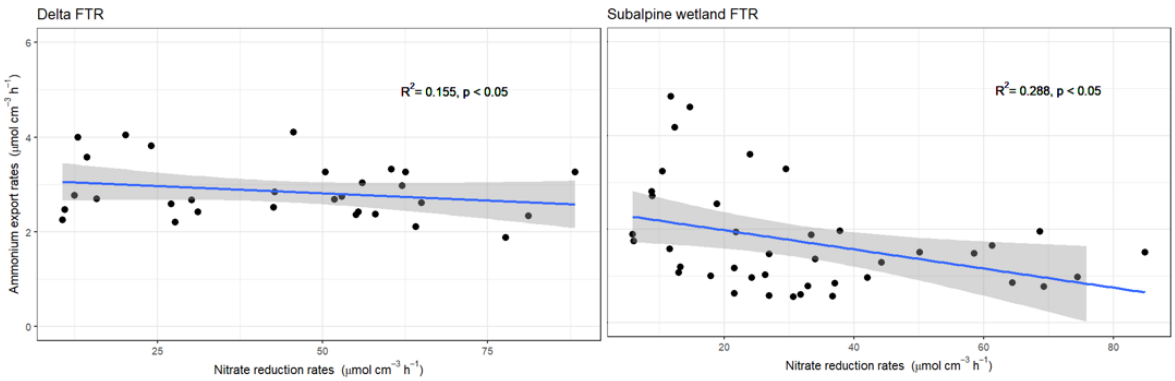

Figure 52. Regression plots between ammonium export rates and nitrate reduction rates from both wetland geographies. Grey envelope represents 95% confidence intervals.

There were weak associations between ammonium export rates and nitrate reduction rates across both geographies (Figure 52). Comparatively, the regression coefficient for the subalpine wetland soils was higher (R^2 = 0.288, p << 0.05) than for the Delta soils (R^2 = 0.155, p < 0.05).

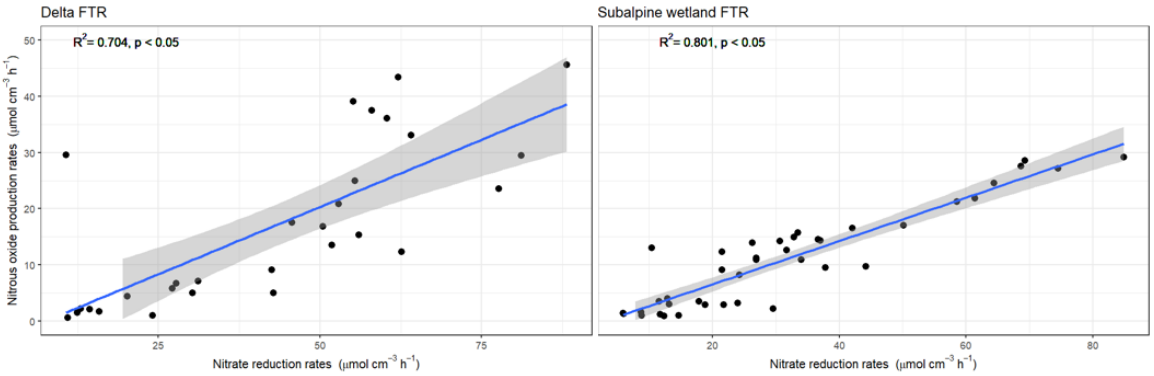

Figure 53. Regression plots between nitrous oxide production rates and nitrate reduction rates from both wetland geographies. Grey envelope represents 95% confidence intervals.

Conversely, nitrate reduction rates were found to be a strong predictor of nitrous oxide production rates across both geographies (Figure 53), with R^2 values of 0.704 and 0.801 for Delta and subalpine wetlands respectively (p << 0.05).

4. Discussion

4.1 Site characteristics and impact on nitrate reduction rates across geographies.

The maximum potential nitrate reduction rates, or R_{max} ,obtained in this study lie between 30-130 nmol $cm^{-3}h^{-1}$, which are on the lower-end of values reported in Laverman et. al[175] from coastal lakes and intertidal marshes ranging from 98-933 nmol $cm^{-3}h^{-1}$. However, the range of K_m, or affinity constants, obtained from our experiments (.6234 - 2.438 mM) across all sites and treatments were higher than values reported by Laverman et.al[175] (0.2-0.6 mM). This indicates that soils from our experiments had lower affinity for nitrate combined with lower nitrification rates compared to the other study. Given the highest affinity constants were observed for

burned topsoils in our study, this would indicate a lower selectivity due lack of abundance of microbial communities associated with burned topsoils despite the higher rates of nitrate reduction compared to deeper depths and freshwater soil incubations from Delta sites. This discrepancy could be explained by elevated nitrate concentrations in surface water for burned sites and high ash content in burned sediments derived from the burning of biomass, a proxy for the presence of pyrogenic carbon (pyC). Pyrogenic carbon has been known to increase redox potential in anoxic sediments, and act as an electron snorkel, speeding up anoxic reactions with the supply of extra electrons[77]. The higher affinity for nitrate in deep soils reflect the lower nitrate concentrations persisting at deeper wetland soil depths due to the biogeochemical redox ladder, where most of the nitrate is consumed in the top few centimeters of the soil profile[178]. This would also explain the similar lower affinity for nitrate in shallow unburned soils, where ambient nitrate concentrations, despite being lower than burned sites, were still higher than at depth.

In the Delta system, the highest nitrate reduction rates were observed for East End, the site with the highest abundance of mineral oxides and nitrate concentrations in surface water. Despite the competitive nature of nitrate and ferric iron reduction, it has been shown the presence of iron oxides enhanced nitrate reduction rates in experiments with fermentative bacterium *Bacillus sp*[179]*.* Presence of mineral oxides could also be correlated with higher abundance of reduced iron minerals such as iron sulfides and pyrites, especially given the reducing conditions, which are known to act as electron donors for nitrate reduction[180]. The high carbon content in East End and West Pond soils, and the proximity of those sites to agricultural fields that expose them to higher ambient nitrate concentrations could also stimulate nitrate reduction[148]. These would also induce lower affinities for nitrate reduction compared to higher salinity treatments. Notable among the three sites was Dutch Slough, site with the highest salinity in surface water, where rates weren't significantly lower for higher salinity treatment. A potential explanation for this could be the potential oxidation of hydrogen sulfide (H_2S) coupled to the reduction of nitrate[181,182] at this site, which was also found to possess the highest sulfate and ammonium concentrations in surface water samples. For freshwater sites, lower nitrate reduction rates could be explained by stress induced by higher osmotic pressure[183], resulting in diminished microbial activity.

4.2 Ammonium and nitrous oxide production rate dynamics across wetland sites

Given that subalpine wetlands considered for this study, and generally wetlands at high altitudes, have lower nitrogen (compared to sites from the Delta) due to limits on gross primary productivity[184,185], the response to increasing nitrate concentrations and shifts towards lower C_{org}/nitrate induced a significant decrease in DNRA[167]. Concomitant with this reduction in ammonium export rates, increases in nitrous oxide production rates were also observed,

presumably due to the increasing denitrification rates with increasing input nitrate concentrations[148]. It would appear that these wetlands shift towards denitrification from DNRA with increasing nitrate loading, also reflected in the fits for the regression plot.

Ammonium export rates exhibited no specific trends and tended to be variable for soils from the three Delta sites, whilst nitrous oxide production rates generally increased with increasing nitrate inputs. This could be explained by the greater heterogeneity in soil characteristics from the Delta compared to subalpine wetland soils, including variations in porewater chemistry which could confound some of the effects tested in the experiments. Delta soils. However, both rates were fairly comparable across freshwater (0 ppt) and oligohaline (3 ppt) incubations. This indicates little inhibition in response to increasing salinity, a trend that has been observed in other saline and hypersaline wetland systems as well[186,187], explained by the coupling of nitrate reduction to oxidation of native ferrous iron oxides and sulfides. Subalpine wetlands, on average, possessed higher ammonium export rates than Delta wetlands, which could be explained by higher clay content in Delta soils, leading to higher sorption and retention within the flow-through reactor sediments and less in the output.

4.3 Carbon dynamics in FTR experiments.

Carbon dioxide production rates were significantly higher for shallow soils compared to deep soils, which could be explained by differences in carbon contents of respective soils. This was also reflected in lower dissolved organic carbon production rates, which has also been observed in previous studies comparing shallow and deep soil incubations[59,63].

This implies that carbon dioxide and dissolved organic carbon evolved coupled to nitrate reduction, which is expected given high concentrations of nitrate supplied to the reactors in these experiments. There was no methane detected in the outflow throughout the course of the experiments with the exception of control incubations with no nitrate in the input solution.

4.4 Implications

These experiments answer critical questions about wetland resilience to nitrate loadings spanning two diverse geographies. Across both geographies, maximum nitrate reduction rates were observed for sediments with higher prior exposure to elevated nitrate concentrations, i.e. East End and burned wetland sections. This is a useful adaptation for microbial communities inhabiting wetland systems in a rapidly changing world with anthropogenic disturbances increasingly impacting water and sediment chemistry, such as fire and nitrate loading. Additionally, saline sites were shown to handle increased nitrate loading, with diminishment seen for freshwater sites. This is important information for stewards and agencies involved in drinking water quality for both systems.

Future experiments would complete the full mass balance of nitrogen by supply ^{15}N labeled nitrate solutions in tandem with acetylene and track the isotope ratios of all relevant gas and ionic species. Acetylene is known to inhibit the production of nitrogen from nitrous oxide[188], which would increase the nitrous oxide production rates from these experiments, which would allow us to better estimate nitrous oxide fluxes from these soil incubations. Additionally, it would also allow us to complete the mass balance of nitrogen entering these systems, and attribute it to various nitrate reduction pathways.

Chapter 4: Experiments in changing root exudate chemistry and the impact on greenhouse gas fluxes in the Delta

1. Introduction

Wetlands are critical carbon sinks that sequester carbon at higher rates than other ecosystems[151,189]. Carbon sequestration takes place primarily through the primary productivity of plants adapted to flooded sediments and anoxic environments, and as these plants grow, senesce, and die off, they directly contribute to organic matter being accreted in wetland soils through litterfall and root exudates[190–194]. Specifically, root exudates play an important role in regulating soil carbon dynamics and greenhouse gas emissions in wetland ecosystems[195,196]. The quantity and quality of root exudates can vary significantly depending on plant species, environmental conditions, and anthropogenic activities. Understanding how changes in root exudates impact carbon sequestration and GHG fluxes is important for predicting the response of these ecosystems to regime shifts, notably indicated by shifts in vegetation type, and broadly anthropogenic disturbances.[197,198]. Under environmental stressors like drought[199], and N/P limitation[200], root exudate profiles can shift, from high glucose to organic acid rich compounds to solubilize phosphate minerals for nutrition[201].

Few studies so far have investigated the impact of exudates in controlling CO_2 and CH_4 fluxes from wetland soils. Hoyos-Santillan et al.[202] showed that the quality, rather than quantity, of organic matter derived from root exudates was a key driver of CO_2 and CH_4 production in neotropical peat profiles. They linked higher GHG production to the presence of long chain fatty acids and lignin compounds in surface peat layers, originating from fresh root inputs, in comparison to more decomposed organic matter at depth. Girkin et al.[196] showed that the quality of root exudate analogues, specifically the ratio of carbohydrates and sugars to organic acids, impacted CO_2 and CH_4 fluxes in tropical peat soils. Labile carbon inputs in the form of root exudates stimulated microbial activity and methanogenesis, with the magnitude and duration of the response dependent on the chemical composition of the exudates. Additionally, changes in vegetation composition due to natural succession, land use change, or climate change, what is also referred to as a "regime shift"[203], can change the quantity and quality of root exudates entering wetland soils, which subsequently affects carbon storage and GHG emissions. Waldo et al.[204] found that the presence of certain wetland sedges increased CH_4 emissions not only by providing a direct conduit for gas transport through aerenchyma, but also by releasing root exudates that stimulated both CH_4 production and the decomposition of native soil organic matter through microbial priming. The priming effect was mediated by changes in soil redox conditions and competition for oxygen between heterotrophs and

methanotrophs in the rhizosphere. Akhtar et al.[205] showed that in a fire-degraded tropical peatland, the addition of labile carbon mimicking root exudates from ferns and sedges significantly enhanced both carbon dioxide and methane production, with the response modulated by soil moisture and oxygen availability associated with different microtopographic positions. Furthermore, the temperature sensitivity of CH_4 production was higher under anoxic conditions, highlighting the potential for enhanced emissions under future climate warming scenarios. Priming is still a contentious issue, with a host of native sediment and environmental factors shaping the response to inputs of labile C[31,206], however the impact of additional C inputs, especially ones that can act as substrates for reactions implicated in GHG production is an important one to quantify and add to the burgeoning scientific literature on priming.

It has been observed, especially on a global scale, that changes in root exudates under rising atmospheric CO_2 concentrations and warmer temperature could substantially increase soil organic carbon sequestration in natural ecosystems like forests and grasslands[207,208]. This makes it even more important to study the impacts of exudate quality on wetland ecosystems, given their exceptional carbon density and sequestration abilities. Panchal et al.[207] have suggested that the recalcitrant components of root exudates can be stabilized in soil through various physical and chemical protection mechanisms, contributing to long-term carbon storage. However, realizing this potential requires preserving and restoring these ecosystems, in addition to extensive experimental and modeling based studies that will give us a better understanding of long-term trends, not just in terrestrial ecosystems with oxic soils, but anoxic sediments in wetlands as well.

Here, we wanted to assess how wetland soils from sites with different salinity in the Sacramento-San Joaquin Delta would respond in terms of greenhouse gas and dissolved organic carbon fluxes to different root exudate compounds. For that purpose, we used slurry experiments with top soils from three sites to test the effects of three different model root exudate constituents; glucose, lysine, and ascorbic acid, on the concentrations of greenhouse gases, dissolved ions and organic carbon as a function of time. Glucose was found to prime mineralization and increase emissions of carbon dioxide and methane, whereas lysine was found to increase nitrous oxide emissions by providing an extra source of nitrogen, especially for sites deficient in organic nitrogen.

2. Methods

2.1 Study sites.

Our study focused on three sites in the Sacramento-San Joaquin Delta that are located within a narrow geographic zone (Figure 17) and constitute sites characterized by different salinities. The sites on Twitchell Island (West Pond and East End) are non-tidal and therefore have a low salinity (0.19 and 0.22 ppt respectively), whereas Dutch Slough is tidally connected and has a

higher salinity (0.48 ppt). All three sites have similar mean annual precipitation (338 mm) and air temperature (around 16^{o}C). West Pond and East End have been extensively studied in the past for their carbon fluxes on larger spatial scales[97,136], with eddy covariance (EC) towers established in 2012 and 2014 respectively, whereas Dutch Slough is a relatively new site with its EC tower established in 2021[137]. The dominant vegetation across the sites is cattail and tule grasses, as they were brought in to stabilize berms from persistent wind and water-mediated soil erosion.

Soils on Twitchell Island feature a complex patchwork of alluvium Mollisols adjacent to peat Histosols which were separated from main river channels, which accumulated organic matter over the last hundred or so years[138]. The East End site was established on alluvium soils whereas West Pond was established on peat-rich Histosols. The three sites were sampled in June 2022. Triplicate topsoil cores were taken to a depth of 5 cm of mineral soil at each site within the flux footprint of the EC tower and immediately transferred to a cooler with ice to prevent biogeochemical changes. Shallow depths were sampled as soil cores contained peat-like organic matter at the top which was discarded, and we were more interested in incubating mineral soils underneath that contain higher concentrations of native electron acceptors known to influence greenhouse gas production. Grab water samples were taken in triplicate at each location and instantly acidified with 2% HNO_3 to prevent oxidation of redox-relevant dissolved ions.

Figure 18: Location of the three study sites. US-Tw1 corresponds to West Pond, US-Tw4 corresponds to East End, and US-Dmg corresponds to Dutch Slough.

2.2 Sediment and surface water characterization

Water samples were acidified with dilute (2% w/v) HNO_3 to preserve chemical speciation of dissolved Fe and N cations/anions. Relevant extractable anions and cations were measured using a Dionex ion chromatograph (IC) (electrochemical detector, ED40; analytical column, AS23/AG23; anion self-regenerating suppressor, ASRS-I, 4 mm; mean detection limit: 30 µg/L, error: 5 µg/L) supplied with a carbonate eluant (7.2 mM Na_2CO_3 and 1.28 mM $NaHCO_3$) at a flow rate of 1.0 mL min^{-1}.

Our study focused on mineral soil, which was collected and analyzed after discarding the O horizon, which overlaid soils from all three sites. Soil dry bulk density was determined by drying a known volume of soil for 24 hours at 105°C. Soil pH was measured in a soil slurry after suspending 5g of soil in a 10 mM $CaCl_2$ solution[52]. Total % organic carbon and nitrogen was measured by combusting 30 mg of dried soil using a NC 2100 Elemental Analyzer (CE Instruments, USA). Oxalate-extractable Fe, used as a proxy for poorly-ordered oxides more likely to participate in redox reactions, was determined using Schwertmann's protocol[54].

2.3 Slurry experiments

In order to test the effect of specific root exudates on greenhouse gas emission in wetland soils, we conducted a series of slurry experiments under simplified conditions by testing the effect of three individual soil exudates. Glucose, ascorbic acid, and lysine, all constituents of a root exudate profile, were selected because they are common root exudates with similar molecular weights (180.156 g/mol, 176.12 g/mol, 146.19 g/mol) but different function groups. They also span different oxidation states for C in these compounds, an indicator of how "reduced" the compound has. Lysine is the only exudated tested with a nitrogen group in its chemical constituents.

Anoxic slurry experiments were conducted in 125 mL serum bottles, using a 1:4 (w/w) wet soil: deionized water mixture. Soils from the 0-5 cm depth interval were homogenized prior to the preparing the slurries. The slurries were incubated under gentle orbital shaking to maintain the soil in suspension, and experiments lasted 7 days with temperature maintained at 25°C. Prior to the incubation, the serum bottles were evacuated, and the deionized water was flushed with N_2 to remove most O_2 from both systems. Slurries were sampled for water and gas samples with higher frequency for the first six hours, and subsequently daily lasting 7 days, for water and gas samples. This was done to capture the gas fluxes from the initial kinetic phase of reactions implicated in greenhouse gas production, especially N_2O, known to be driven by 'hot spots and hot moments' in the soil continuum[139]. An equal amount of N_2 was injected into the bottles to maintain vapour pressure during gas sampling.

Following the protocol of Chari and Smith[194], soil samples were slowly injected with 1 mL of each exudate into serum bottles containing sediments from each site, in duplicate, once a day over 7 days. Injection rates and concentrations of all three exudates were kept constant at 0.05 gC d^{-1}, or 55.56 µmolC d^{-1} , based and higher than carbon concentrations used in other exudate manipulation experiments[194,209,210]. Given the dearth of exudate estimates from wetland plants such as cattail and tule and higher GPP estimates compared to ecosystems in the study listed[211], a greater value was chosen. Control experiments featured no injection of model compounds.

Liquid samples were filtered through a 0.22 µm PTFE membrane syringe filter (Whatman; 25 mm filter size) prior to chemical analyses. Liquid samples were analysed as described in Section 2.2. Gas samples were analysed on an Agilent 7890B GC (Agilent, Santa Clara, CA) for CO_2, CH_4, and N_2O using thermal conductivity, flame ionization, and nitrogen chemiluminescence detectors (TCD, FID, and NCD) respectively. Concentrations of CO_2, CH_4, and N_2O were then used to calculate potential CO_2, CH_4, and N_2O fluxes according to:

$$F = \frac{V}{A*m} * \frac{\Delta C}{\Delta T} \quad (1)$$

Where *F* is the gas flux (µmol [CO_2 or CH_4] g $soil^{-1}$ m^{-2} s^{-1}), V is the volume of the slurry, Δ*C* is the gas concentration difference between consecutive time points (mol m^{-3} [CO_2, CH_4, and N_2O]), *m* is the mass of dry soil, and Δ*t* is the time increment. Values were converted from ppm to mol m^{-3} using the ideal gas equation.

Two potential fluxes of CO_2, CH_4 and N_2O production were calculated from the initial linear increases (0-24 hr) in CO_2, CH_4, and N_2O concentration, respectively and final stable values (> 96 hr)

2.3 Statistical analyses

All statistical analyses were carried out in R[69]. Differences between all measured water, sediment, and gas variables were determined using a t-test with a threshold of p <= 0.05. Tukey's honest significance difference test was used to determine which sites, if found significant (α = 0.05), were different. Pearson's correlation coefficients were calculated between measured water, sediment, and gas variables and visualized using the 'corrplot' function in R[70]. Multivariate analyses were performed to evaluate differences in water, sediment, and gas concentrations. Given these concentrations vary by orders of magnitude, it was desirable to relativize them by column totals through the 'decostand' function using the 'vegan' package[71]. These were then visualized using Principal Components Analysis (PCA) ordinations. PCA was performed in R using the 'prcomp' function which is a part of the 'stats' package[29].

3. Results

3.1 Soil characteristics

Table 10. Physical and chemical characteristics of surface soils (depth interval 0-5 cm) and surface waters from the three study sites. Values are reported as means from triplicate samples. Different letters denote significance at p <= 0.1. Standard errors were found to not exceed >30% of measured values.

Site characteristics	Dutch Slough	East End	West Pond
Soil (0-5 cm)			
Sand	79.6±13.5[a]	55.2±11.2[b]	59.3±7.75[b]
Silt	10.1±2.3[a]	33.2±6.7[b]	21.2±3.4[c]
Clay	11.1±3.1[a]	12.4±2.6[a]	20.1±4.7[b]
Textural class	Loamy sand	Loam	Sandy clay loam
Dry bulk density	1.22±.29[a]	1.07±.18[b]	1.16±.25[a]
pH	7.57±.36[a]	5.96±.44[b]	6.49±.29[c]
C_{org} content (%)	7.89±1.19[a]	15.32±3.65[b]	18.95±2.77[c]
Total N content (%)	0.47±.06[a]	0.91±.14[b]	0.93±.22[b]
Molar C_{org}:N ratio	17.54±1.15[a]	16.38±3.11[a]	19.17±2.79[a]
Extractable Fe content (mg g of $soil^{-1}$)	2.17±.33[a]	11.89±2.96[b]	8.16±1.47[c]
Extractable Mn content (mg g of $soil^{-1}$)	0.12±.03[a]	0.78±.17[b]	0.31±0.06[c]
Extractable Al content (mg g of $soil^{-1}$)	1.41±.23[a]	5.59±1.14[b]	3.27±0.55[c]
Extractable Ca content (mg g of $soil^{-1}$)	44.32±10.71[a]	121.42±20.39[b]	78.13±15.52[c]
Surface water			
Salinity (ppt)	0.48±.06	0.22±.03	0.19±.02
NH_4^+ concentrations (ppm)	1.67±.44[a]	1.19±.16[b]	2.12±.079[c]
NO_3^- concentrations (ppm)	0.27±.03[a]	0.86±.17[b]	0.13±.03[c]
Cl^- concentrations (ppm)	267.81±15.39[a]	122.31±15.32[b]	110.57±20.91[b]
SO_4^{-2} concentrations (ppm)	20.87±4.11[a]	0.78±.11[b]	0.56±.09[c]

Dutch Slough was characterized by soils that had significantly lower C_{org} and N contents ($p = 0.008, 0.01$), as well as significantly lower contents of extractable Fe, Mn, Al and Ca and a higher pH (7.9 versus <6.5 for the other two sites). Both SO_4^{2-} and Cl^- concentrations in surface water were statistically significantly higher in Dutch Slough than in the other sites, by factors of 27-37 and 2.1-2.4, respectively. East End soils had significantly higher contents of Fe, Mn, Al and Ca than those of West Pond, but lower C_{org} and N content and a more acidic pH. Its surface water was characterized by slightly higher NO_3^-, Cl^- and SO_4^{2-} concentrations than the one of West End. All of the sites had similar C_{org}/N ratios. The surface water concentrations make the freshwater/salinity gradient clear, with Dutch Slough having the highest chloride and sulfate concentrations (267.81 and 20.87 ppm) ($p <<< 0.05$), followed by East End and West Pond. The sulfate concentrations were found to be greater by an order of magnitude; 20.87 ppm compared to <1 ppm for the other two sites.

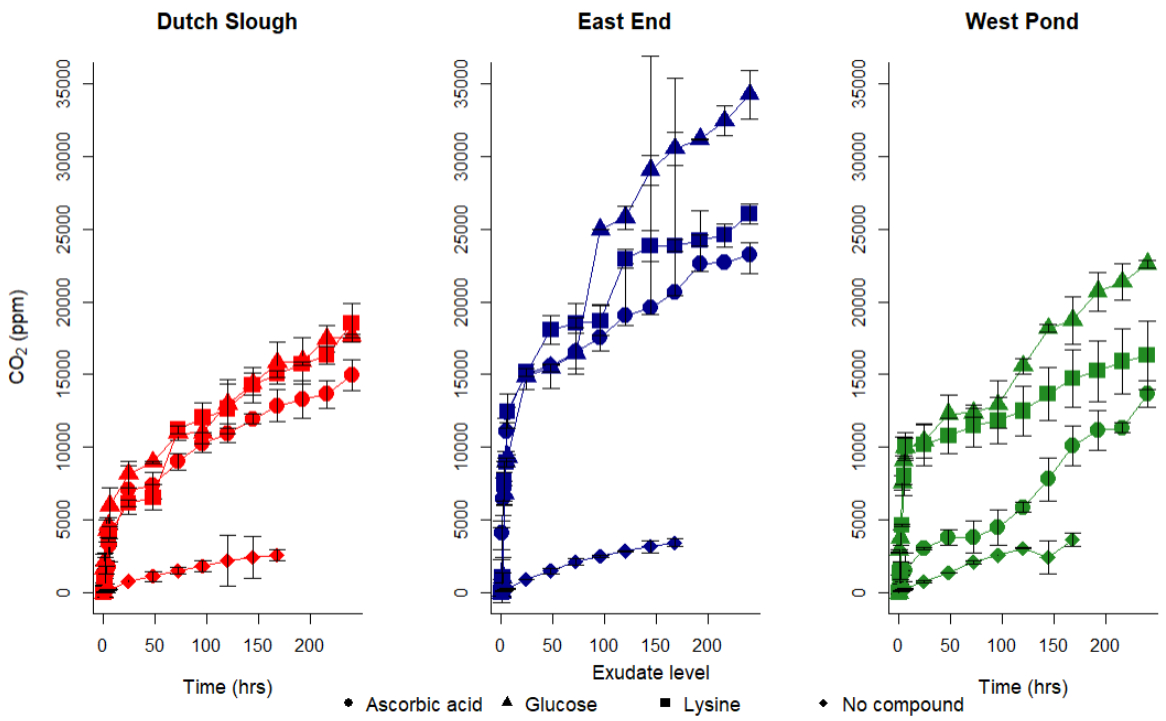

Figure 55. Effect of the addition of three model exudate compounds, ascorbic acid (circles), glucose (triangles), and lysine (squares) on CO_2 concentrations produced over time in slurry experiments with topsoil (0-5 cm) from the three Delta study sites. Error bars represent standard deviations for each time point found not to exceed >40% of measured value for individual time points.

3.2 Greenhouse gas concentrations and fluxes in response to exudate additions.

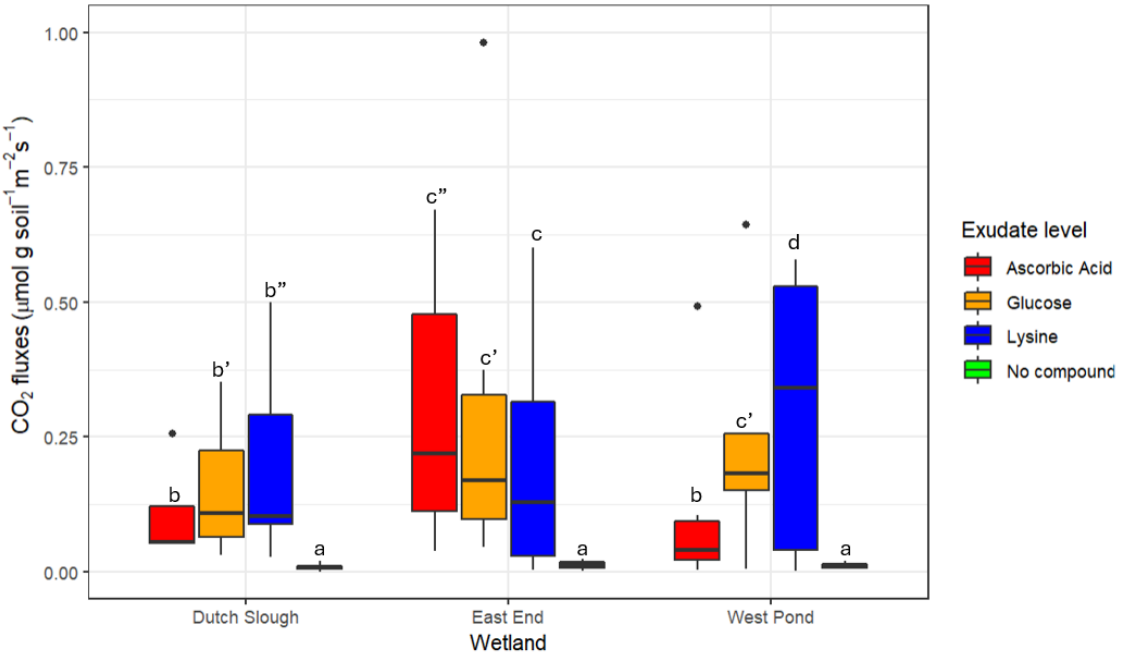

Figure 56. Average CO_2 fluxes calculated for the initial rapid evolution phase of the slurry experiments (1-24 hours) in response to addition of ascorbic acid (red), glucose (orange), lysine (blue), and for control experiments without addition (green). Different letters indicate significant differences at p<= 0.05. Letter' represents differences at significance level p <=0.1. Error bars represent standard deviations found not to exceed >30% of measured mean CO_2 fluxes.

Figure 55 shows the time evolution of CO_2 concentrations in response to the addition of model exudates for the three study sites. On average, East End produced 23.8% more carbon dioxide compared to Dutch Slough and West Pond sediments ($p << 0.05$). For the three study sites, the addition of the model exudates led to CO_2 concentrations that were 1-2 orders of magnitude higher than in the control experiments. There was also a steeper initial increase in concentrations, followed by stabilization at the final time points of the experiments. Across the three different exudates tested, glucose additions led to significantly higher cumulative carbon dioxide concentrations than lysine, ascorbic acid, and control treatments ($p << 0.05$). This trend was especially more pronounced for East End soils, but also for West Pond soils($p < 0.05$). Given constant additions of exudates to these slurry experiments, CO_2 concentrations did not stabilize 218 hours after the beginning of the experiments.

Figure 56 shows the initial average CO_2 fluxes calculated from the 1-24h data points from Figure 55. On average, East End and West Pond soils produced higher initial fluxes compared to Dutch Slough ($p << 0.05$) but were not significantly different from each other. The addition of the model exudates led to much higher initial average CO_2 fluxes than in the control experiments. The initial average CO_2 fluxes were found to be significantly different for site plus exudate

addition combination. For Dutch Slough and West Pond soils, lysine addition led to the highest initial fluxes (p = 0.077, 0.028) compared to glucose and ascorbic acid additions. For the East End soils, ascorbic acid additions led to the highest initial fluxes (p = 0.058) compared to glucose and lysine additions. On average, significantly higher cumulative fluxes were observed for glucose additions, compared to lysine and ascorbic acid additions (p = 0.067). No differences were observed between carbon dioxide fluxes from East End and West Pond soils, both of which were significantly higher than Dutch Slough soils (p = 0.019).

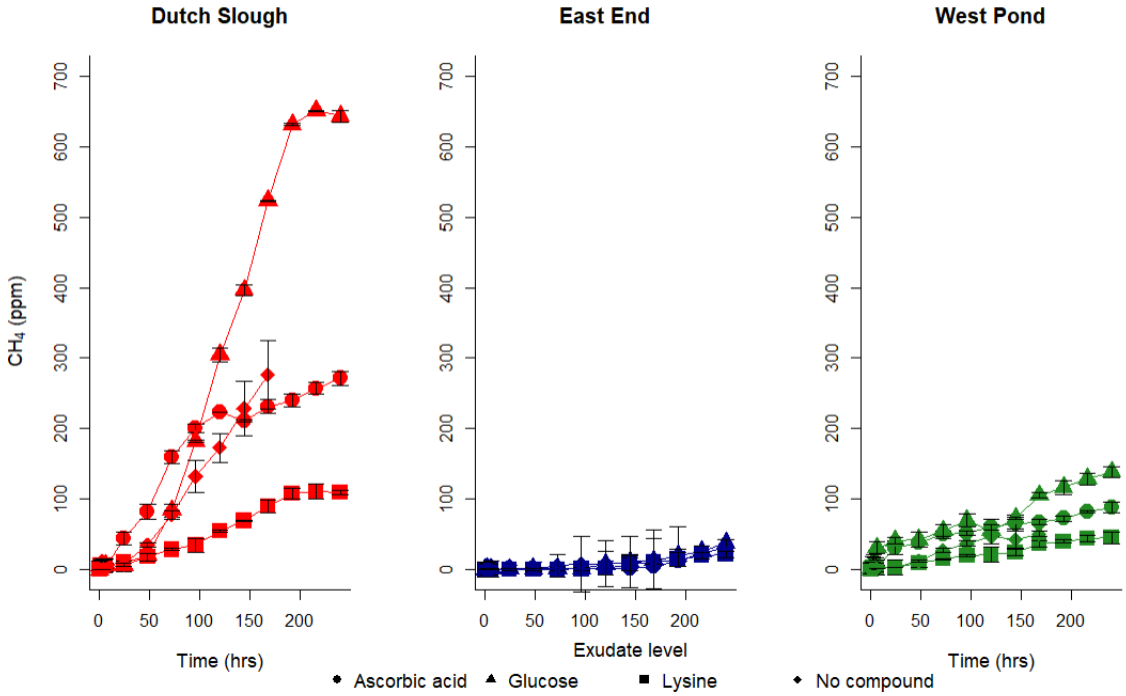

Figure 57. Effect of the addition of three model exudate compounds, ascorbic acid (circles), glucose (triangles), and lysine (squares) on CH_4 concentrations produced over time in slurry experiments with top soil (0-5 cm) from the three Delta study sites. Error bars represent standard deviations for each time point found not to exceed >40% of measured value for individual time points.

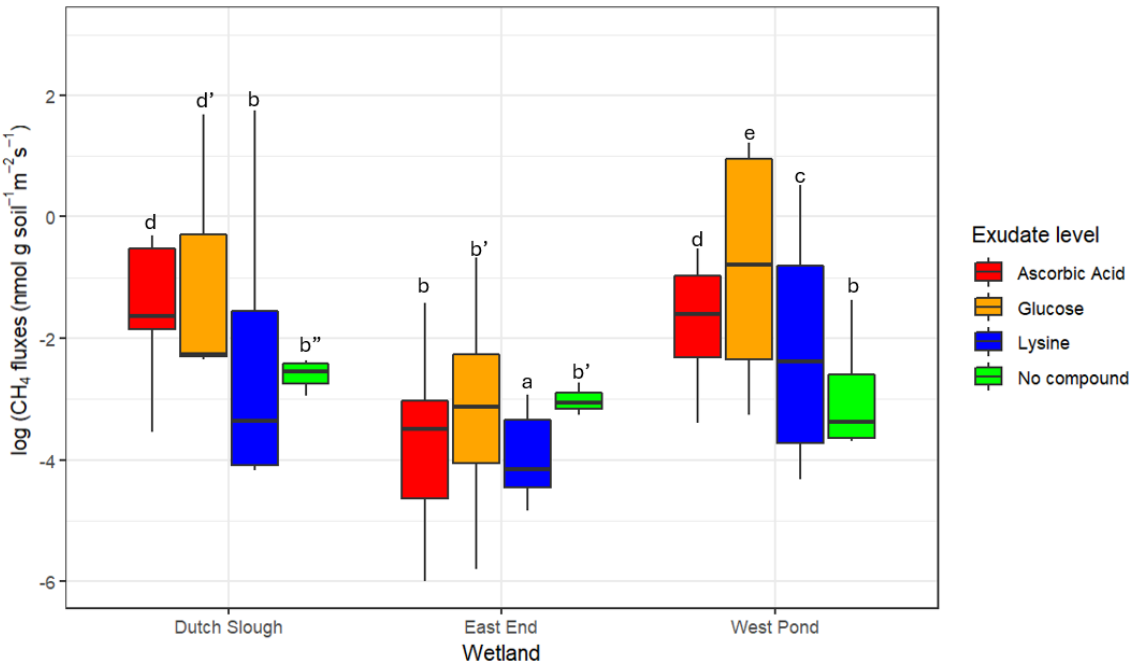

Figure 58. Average log transformed CH_4 fluxes calculated for the initial rapid evolution phase of the slurry experiments (1-24 hours) in response to addition of ascorbic acid (red), glucose (orange), lysine (blue), and for control experiments without addition (green). Different letters indicate significant differences at p<= 0.05. Letter' represents differences at significance level p <=0.1. Log transformations were made for visualization of responses on the same axes.

Figure 57 shows the time evolution of CH_4 concentrations in response to the addition of model exudates for the three study sites. Dutch Slough was characterized by the highest CH_4 concentrations compared to the other sites, both for control experiments ($p <<< 0.05$) and in response to the three model exudates, with concentrations significantly higher by two orders of magnitude. East End was characterized by very limited production of CH_4 for all time points and conditions tested. CH_4 concentrations did stabilize with time across the three wetland sites and exudate additions, contrary to what was observed with carbon dioxide concentrations (Figure 55). Methane concentrations varied significantly across treatments and sites. Glucose additions were found to increase CH_4 concentrations significantly in Dutch Slough and West Pond soils ($p << 0.05$). Lysine additions were found to significantly lower CH_4 concentrations in comparison to control treatments for Dutch Slough and West Pond soils. Methane concentrations were also consistently higher for glucose additions, on average, followed by lysine and ascorbic acid additions.

Figure 58 shows the log transformed initial average CH_4 fluxes calculated from the 1-24h data points from Figure 57. Dutch Slough soils produced the highest fluxes across different treatments, on average ($p << 0.05$). This was followed by West Pond soils which produced significantly higher fluxes than East End soils ($p << 0.05$). Across the three sites, glucose additions were found to elicit the highest response in CH_4 fluxes compared to the other

treatments (p = 0.013). For Dutch Slough and West Pond soils, ascorbic acid had significantly higher CH_4 fluxes compared to lysine and control. Curiously, control treatments were found to emit higher CH_4 fluxes for East End soils compared to ascorbic acid and lysine (p = 0.025). On average, lysine additions were shown to produce the lowest CH_4 fluxes across the three sites, however there were significant differences in fluxes across site for this exudate compound addition (p = 0.017).

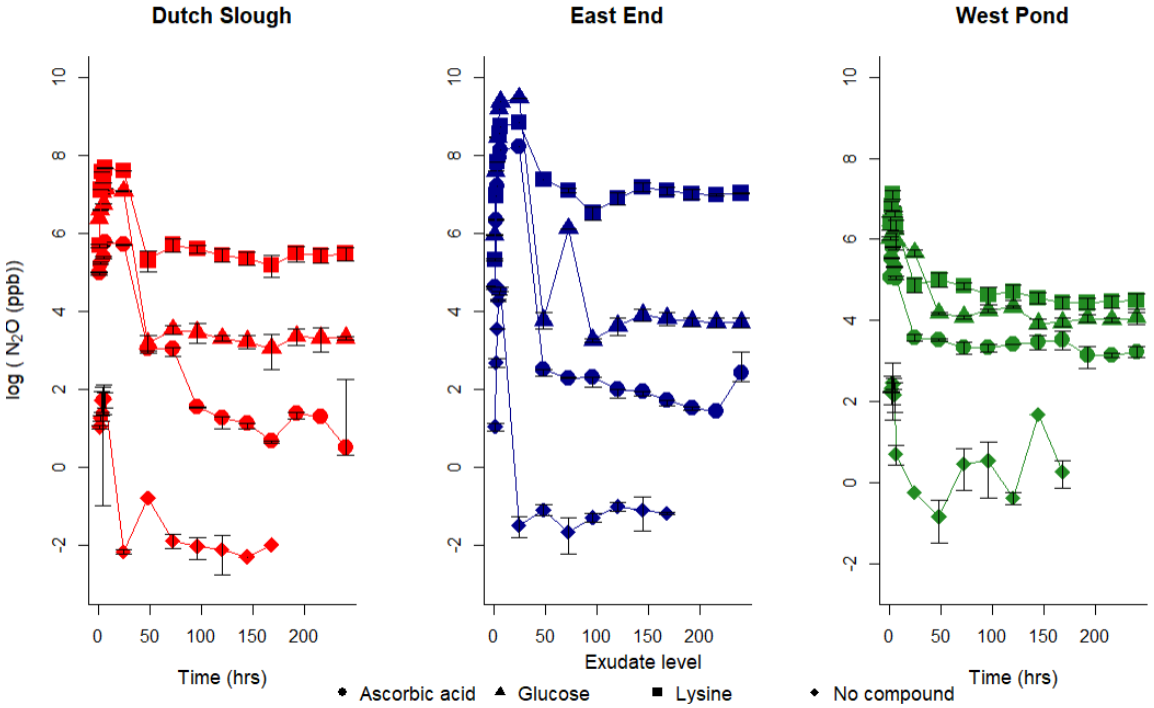

Figure 59. Effect of the addition of three model exudate compounds, ascorbic acid (circles), glucose (triangles), and lysine (squares) on log transformed N_2O concentrations produced over time in slurry experiments with topsoil (0-5 cm) from the three Delta study sites. Error bars represent standard deviations for each time point found not to exceed >40% of measured value for individual time points. Log transformations were made for visualization of responses on the same axes.

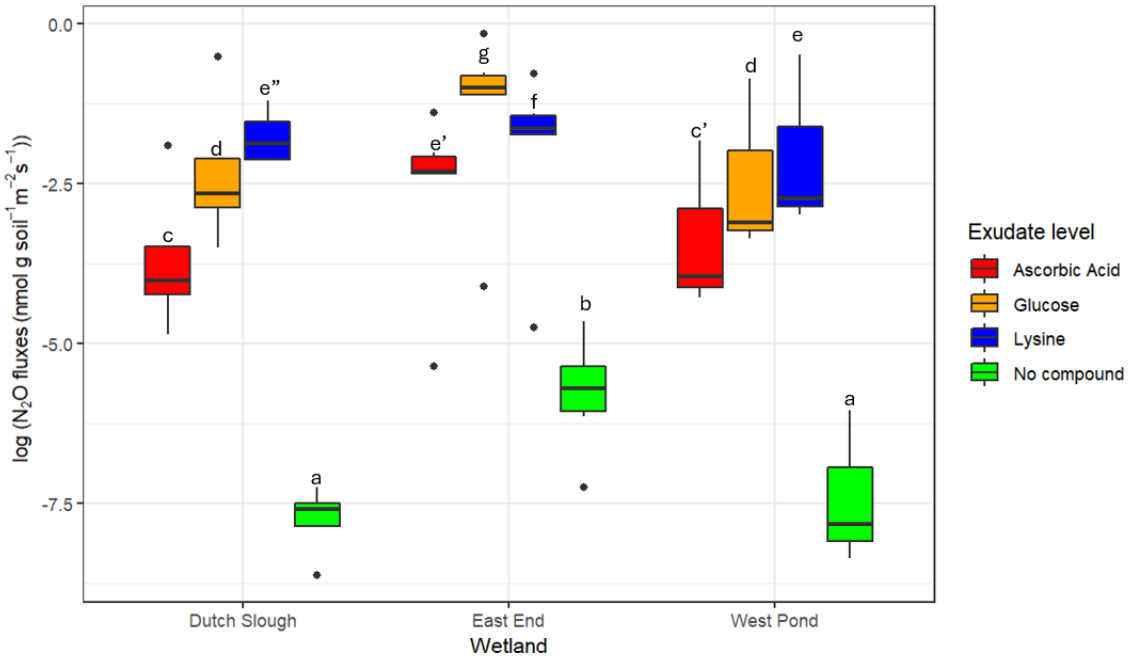

Figure 60. Average log transformed N_2O fluxes calculated for the initial rapid evolution phase of the slurry experiments (1-24 hours) in response to addition of ascorbic acid (red), glucose (orange), lysine (blue), and for control experiments without addition (green). Different letters indicate significant differences at p<= 0.05. Letter' represents differences at significance level p <=0.1. Log transformations were made for visualization of responses on the same axes.

Figure 59 shows the time evolution of log transformed N_2O concentrations in response to the addition of model exudates for the three study sites. Highest concentrations were observed for East End soils, with no differences between concentrations from Dutch Slough and West Pond soils. For the three study sites, the addition of the model exudates led to N_2O concentrations that were 1-2 orders of magnitude higher than in the control experiments. Nitrous oxide concentrations were shown to either stabilize or decrease by the end of the experiments, with consistent exudate additions adding more carbon to the system compared to nitrogen. Lysine additions were consistently found to produce highest cumulative concentrations across the sites, followed by glucose and ascorbic acid additions respectively ($p << 0.05$).

Log transformed initial nitrous oxide fluxes, displayed in Figure 60, highlighted different trends observed for concentration data. The strongest response was seen for lysine additions on East End soils, which produced the highest nitrous oxide concentrations compared to Dutch Slough and West Pond ($p << 0.05$). There were similarities between Dutch Slough and West Pond in terms of magnitude and temporal evolution of nitrous oxide fluxes from sediments. Across sites, East End soils produced the highest cumulative nitrous oxide concentrations ($p << 0.05$) compared to the other two sites.

Lysine additions stimulated nitrous oxide fluxes significantly from Dutch Slough and West Pond soils compared to the other two exudate additions ($p << 0.05$). However, highest fluxes

measured for glucose additions on East End soils compared to the other two treatments ($p < 0.05$). On average, initial fluxes were significantly higher for East End soils ($p << 0.05$), followed by less pronounced differences between West Pond and Dutch Slough soils ($p = 0.087$). Control treatments were significantly higher for East End soils ($p << 0.05$) compared to West Pond and Dutch Slough soils, who behaved statistically similarly.

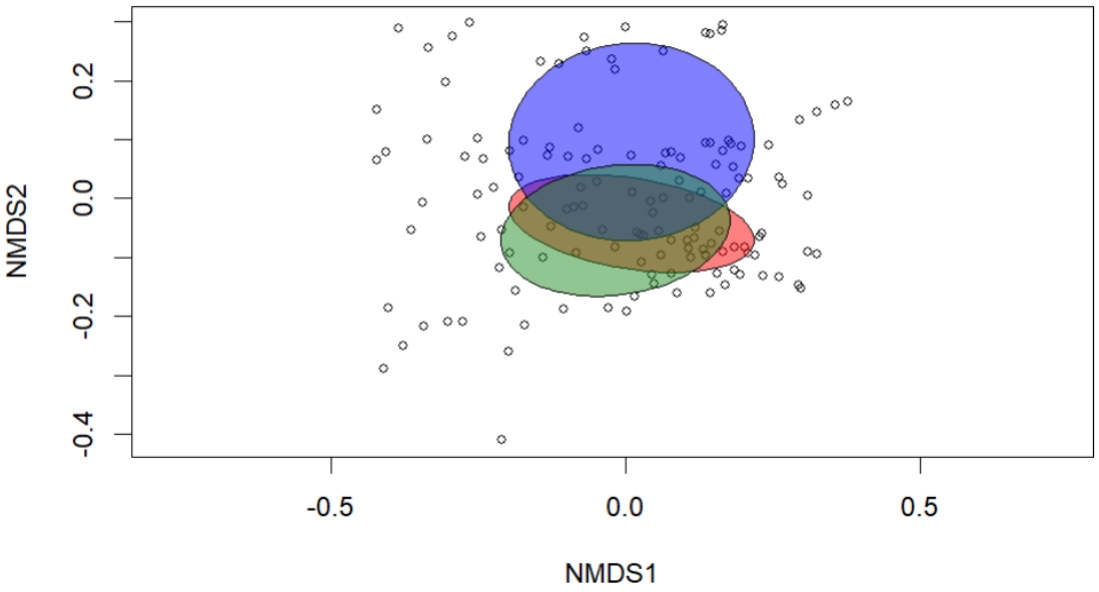

Figure 61. NMDS plot of all measured variables from the root exudate slurry experiments. Red, blue, and forest green ellipses represent measured variables from Dutch Slough, East End, and West Pond soils respectively.

With respect to the NMDS ordination displayed in Figure 61, there is almost complete overlap between Dutch Slough and West Pond wetland sites, with East End visibly distinguishing itself as most dissimilar from the either two sites, some overlap notwithstanding. In terms of response to an altering exudate regime, Dutch Slough and West Pond exhibited similar levels and trends in carbon dioxide, methane, nitrous oxide, dissolved organic carbon fluxes.

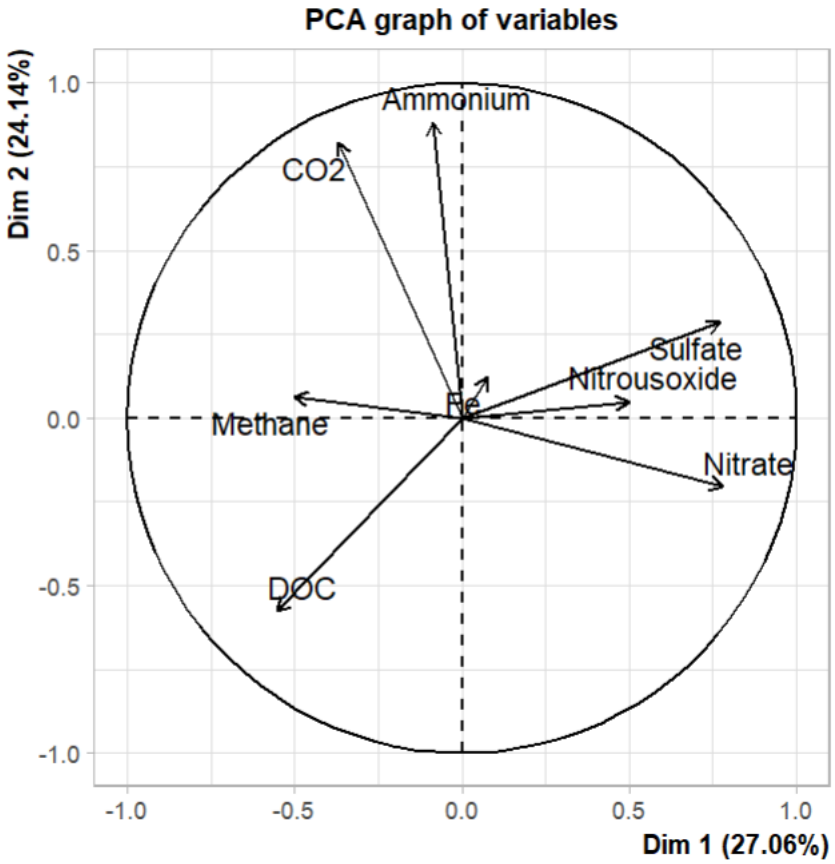

Figure 62. PCA plot of all measure variables from the exudate-addition experiments.

The PCA ordination plot, shown in Figure 62, reveals interesting associations between measured variables. Dissolved organic carbon was found to be not associated with carbon dioxide fluxes. Strong associations were found between methane, sulfate, nitrous oxide and nitrate concentrations from exudate amendment study.

4. Discussion

4.1 Site characteristics and influence on greenhouse gas fluxes.

Of the three sites, East End was characterized by the highest sediment nitrate, oxalate-extractable Fe(III) and Mn oxides contents, which are a proxy for poorly ordered mineral oxides more likely to participate in redox reactions, and the lowest C:N ratio. This indicates a higher potential to support alternative respiration pathways leading to the higher CO_2 fluxes we observed compared to Dutch Slough and West Pond. For Dutch Slough and West Pond, nitrogen was the limiting nutrient relative to carbon given their relatively high C:N ratios, therefore their response to glucose additions was muted in comparison to East End. This would explain why they responded more positively to additions of lysine, an amino acid, compared to

glucose. This highlights the "positive priming" effect of root exudates, which has now been suggested as the dominant effect in similar experiments by a recent meta-analysis[212].

A plausible explanation for lowest fluxes for East End this could be the presence of mineral oxides, which led to East End soils with the highest oxalate extractable iron and manganese oxides exhibiting the lowest methane concentrations. On the other hand, Dutch Slough soils, with the least quantity of mineral oxides among the three sites, specifically iron and manganese oxides known to participate in redox reactions, produced the most methane. This could be due to methanogens utilizing substrates produced by halophilic and sulfate-reducing bacteria in soils from Dutch Slough, which also happened to be the most saline site[152]. Presence of redox-relevant mineral oxides has been known to inhibit methane production in coastal and freshwater wetlands as it is thermodynamically favourable[213]. In addition, lower fluxes could be explained by these minerals oxidizing methane produced to carbon dioxide, referred to as the anaerobic oxidation of methane.[214–216]

The extent of nitrous oxide production was most pronounced for East End sediments compared to the other two sites. This response was observed across the three sites, indicating higher denitrification rates. East End had the lowest ammonium concentrations across the three sites and these were also found to be negatively correlated with nitrate concentrations, with higher nitrate concentrations preferring denitrification whereas ammonium was produced mostly at lower concentrations. Given that East End had lower C_{org}/N ratios and higher nitrate in surface water compared to West Pond and Dutch Slough, this could explain the differences in nitrous oxide production, with denitrification being the dominant pathway at East End, dissimilatory nitrate reduction to ammonium dominating at the other two sites[155,167]. A similar spike pattern was observed for nitrous oxide production across all three sites and exudate treatments. This is presumably due to the fact nitrous oxide is seldom continuously produced and relies on hot-spots and hot-moments of microbial activity in the environment[139].

In terms of overall site response to exudate additions, East End behaved differently compared to the other sites, as evidenced by the NMDS ordination plot in Figure 61. This suggests that inherent soil properties might be the biggest predictors to our understanding of wetland response to an altering exudate regime. It has been established that given the presence of mineral oxides, root exudate compounds such as organic acids could be sorbed directly on to mineral surfaces instead of instantly priming native microbial populations[217] . Root exudates have also been known to be integral to soil organic matter formation and turnover rates, with amino acids increasing microbial biomass and glucose increasing the turnover rates of native sediment organic matter[194], and results from the East End site are consistent with this theory.

4.2 Influence of chemical composition of exudates on greenhouse gas fluxes and interaction with site properties.

For Dutch Slough and West Pond, the differences in CO_2 fluxes between experiments with glucose and lysine are presumably explained by the presence of nitrogen in lysine. Since these sites were nitrogen-limited in comparison to East End, the lysine additions could have been mineralized to inorganic nitrogen and utilized for alternative respiration strategies and increase in microbial biomass[218–220]. Ascorbic acid additions featured the lowest carbon dioxide concentrations and lower cumulative fluxes compared to the other two treatments across all sites. This could be explained by the reduction in pH leading to inhibition of microbial activity and mineralization of organic matter[221,222].

The positive effect we observed for glucose additions on CH_4 concentrations across the three sites is presumably due to decomposition/fermentation byproducts of glucose, such as ethanol and acetate, which are being readily utilized by methanogens in these anoxic systems[223,224]. Ascorbic acid has been known to react with oxygen in the presence of iron oxides to produce CH_4 in model systems[225], which could be a reason for the increase in CH_4 concentrations in wetland sediments. Compared to the other two treatments, CH_4 production was suppressed in the presence of lysine additions. This could be explained by the mineralization of lysine to nitrate, which would lead to lower CH_4 emissions due to thermodynamic favorability of nitrate reduction over organic matter fermentation[226].

Nitrous oxide concentrations and fluxes were found to be significantly elevated for lysine additions compared to the other model exudate constituents. However, due to persistent lysine additions in our experiments, we did see considerable fluxes of nitrous oxide throughout the course of the experiments across the three sites. Increases were observed for glucose and ascorbic acid amendments as well, but to a lower extent. This could be explained by the consistent inputs of carbon compounds that stimulate microbial activity and mining of native sediment inorganic nitrogen, which would primarily produce ammonium and carbon dioxide but also some quantities of nitrous oxide as well till all the nitrogen was exhausted. In fact, strong associations were observed between ammonium and carbon dioxide concentrations, as evident from the ordinations plot (Figure 50) .Glucose additions featured lower nitrous oxide fluxes, given that it further increases the C_{org}/N ratios, however there was a positive effect observed over treatments with no addition of model exudate compounds. This effect was also seen in experiments with grassland soils with glucose amendments and nitrous oxide measurements, where an initial pulse of nitrous oxide was succeeded by decline in nitrous oxide concentrations due to nitrate limitation[227]. Ascorbic acid amendments produced higher fluxes of nitrous oxide compared to control treatments. This could be explained by the promotion of denitrification at lower pH values[228] induced by ascorbic acid additions. However, evidence for this effect is still contentious[229], and fluxes were observed to be significantly lower than the other two amendments.

4.3 Implications

Across all experiments, differences in measured greenhouse gases were driven by a combination of site characteristics and chemical composition of the model compounds standing in for exudates used for this project. As root exudate compositions change with environmental stressors, greenhouse gas emissions and dissolved organic carbon fluxes will change dependent on substrate lability, with higher mineralization for sugar rich exudates, and effects on porewater and soil pH, which can alter microbial activity. Sites will also respond differently to these shifts dependent on their native soil properties, with East End behaving significantly differently from the other two sites in our study, as evident from the NMDS ordination.

Broadly, root exudates are a dynamic component of the carbon cycle in wetland soils, and their changing nature in response to various environmental drivers can have profound impacts on greenhouse gas emissions and soil carbon sequestration, as was observed in this study. As wetlands are among the largest natural sources of methane and store vast amounts of soil organic carbon, improving our mechanistic understanding of how root exudate dynamics influence these processes is essential for predicting ecosystem feedbacks to global change and informing climate mitigation strategies. Future research should focus on integrating field measurements, detailed characterization of exudate profiles across commonly found wetland plant species, controlled experiments, and modeling approaches to elucidate the complex interactions between plants, microbes, and soil biogeochemistry mediated by root exudates across diverse wetland ecosystems.

References

(1) *Why do we blame climate change on carbon dioxide, when water vapor is a much more common greenhouse gas? | MIT Climate Portal*. https://climate.mit.edu/ask-mit/why-do-we-blame-climate-change-carbon-dioxide-when-water-vapor-much-more-common-greenhouse (accessed 2024-04-19).

(2) Dynarski, K. A.; Bossio, D. A.; Scow, K. M. Dynamic Stability of Soil Carbon: Reassessing the "Permanence" of Soil Carbon Sequestration. *Front. Environ. Sci.* **2020**, *8*. https://doi.org/10.3389/fenvs.2020.514701.

(3) Archer, D.; Eby, M.; Brovkin, V.; Ridgwell, A.; Cao, L.; Mikolajewicz, U.; Caldeira, K.; Matsumoto, K.; Munhoven, G.; Montenegro, A.; Tokos, K. Atmospheric Lifetime of Fossil Fuel Carbon Dioxide. *Annual Review of Earth and Planetary Sciences* **2009**, *37* (Volume 37, 2009), 117–134. https://doi.org/10.1146/annurev.earth.031208.100206.

(4) Trumbore, S. E. Comparison of Carbon Dynamics in Tropical and Temperate Soils Using Radiocarbon Measurements. *Global Biogeochemical Cycles* **1993**, *7* (2), 275–290. https://doi.org/10.1029/93GB00468.

(5) Leifeld, J.; Keel, S. G. Quantifying Negative Radiative Forcing of Non-Permanent and Permanent Soil Carbon Sinks. *Geoderma* **2022**, *423*, 115971. https://doi.org/10.1016/j.geoderma.2022.115971.

(6) Matthews, H. D.; Zickfeld, K.; Dickau, M.; MacIsaac, A. J.; Mathesius, S.; Nzotungicimpaye, C.-M.; Luers, A. Temporary Nature-Based Carbon Removal Can Lower Peak Warming in a Well-below 2 °C Scenario. *Commun Earth Environ* **2022**, *3* (1), 1–8. https://doi.org/10.1038/s43247-022-00391-z.

(7) Kolka, R.; Trettin, C.; Windham-Myers, L. The Importance of Wetland Carbon Dynamics to Society. In *Wetland Carbon and Environmental Management*; American Geophysical Union (AGU), 2021; pp 421–436. https://doi.org/10.1002/9781119639305.ch24.

(8) Oldfield, E. E.; Bradford, M. A.; Wood, S. A. Global Meta-Analysis of the Relationship between Soil Organic Matter and Crop Yields. *SOIL* **2019**, *5* (1), 15–32. https://doi.org/10.5194/soil-5-15-2019.

(9) Oldfield, E. E.; Wood, S. A.; Bradford, M. A. Direct Evidence Using a Controlled Greenhouse Study for Threshold Effects of Soil Organic Matter on Crop Growth. *Ecological Applications* **2020**, *30* (4). https://doi.org/10.1002/eap.2073.

(10) Mitsch, W. J.; Bernal, B.; Nahlik, A. M.; Mander, Ü.; Zhang, L.; Anderson, C. J.; Jørgensen, S. E.; Brix, H. Wetlands, Carbon, and Climate Change. *Landscape Ecol* **2013**, *28* (4), 583–597. https://doi.org/10.1007/s10980-012-9758-8.

(11) Bridgham, S. D.; Megonigal, J. P.; Keller, J. K.; Bliss, N. B.; Trettin, C. The Carbon Balance of North American Wetlands. *Wetlands* **2006**, *26* (4), 889–916. https://doi.org/10.1672/0277-5212(2006)26[889:TCBONA]2.0.CO;2.

(12) Nahlik, A. M.; Fennessy, M. S. Carbon Storage in US Wetlands. *Nat Commun* **2016**, *7* (1), 13835. https://doi.org/10.1038/ncomms13835.

(13) *Global Wetland Outlook*. Global Wetland Outlook. https://www.global-wetland-outlook.ramsar.org (accessed 2024-04-19).

(14) Keller, J. K. Wetlands and the Global Carbon Cycle: What Might the Simulated Past Tell Us about the Future? *New Phytologist* **2011**, *192* (4), 789–792. https://doi.org/10.1111/j.1469-8137.2011.03954.x.
(15) *"Out of control" wildfires are ravaging Brazil's wildlife-rich Pantanal wetlands - CBS News*. https://www.cbsnews.com/news/brazil-wildfires-pantanal-wetlands-2023-animal-deaths/ (accessed 2024-04-19).
(16) Hansen, A. T.; Dolph, C. L.; Foufoula-Georgiou, E.; Finlay, J. C. Contribution of Wetlands to Nitrate Removal at the Watershed Scale. *Nature Geosci* **2018**, *11* (2), 127–132. https://doi.org/10.1038/s41561-017-0056-6.
(17) Herbert, E. R.; Boon, P.; Burgin, A. J.; Neubauer, S. C.; Franklin, R. B.; Ardón, M.; Hopfensperger, K. N.; Lamers, L. P. M.; Gell, P. A Global Perspective on Wetland Salinization: Ecological Consequences of a Growing Threat to Freshwater Wetlands. *Ecosphere* **2015**, *6* (10), art206. https://doi.org/10.1890/ES14-00534.1.
(18) Dacal, M.; Delgado-Baquerizo, M.; Barquero, J.; Berhe, A. A.; Gallardo, A.; Maestre, F. T.; García-Palacios, P. Temperature Increases Soil Respiration Across Ecosystem Types and Soil Development, But Soil Properties Determine the Magnitude of This Effect. *Ecosystems* **2021**, 1–15. https://doi.org/10.1007/s10021-021-00648-2.
(19) Pausas, J. G.; Keeley, J. E. Wildfires as an Ecosystem Service. *Frontiers in Ecology and the Environment* **2019**, *17* (5), 289–295. https://doi.org/10.1002/fee.2044.
(20) Bird, M. I.; Wynn, J. G.; Saiz, G.; Wurster, C. M.; McBeath, A. The Pyrogenic Carbon Cycle. *Annual Review of Earth and Planetary Sciences* **2015**, *43*, 273–298. https://doi.org/10.1146/annurev-earth-060614-105038.
(21) Cotrufo, M. F.; Boot, C.; Abiven, S.; Foster, E. J.; Haddix, M.; Reisser, M.; Wurster, C. M.; Bird, M. I.; Schmidt, M. W. I. Quantification of Pyrogenic Carbon in the Environment: An Integration of Analytical Approaches. *Organic Geochemistry* **2016**, *100*, 42–50. https://doi.org/10.1016/j.orggeochem.2016.07.007.
(22) Pingree, M. R. A.; DeLuca, T. H. Function of Wildfire-Deposited Pyrogenic Carbon in Terrestrial Ecosystems. *Frontiers in Environmental Science* **2017**, *5* (AUG), 53. https://doi.org/10.3389/FENVS.2017.00053.
(23) Reisser, M.; Purves, R. S.; Schmidt, M. W. I.; Abiven, S. Pyrogenic Carbon in Soils: A Literature-Based Inventory and a Global Estimation of Its Content in Soil Organic Carbon and Stocks. *Frontiers in Earth Science* **2016**, *4*, 80. https://doi.org/10.3389/FEART.2016.00080.
(24) Forbes, M. S.; Raison, R. J.; Skjemstad, J. O. Formation, Transformation and Transport of Black Carbon (Charcoal) in Terrestrial and Aquatic Ecosystems. *Science of The Total Environment* **2006**, *370* (1), 190–206. https://doi.org/10.1016/J.SCITOTENV.2006.06.007.
(25) Kuzyakov, Y.; Bogomolova, I.; Glaser, B. Biochar Stability in Soil: Decomposition during Eight Years and Transformation as Assessed by Compound-Specific 14C Analysis. *Soil Biology and Biochemistry* **2014**, *70*, 229–236. https://doi.org/10.1016/J.SOILBIO.2013.12.021.
(26) Lehmann, J.; Gaunt, J.; Rondon, M. Bio-Char Sequestration in Terrestrial Ecosystems - A Review. *Mitigation and Adaptation Strategies for Global Change* **2006**, *11* (2), 403–427. https://doi.org/10.1007/s11027-005-9006-5.

(27) Liang, B.; Lehmann, J.; Solomon, D.; Sohi, S.; Thies, J. E.; Skjemstad, J. O.; Luizão, F. J.; Engelhard, M. H.; Neves, E. G.; Wirick, S. Stability of Biomass-Derived Black Carbon in Soils. *Geochimica et Cosmochimica Acta* **2008**, *72* (24), 6069–6078. https://doi.org/10.1016/j.gca.2008.09.028.
(28) Lehmann, J.; Kleber, M. The Contentious Nature of Soil Organic Matter. *Nature* **2015**, *528* (7580), 60–68. https://doi.org/10.1038/nature16069.
(29) De la Rosa, J. M.; Miller, A. Z.; Knicker, H. Soil-Borne Fungi Challenge the Concept of Long-Term Biochemical Recalcitrance of Pyrochar. *Sci Rep* **2018**, *8* (1), 2896. https://doi.org/10.1038/s41598-018-21257-5.
(30) VanderRoest, J. P.; Fowler, J. A.; Rhoades, C. C.; Roth, H. K.; Broeckling, C. D.; Fegel, T. S.; McKenna, A. M.; Bechtold, E. K.; Boot, C. M.; Wilkins, M. J.; Borch, T. Fire Impacts on the Soil Metabolome and Organic Matter Biodegradability. *Environ. Sci. Technol.* **2024**, *58* (9), 4167–4180. https://doi.org/10.1021/acs.est.3c09797.
(31) Whitman, T.; Enders, A.; Lehmann, J. Pyrogenic Carbon Additions to Soil Counteract Positive Priming of Soil Carbon Mineralization by Plants. *Soil Biology and Biochemistry* **2014**, *73*, 33–41. https://doi.org/10.1016/j.soilbio.2014.02.009.
(32) Zimmerman, A. R.; Gao, B.; Ahn, M.-Y. Positive and Negative Carbon Mineralization Priming Effects among a Variety of Biochar-Amended Soils. *Soil Biology and Biochemistry* **2011**, *43* (6), 1169–1179. https://doi.org/10.1016/j.soilbio.2011.02.005.
(33) Liu, X.-J. A.; Finley, B. K.; Mau, R. L.; Schwartz, E.; Dijkstra, P.; Bowker, M. A.; Hungate, B. A. The Soil Priming Effect: Consistent across Ecosystems, Elusive Mechanisms. *Soil Biology and Biochemistry* **2020**, *140*, 107617. https://doi.org/10.1016/j.soilbio.2019.107617.
(34) Chen, L.; Liu, L.; Qin, S.; Yang, G.; Fang, K.; Zhu, B.; Kuzyakov, Y.; Chen, P.; Xu, Y.; Yang, Y. Regulation of Priming Effect by Soil Organic Matter Stability over a Broad Geographic Scale. *Nat Commun* **2019**, *10* (1), 5112. https://doi.org/10.1038/s41467-019-13119-z.
(35) Sun, T.; Levin, B. D. A.; Guzman, J. J. L.; Enders, A.; Muller, D. A.; Angenent, L. T.; Lehmann, J. Rapid Electron Transfer by the Carbon Matrix in Natural Pyrogenic Carbon. *Nature Communications 2017 8:1* **2017**, *8* (1), 1–12. https://doi.org/10.1038/ncomms14873.
(36) Minshall, G. W.; Brock, J. T.; Andrews, D. A.; Robinson, C. T. Water Quality, Substratum and Biotic Responses of Five Central Idaho (USA) Streams during the First Year Following the Mortar Creek Fire. *International Journal of Wildland Fire* **2001**, *10* (2), 185–199. https://doi.org/10.1071/WF01017.
(37) Schindler, D. W.; Curtis, P. J.; Bayley, S. E.; Parker, B. R.; Beaty, K. G.; Stainton, M. P. Climate-Induced Changes in the Dissolved Organic Carbon Budgets of Boreal Lakes. *Biogeochemistry 1997 36:1* **1997**, *36* (1), 9–28. https://doi.org/10.1023/A:1005792014547.
(38) Hohner, A. K.; Rhoades, C. C.; Wilkerson, P.; Rosario-Ortiz, F. L. Wildfires Alter Forest Watersheds and Threaten Drinking Water Quality. *Acc. Chem. Res.* **2019**, *52* (5), 1234–1244. https://doi.org/10.1021/acs.accounts.8b00670.
(39) Rhoades, C. C.; Chow, A. T.; Covino, T. P.; Fegel, T. S.; Pierson, D. N.; Rhea, A. E. The Legacy of a Severe Wildfire on Stream Nitrogen and Carbon in Headwater

Catchments. *Ecosystems 2018 22:3* **2018**, *22* (3), 643–657. https://doi.org/10.1007/S10021-018-0293-6.
(40) McEachern, P.; Prepas, E. E.; Gibson, J. J.; Dinsmore, W. P. Forest Fire Induced Impacts on Phosphorus, Nitrogen, and Chlorophyll a Concentrations in Boreal Subarctic Lakes of Northern Alberta. *https://doi.org/10.1139/f00-124* **2011**, *57* (S2), 73–81. https://doi.org/10.1139/F00-124.
(41) Wei, X.; Hayes, D. J.; Fernandez, I. Fire Reduces Riverine DOC Concentration Draining a Watershed and Alters Post-Fire DOC Recovery Patterns. *Environmental Research Letters* **2021**, *16* (2), 024022. https://doi.org/10.1088/1748-9326/ABD7AE.
(42) Leifeld, J.; Alewell, C.; Bader, C.; Krüger, J. P.; Mueller, C. W.; Sommer, M.; Steffens, M.; Szidat, S. Pyrogenic Carbon Contributes Substantially to Carbon Storage in Intact and Degraded Northern Peatlands. *Land Degradation & Development* **2018**, *29* (7), 2082–2091. https://doi.org/10.1002/LDR.2812.
(43) Shibata, H.; Petrone, K. C.; Hinzman, L. D.; Boone, R. D. Effect of Fire on Dissolved Organic Carbon and Inorganic Solutes in Spruce Forest in the Permafrost Region of Interior Alaska. *http://dx.doi.org/10.1080/00380768.2003.10409975* **2011**, *49* (1), 25–29. https://doi.org/10.1080/00380768.2003.10409975.
(44) Smith, H. G.; Sheridan, G. J.; Lane, P. N. J.; Nyman, P.; Haydon, S. *Wildfire effects on water quality in forest catchments: A review with implications for water supply*. Journal of Hydrology. https://doi.org/10.1016/j.jhydrol.2010.10.043.
(45) Mast, M. A.; Clow, D. W. Effects of 2003 Wildfires on Stream Chemistry in Glacier National Park, Montana. *Hydrological Processes* **2008**, *22* (26), 5013–5023. https://doi.org/10.1002/HYP.7121.
(46) Baldock, J. A.; Masiello, C. A.; Gélinas, Y.; Hedges, J. I. Cycling and Composition of Organic Matter in Terrestrial and Marine Ecosystems. *Marine Chemistry* **2004**, *92* (1–4), 39–64. https://doi.org/10.1016/J.MARCHEM.2004.06.016.
(47) Certini, G. Effects of Fire on Properties of Forest Soils: A Review. *Oecologia 2005 143:1* **2005**, *143* (1), 1–10. https://doi.org/10.1007/S00442-004-1788-8.
(48) Sulwiński, M.; Mętrak, M.; Wilk, M.; Suska-Malawska, M. Smouldering Fire in a Nutrient-Limited Wetland Ecosystem: Long-Lasting Changes in Water and Soil Chemistry Facilitate Shrub Expansion into a Drained Burned Fen. *Science of The Total Environment* **2020**, *746*, 141142. https://doi.org/10.1016/J.SCITOTENV.2020.141142.
(49) *Mullen Fire Information - InciWeb the Incident Information System*. https://inciweb.nwcg.gov/incident/7208/ (accessed 2021-07-14).
(50) Hesslein, R. H. An in Situ Sampler for Close Interval Pore Water Studies. *Limnology and Oceanography* **1976**, *21* (6), 912–914. https://doi.org/10.4319/lo.1976.21.6.0912.
(51) Mayer, L. M. Chemical Water Sampling in Lakes and Sediments with Dialysis Bags. *Limnology and Oceanography* **1976**, *21* (6), 909–912. https://doi.org/10.4319/lo.1976.21.6.0909.
(52) Thomas, G. W. Soil pH and Soil Acidity. In *Methods of Soil Analysis*; John Wiley & Sons, Ltd, 1996; pp 475–490. https://doi.org/10.2136/sssabookser5.3.c16.
(53) US EPA, O. *EPA Method 3050B: Acid Digestion of Sediments, Sludges, and Soils*. https://www.epa.gov/esam/epa-method-3050b-acid-digestion-sediments-sludges-and-soils (accessed 2024-05-04).

(54) SCHWERTMANN, U. Use of Oxalate for Fe Extraction From Soils. *Canadian Journal of Soil Science* **1973**, *53* (2), 244–246. https://doi.org/10.4141/cjss73-037.
(55) *Standard Test Methods for Determining the Water (Moisture) Content, Ash Content, and Organic Material of Peat and Other Organic Soils*. https://www.astm.org/d2974-20e01.html (accessed 2024-05-04).
(56) Burdige, D. J. The Effects of Sediment Slurrying on Microbial Processes, and the Role of Amino Acids as Substrates for Sulfate Reduction in Anoxic Marine Sediments. *Biogeochemistry* **1989**, *8* (1), 1–23.
(57) Hutchinson, G. L.; Livingston, G. P.; Healy, R. W.; Striegl, R. G. Chamber Measurement of Surface-Atmosphere Trace Gas Exchange: Numerical Evaluation of Dependence on Soil, Interfacial Layer, and Source/Sink Properties. *Journal of Geophysical Research: Atmospheres* **2000**, *105* (D7), 8865–8875. https://doi.org/10.1029/1999JD901204.
(58) Pallud, C.; Van Cappellen, P. Kinetics of Microbial Sulfate Reduction in Estuarine Sediments. *Geochimica et Cosmochimica Acta* **2006**, *70* (5), 1148–1162. https://doi.org/10.1016/J.GCA.2005.11.002.
(59) Schilling, K.; Borch, T.; Rhoades, C. C.; Pallud, C. E. Temperature Sensitivity of Microbial Fe(III) Reduction Kinetics in Subalpine Wetland Soils. *Biogeochemistry* **2019**. https://doi.org/10.1007/s10533-018-0520-4.
(60) US Department of Commerce, N. *National Weather Service*. https://forecast.weather.gov/MapClick.php?lat=41.89729401198026&lon=-106.20311737060547 (accessed 2024-04-15).
(61) Jepsen, S. M.; Harmon, T. C.; Sadro, S.; Reid, B.; Chandra, S. Water Residence Time (Age) and Flow Path Exert Synchronous Effects on Annual Characteristics of Dissolved Organic Carbon in Terrestrial Runoff. *Science of The Total Environment* **2019**, *656*, 1223–1237. https://doi.org/10.1016/j.scitotenv.2018.11.392.
(62) Daugherty, E. E.; McKee, G. A.; Bergstrom, R.; Burton, S.; Pallud, C.; Hubbard, R. M.; Kelly, E. F.; Rhoades, C. C.; Borch, T. Hydrogeomorphic Controls on Soil Carbon Composition in Two Classes of Subalpine Wetlands. *Biogeochemistry* **2019**, *145* (1), 161–175. https://doi.org/10.1007/s10533-019-00597-y.
(63) Pallud, C.; Rhoades, C. C.; Schneider, L.; Dwivedi, P.; Borch, T. Temperature-Induced Iron (III) Reduction Results in Decreased Dissolved Organic Carbon Export in Subalpine Wetland Soils, Colorado, USA. *Geochimica et Cosmochimica Acta* **2020**. https://doi.org/10.1016/j.gca.2020.03.023.
(64) Stookey, L. L. Ferrozine---a New Spectrophotometric Reagent for Iron. *Analytical Chemistry* **1970**, *42* (7), 779–781. https://doi.org/10.1021/ac60289a016.
(65) Richards, C. M.; Pallud, C. Kinetics of Sulfate Reduction and Sulfide Precipitation Rates in Sediments of a Bar-Built Estuary (Pescadero, California). *Water Research* **2016**, *94*, 86–102. https://doi.org/10.1016/j.watres.2016.01.044.
(66) Pallud, C.; Kausch, M.; Fendorf, S.; Meile, C. Spatial Patterns and Modeling of Reductive Ferrihydrite Transformation Observed in Artificial Soil Aggregates. *Environmental Science and Technology* **2010**, *44* (1), 74–79. https://doi.org/10.1021/es901736t.

(67) Daugherty, E. E.; Gilbert, B.; Nico, P. S.; Borch, T. Complexation and Redox Buffering of Iron(II) by Dissolved Organic Matter. *Environ. Sci. Technol.* **2017**, *51* (19), 11096–11104. https://doi.org/10.1021/acs.est.7b03152.
(68) Chen, M.; Ye, T.-R.; Krumholz, L. R.; Jiang, H.-L. Temperature and Cyanobacterial Bloom Biomass Influence Phosphorous Cycling in Eutrophic Lake Sediments. *PLOS ONE* **2014**, *9* (3), e93130. https://doi.org/10.1371/journal.pone.0093130.
(69) *R: The R Project for Statistical Computing*. https://www.r-project.org/ (accessed 2024-04-15).
(70) Wei, T.; Simko, V.; Levy, M.; Xie, Y.; Jin, Y.; Zemla, J.; Freidank, M.; Cai, J.; Protivinsky, T. Corrplot: Visualization of a Correlation Matrix, 2021. https://cran.r-project.org/web/packages/corrplot/index.html (accessed 2024-04-15).
(71) Oksanen, J.; Simpson, G. L.; Blanchet, F. G.; Kindt, R.; Legendre, P.; Minchin, P. R.; O'Hara, R. B.; Solymos, P.; Stevens, M. H. H.; Szoecs, E.; Wagner, H.; Barbour, M.; Bedward, M.; Bolker, B.; Borcard, D.; Carvalho, G.; Chirico, M.; Caceres, M. D.; Durand, S.; Evangelista, H. B. A.; FitzJohn, R.; Friendly, M.; Furneaux, B.; Hannigan, G.; Hill, M. O.; Lahti, L.; McGlinn, D.; Ouellette, M.-H.; Cunha, E. R.; Smith, T.; Stier, A.; Braak, C. J. F. T.; Weedon, J. Vegan: Community Ecology Package, 2022. https://cran.r-project.org/web/packages/vegan/index.html (accessed 2024-04-15).
(72) Maestrini, B.; Nannipieri, P.; Abiven, S. A Meta-Analysis on Pyrogenic Organic Matter Induced Priming Effect. *GCB Bioenergy* **2015**, *7* (4), 577–590. https://doi.org/10.1111/gcbb.12194.
(73) Nelson, A. R.; Narrowe, A. B.; Rhoades, C. C.; Fegel, T. S.; Daly, R. A.; Roth, H. K.; Chu, R. K.; Amundson, K. K.; Young, R. B.; Steindorff, A. S.; Mondo, S. J.; Grigoriev, I. V.; Salamov, A.; Borch, T.; Wilkins, M. J. Wildfire-Dependent Changes in Soil Microbiome Diversity and Function. *Nat Microbiol* **2022**, *7* (9), 1419–1430. https://doi.org/10.1038/s41564-022-01203-y.
(74) Wu, S.; Wang, D.; Liu, C.; Fang, G.; Sun, T.-R.; Cui, P.; Yan, H.; Wang, Y.; Zhou, D. Pyridinic- and Pyrrolic Nitrogen in Pyrogenic Carbon Improves Electron Shuttling during Microbial Fe(III) Reduction. *ACS Earth Space Chem.* **2021**, *5* (4), 900–909. https://doi.org/10.1021/acsearthspacechem.1c00012.
(75) Whitman, T.; DeCiucies, S.; Hanley, K.; Enders, A.; Woolet, J.; Lehmann, J. Microbial Community Shifts Reflect Losses of Native Soil Carbon with Pyrogenic and Fresh Organic Matter Additions and Are Greatest in Low-Carbon Soils. *Applied and Environmental Microbiology* **2021**, *87* (8), e02555-20. https://doi.org/10.1128/AEM.02555-20.
(76) Klüpfel, L.; Keiluweit, M.; Kleber, M.; Sander, M. Redox Properties of Plant Biomass-Derived Black Carbon (Biochar). *Environ. Sci. Technol.* **2014**, *48* (10), 5601–5611. https://doi.org/10.1021/es500906d.
(77) Sun, T.; Guzman, J. J. L.; Seward, J. D.; Enders, A.; Yavitt, J. B.; Lehmann, J.; Angenent, L. T. Suppressing Peatland Methane Production by Electron Snorkeling through Pyrogenic Carbon in Controlled Laboratory Incubations. *Nature Communications 2021 12:1* **2021**, *12* (1), 1–9. https://doi.org/10.1038/s41467-021-24350-y.

(78) Updegraff, K.; Pastor, J.; Bridgham, S. D.; Johnston, C. A. Environmental and Substrate Controls over Carbon and Nitrogen Mineralization in Northern Wetlands. *Ecological Applications* **1995**, *5* (1), 151–163. https://doi.org/10.2307/1942060.
(79) Steinmuller, H. E.; Dittmer, K. M.; White, J. R.; Chambers, L. G. Understanding the Fate of Soil Organic Matter in Submerging Coastal Wetland Soils: A Microcosm Approach. *Geoderma* **2019**, *337*, 1267–1277. https://doi.org/10.1016/j.geoderma.2018.08.020.
(80) Chari, N. R.; Lin, Y.; Lin, Y. S.; Silver, W. L. Interactive Effects of Temperature and Redox on Soil Carbon and Iron Cycling. *Soil Biology and Biochemistry* **2021**, *157*, 108235. https://doi.org/10.1016/j.soilbio.2021.108235.
(81) Lalonde, K.; Mucci, A.; Ouellet, A.; Gélinas, Y. Preservation of Organic Matter in Sediments Promoted by Iron. *Nature* **2012**, *483* (7388), 198–200. https://doi.org/10.1038/nature10855.
(82) Mu, C. C.; Zhang, T. J.; Zhao, Q.; Guo, H.; Zhong, W.; Su, H.; Wu, Q. B. Soil Organic Carbon Stabilization by Iron in Permafrost Regions of the Qinghai-Tibet Plateau. *Geophysical Research Letters* **2016**, *43* (19), 10,286-10,294. https://doi.org/10.1002/2016GL070071.
(83) Christ, M. J.; David, M. B. Temperature and Moisture Effects on the Production of Dissolved Organic Carbon in a Spodosol. *Soil Biology and Biochemistry* **1996**, *28* (9), 1191–1199. https://doi.org/10.1016/0038-0717(96)00120-4.
(84) Clark, J. M.; Ashley, D.; Wagner, M.; Chapman, P. J.; Lane, S. N.; Evans, C. D.; Heathwaite, A. L. Increased Temperature Sensitivity of Net DOC Production from Ombrotrophic Peat Due to Water Table Draw-Down. *Global Change Biology* **2009**, *15* (4), 794–807. https://doi.org/10.1111/j.1365-2486.2008.01683.x.
(85) Wu, Q.; Ye, R.; Bridgham, S. D.; Jin, Q. Limitations of the Q10 Coefficient for Quantifying Temperature Sensitivity of Anaerobic Organic Matter Decomposition: A Modeling Based Assessment. *Journal of Geophysical Research: Biogeosciences* **2021**, *126* (8), e2021JG006264. https://doi.org/10.1029/2021JG006264.
(86) Hamdi, S.; Moyano, F.; Sall, S.; Bernoux, M.; Chevallier, T. Synthesis Analysis of the Temperature Sensitivity of Soil Respiration from Laboratory Studies in Relation to Incubation Methods and Soil Conditions. *Soil Biology and Biochemistry* **2013**, *58*, 115–126. https://doi.org/10.1016/j.soilbio.2012.11.012.
(87) Li, Z.; Grant, R. F.; Chang, K.-Y.; Hodgkins, S. B.; Tang, J.; Cory, A.; Mekonnen, Z. A.; Saleska, S. R.; Brodie, E. L.; Varner, R. K.; Rich, V. I.; Wilson, R. M.; Chanton, J. P.; Crill, P.; Riley, W. J. Soil Incubation Methods Lead to Large Differences in Inferred Methane Production Temperature Sensitivity. *Environ. Res. Lett.* **2024**, *19* (4), 044069. https://doi.org/10.1088/1748-9326/ad3565.
(88) Lupascu, M.; Wadham, J. L.; Hornibrook, E. R. C.; Pancost, R. D. Temperature Sensitivity of Methane Production in the Permafrost Active Layer at Stordalen, Sweden: A Comparison with Non-Permafrost Northern Wetlands. *Arctic, Antarctic, and Alpine Research* **2012**, *44* (4), 469–482. https://doi.org/10.1657/1938-4246-44.4.469.
(89) Fan, L.; Dippold, M. A.; Thiel, V.; Ge, T.; Wu, J.; Kuzyakov, Y.; Dorodnikov, M. Temperature Sensitivity of Anaerobic Methane Oxidation versus Methanogenesis in

Paddy Soil: Implications for the CH4 Balance under Global Warming. *Global Change Biology* **2022**, *28* (2), 654–664. https://doi.org/10.1111/gcb.15935.
(90) Meier, J.; Costa, R.; Smalla, K.; Boehrer, B.; Wendt-Potthoff, K. Temperature Dependence of Fe(III) and Sulfate Reduction Rates and Its Effect on Growth and Composition of Bacterial Enrichments from an Acidic Pit Lake Neutralization Experiment. *Geobiology* **2005**, *3* (4), 261–274. https://doi.org/10.1111/j.1472-4669.2006.00065.x.
(91) Osborne, T. Z.; Kobziar, L. N.; Inglett, P. W. Fire and Water: New Perspectives on Fire's Role in Shaping Wetland Ecosystems. *fire ecol* **2013**, *9* (1), 1–5. https://doi.org/10.4996/fireecology.0901001.
(92) Scott, D. N.; Wohl, E. E. Evaluating Carbon Storage on Subalpine Lake Deltas. *Earth Surface Processes and Landforms* **2017**, *42* (10), 1472–1481. https://doi.org/10.1002/esp.4110.
(93) Heikkinen, J. E. P.; Elsakov, V.; Martikainen, P. J. Carbon Dioxide and Methane Dynamics and Annual Carbon Balance in Tundra Wetland in NE Europe, Russia. *Global Biogeochemical Cycles* **2002**, *16* (4), 62-1-62–15. https://doi.org/10.1029/2002GB001930.
(94) Abdul Malak, D.; Marín, A.; Trombetti, M.; Sonsoles, S. *Carbon Pools and Sequestration Potential of Wetlands in the European Union European Topic Centre on Urban, Land and Soil Systems Similarities and Diversity of European Cities A Typology Tool to Support Urban Sustainability*; 2021. https://doi.org/10.13140/RG.2.2.34986.34243.
(95) Mitsch, W. J.; Gosselink, J. G. *Wetlands*. https://books.google.com/books?hl=en&lr=&id=-vcwBgAAQBAJ&oi=fnd&pg=PR5&ots=3sQIdhMt5E&sig=LtVofotG0eTRP-0V_q2ddj_ESd4#v=onepage&q&f=false (accessed 2021-06-08).
(96) Kayranli, B.; Scholz, M.; Mustafa, A.; Hedmark, Å. Carbon Storage and Fluxes within Freshwater Wetlands: A Critical Review. *Wetlands* **2010**, *30* (1), 111–124. https://doi.org/10.1007/s13157-009-0003-4.
(97) Chamberlain, S. D.; Anthony, T. L.; Silver, W. L.; Eichelmann, E.; Hemes, K. S.; Oikawa, P. Y.; Sturtevant, C.; Szutu, D. J.; Verfaillie, J. G.; Baldocchi, D. D. Soil Properties and Sediment Accretion Modulate Methane Fluxes from Restored Wetlands. *Global Change Biology* **2018**, *24* (9), 4107–4121. https://doi.org/10.1111/GCB.14124.
(98) Hutton, P. H.; Rath, J. S.; Chen, L.; Ungs, M. J.; Roy, S. B. Nine Decades of Salinity Observations in the San Francisco Bay and Delta: Modeling and Trend Evaluations. *Journal of Water Resources Planning and Management* **2016**, *142* (3), 04015069. https://doi.org/10.1061/(ASCE)WR.1943-5452.0000617.
(99) Kalcic, M.; Crumpton, W.; Liu, X.; D'Ambrosio, J.; Ward, A.; Witter, J. Assessment of Beyond-the-Field Nutrient Management Practices for Agricultural Crop Systems with Subsurface Drainage. *Journal of Soil and Water Conservation* **2018**, *73* (1), 62–74. https://doi.org/10.2489/jswc.73.1.62.
(100) Creed, I. F.; Lane, C. R.; Serran, J. N.; Alexander, L. C.; Basu, N. B.; Calhoun, A. J. K.; Christensen, J. R.; Cohen, M. J.; Craft, C.; D'Amico, E.; DeKeyser, E.; Fowler, L.; Golden, H. E.; Jawitz, J. W.; Kalla, P.; Kirkman, L. K.; Lang, M.; Leibowitz, S. G.; Lewis,

D. B.; Marton, J.; McLaughlin, D. L.; Raanan-Kiperwas, H.; Rains, M. C.; Rains, K. C.; Smith, L. Enhancing Protection for Vulnerable Waters. *Nature Geosci* **2017**, *10* (11), 809–815. https://doi.org/10.1038/ngeo3041.

(101) Griffis, T. J.; Chen, Z.; Baker, J. M.; Wood, J. D.; Millet, D. B.; Lee, X.; Venterea, R. T.; Turner, P. A. Nitrous Oxide Emissions Are Enhanced in a Warmer and Wetter World. *Proceedings of the National Academy of Sciences* **2017**, *114* (45), 12081–12085. https://doi.org/10.1073/pnas.1704552114.

(102) Parker, V. T.; Boyer, K. E. Sea-Level Rise and Climate Change Impacts on an Urbanized Pacific Coast Estuary. *Wetlands* **2019**, *39* (6), 1219–1232. https://doi.org/10.1007/s13157-017-0980-7.

(103) Wankel, S. D.; Kendall, C.; Francis, C. A.; Paytan, A. Nitrogen Sources and Cycling in the San Francisco Bay Estuary: A Nitrate Dual Isotopic Composition Approach. *Limnology and Oceanography* **2006**, *51* (4), 1654–1664. https://doi.org/10.4319/lo.2006.51.4.1654.

(104) *San Francisco Bay-Delta Fish and Wildlife Office | Species | U.S. Fish & Wildlife Service*. https://www.fws.gov/office/san-francisco-bay-delta-fish-and-wildlife (accessed 2024-04-16).

(105) *Voyager: How does water get from Northern California to Southern California? | Scripps Institution of Oceanography*. https://scripps.ucsd.edu/news/voyager-how-does-water-get-northern-california-southern-california (accessed 2024-04-16).

(106) *A History of California Water*. California Water Impact Network. https://www.c-win.org/a-history-of-california-water (accessed 2024-04-16).

(107) Syvitski, J. P. M.; Kettner, A. J.; Overeem, I.; Hutton, E. W. H.; Hannon, M. T.; Brakenridge, G. R.; Day, J.; Vörösmarty, C.; Saito, Y.; Giosan, L.; Nicholls, R. J. Sinking Deltas Due to Human Activities. *Nature Geosci* **2009**, *2* (10), 681–686. https://doi.org/10.1038/ngeo629.

(108) Callaway, J. C.; Parker, V. T.; Vasey, M. C.; Schile, L. M.; Herbert, E. R. Tidal Wetland Restoration in San Francisco Bay: History and Current Issues. *San Francisco Estuary and Watershed Science* **2011**, *9* (3). https://doi.org/10.15447/sfews.2011v9iss3art2.

(109) Drexler, J. Z.; de Fontaine, C. S.; Deverel, S. J. The Legacy of Wetland Drainage on the Remaining Peat in the Sacramento — San Joaquin Delta, California, USA. *Wetlands* **2009**, *29* (1), 372–386. https://doi.org/10.1672/08-97.1.

(110) California, S. of. *The Delta*. https://water.ca.gov/Water-Basics/The-Delta (accessed 2024-04-15).

(111) Medellín-Azuara, J.; Howitt, R. E.; Hanak, E.; Lund, J. R.; Fleenor, W. E. Agricultural Losses from Salinity in California's Sacramento-San Joaquin Delta. *San Francisco Estuary and Watershed Science* **2014**, *12* (1). https://doi.org/10.15447/sfews.2014v12iss1art3.

(112) Luoma, S. N.; Dahm, C. N.; Healey, M.; Moore, J. N. Challenges Facing the Sacramento–San Joaquin Delta: Complex, Chaotic, or Simply Cantankerous? *San Francisco Estuary and Watershed Science* **2015**, *13* (3). https://doi.org/10.15447/sfews.2015v13iss3art7.

(113) Gross, E. S.; Hutton, P. H.; Draper, A. J. A Comparison of Outflow and Salt Intrusion in the Pre-Development and Contemporary San Francisco Estuary. *San Francisco*

Estuary and Watershed Science **2018**, *16* (3). https://doi.org/10.15447/sfews.2018v16iss3art6.
(114) Durand, J. R.; Bombardelli, F.; Fleenor, W. E.; Henneberry, Y.; Herman, J.; Jeffres, C.; Leinfelder–Miles, M.; Lund, J. R.; Lusardi, R.; Manfree, A. D.; Medellín-Azuara, J.; Milligan, B.; Moyle, P. B. Drought and the Sacramento-San Joaquin Delta, 2012–2016: Environmental Review and Lessons. *San Francisco Estuary and Watershed Science* **2020**, *18* (2). https://doi.org/10.15447/sfews.2020v18iss2art2.
(115) Weston, N. B.; Vile, M. A.; Neubauer, S. C.; Velinsky, D. J. Accelerated Microbial Organic Matter Mineralization Following Salt-Water Intrusion into Tidal Freshwater Marsh Soils. *Biogeochemistry* **2011**, *102* (1), 135–151. https://doi.org/10.1007/s10533-010-9427-4.
(116) Neubauer, S. C. Ecosystem Responses of a Tidal Freshwater Marsh Experiencing Saltwater Intrusion and Altered Hydrology. *Estuaries and Coasts* **2013**, *36* (3), 491–507. https://doi.org/10.1007/s12237-011-9455-x.
(117) Chambers, L. G.; Reddy, K. R.; Osborne, T. Z. Short-Term Response of Carbon Cycling to Salinity Pulses in a Freshwater Wetland. *Soil Science Society of America Journal* **2011**, *75* (5), 2000–2007. https://doi.org/10.2136/sssaj2011.0026.
(118) Setia, R.; Marschner, P.; Baldock, J.; Chittleborough, D. Is CO2 Evolution in Saline Soils Affected by an Osmotic Effect and Calcium Carbonate? *Biol Fertil Soils* **2010**, *46* (8), 781–792. https://doi.org/10.1007/s00374-010-0479-3.
(119) Setia, R.; Setia, D.; Marschner, P. Short-Term Carbon Mineralization in Saline–Sodic Soils. *Biol Fertil Soils* **2012**, *48* (4), 475–479. https://doi.org/10.1007/s00374-011-0643-4.
(120) Hemminga, M. A.; De Leeuw, J.; De Munek, W.; Koutstaal, B. P. Decomposition in Estuarine Salt Marshes: The Effect of Soil Salinity and Soil Water Content. *Vegetatio* **1991**, *94* (1), 25–33. https://doi.org/10.1007/BF00044913.
(121) Luo, M.; Huang, J.-F.; Zhu, W.-F.; Tong, C. Impacts of Increasing Salinity and Inundation on Rates and Pathways of Organic Carbon Mineralization in Tidal Wetlands: A Review. *Hydrobiologia* **2019**, *827* (1), 31–49. https://doi.org/10.1007/s10750-017-3416-8.
(122) Marks, B. M.; Chambers, L.; White, J. R. Effect of Fluctuating Salinity on Potential Denitrification in Coastal Wetland Soil and Sediments. *Soil Science Society of America Journal* **2016**, *80* (2), 516–526. https://doi.org/10.2136/sssaj2015.07.0265.
(123) Ji, J.; Peng, Y.; Wang, B.; Mai, W.; Li, X.; Zhang, Q.; Wang, S. Effects of Salinity Build-up on the Performance and Microbial Community of Partial-Denitrification Granular Sludge with High Nitrite Accumulation. *Chemosphere* **2018**, *209*, 53–60. https://doi.org/10.1016/j.chemosphere.2018.05.193.
(124) Wang, H.; Dai, Z.; Krauss, K. W.; Trettin, C. C.; Noe, G. B.; Burton, A. J.; Ward, E. J. Modeling Impacts of Saltwater Intrusion on Methane and Nitrous Oxide Emissions in Tidal Forested Wetlands. *Ecological Applications* **2023**, *33* (5), e2858. https://doi.org/10.1002/eap.2858.
(125) Ardón, M.; Helton, A. M.; Bernhardt, E. S. Salinity Effects on Greenhouse Gas Emissions from Wetland Soils Are Contingent upon Hydrologic Setting: A Microcosm

Experiment. *Biogeochemistry* **2018**, *140* (2), 217–232. https://doi.org/10.1007/s10533-018-0486-2.
(126) Reddy, N.; Crohn, D. M. Effects of Soil Salinity and Carbon Availability from Organic Amendments on Nitrous Oxide Emissions. *Geoderma* **2014**, *235–236*, 363–371. https://doi.org/10.1016/j.geoderma.2014.07.022.
(127) Batjes, N. h. Total Carbon and Nitrogen in the Soils of the World. *European Journal of Soil Science* **1996**, *47* (2), 151–163. https://doi.org/10.1111/j.1365-2389.1996.tb01386.x.
(128) Wang, R.; Chen, H.; Luo, Y.; Moran, P.; Grieneisen, M.; Zhang, M. Nitrate Runoff Contributing from the Agriculturally Intensive San Joaquin River Watershed to Bay-Delta in California. *Sustainability* **2019**, *11* (10), 2845. https://doi.org/10.3390/su11102845.
(129) Bergamaschi, B. A.; Downing, B. D.; Kraus, T. E. C.; Pellerin, B. A. *Designing a High-Frequency Nutrient and Biogeochemical Monitoring Network for the Sacramento–San Joaquin Delta, Northern California*; 2017–5058; U.S. Geological Survey, 2017. https://doi.org/10.3133/sir20175058.
(130) Evenson, G. R.; Golden, H. E.; Christensen, J. R.; Lane, C. R.; Rajib, A.; D'Amico, E.; Mahoney, D. T.; White, E.; Wu, Q. Wetland Restoration Yields Dynamic Nitrate Responses across the Upper Mississippi River Basin. *Environ Res Commun* **2021**, *3*, 1–10. https://doi.org/10.1088/2515-7620/ac2125.
(131) Sanders, C. J.; Eyre, B. D.; Santos, I. R.; Machado, W.; Luiz-Silva, W.; Smoak, J. M.; Breithaupt, J. L.; Ketterer, M. E.; Sanders, L.; Marotta, H.; Silva-Filho, E. Elevated Rates of Organic Carbon, Nitrogen, and Phosphorus Accumulation in a Highly Impacted Mangrove Wetland. *Geophysical Research Letters* **2014**, *41* (7), 2475–2480. https://doi.org/10.1002/2014GL059789.
(132) Pasut, C.; Tang, F. H. M.; Hamilton, D.; Riley, W. J.; Maggi, F. Spatiotemporal Assessment of GHG Emissions and Nutrient Sequestration Linked to Agronutrient Runoff in Global Wetlands. *Global Biogeochemical Cycles* **2021**, *35* (4), e2020GB006816. https://doi.org/10.1029/2020GB006816.
(133) Jordan, S. J.; Stoffer, J.; Nestlerode, J. A. Wetlands as Sinks for Reactive Nitrogen at Continental and Global Scales: A Meta-Analysis. *Ecosystems* **2011**, *14* (1), 144–155. https://doi.org/10.1007/s10021-010-9400-z.
(134) Crumpton, W. G.; Stenback, G. A.; Fisher, S. W.; Stenback, J. Z.; Green, D. I. S. Water Quality Performance of Wetlands Receiving Nonpoint-Source Nitrogen Loads: Nitrate and Total Nitrogen Removal Efficiency and Controlling Factors. *Journal of Environmental Quality* **2020**, *49* (3), 735–744. https://doi.org/10.1002/jeq2.20061.
(135) Windham–Myers, L.; Oikawa, P.; Deverel, S.; Chapple, D.; Drexler, J. Z.; Stern, D. Carbon Sequestration and Subsidence Reversal in the Sacramento–San Joaquin Delta and Suisun Bay: Management Opportunities for Climate Mitigation and Adaptation. *San Francisco Estuary and Watershed Science* **2023**, *20* (4). https://doi.org/10.15447/sfews.2023v20iss4art7.
(136) Eichelmann, E.; Hemes, K. S.; Knox, S. H.; Oikawa, P. Y.; Chamberlain, S. D.; Sturtevant, C.; Verfaillie, J.; Baldocchi, D. D. The Effect of Land Cover Type and Structure on Evapotranspiration from Agricultural and Wetland Sites in the

Sacramento–San Joaquin River Delta, California. *Agricultural and Forest Meteorology* **2018**, *256–257*, 179–195. https://doi.org/10.1016/j.agrformet.2018.03.007.
(137) Arias-Ortiz, A.; Baldocchi, D. *AmeriFlux AmeriFlux US-Dmg Dutch Slough Marsh Gilbert Tract*; Lawrence Berkeley National Laboratory (LBNL), Berkeley, CA (United States). AmeriFlux; Univ. of California, Berkeley, CA (United States), 2023. https://doi.org/10.17190/AMF/1964086.
(138) *Web Soil Survey - Home*. https://websoilsurvey.nrcs.usda.gov/app/ (accessed 2024-04-25).
(139) Anthony, T. L.; Silver, W. L. Hot Moments Drive Extreme Nitrous Oxide and Methane Emissions from Agricultural Peatlands. *Global Change Biology* **2021**, *27* (20), 5141–5153. https://doi.org/10.1111/gcb.15802.
(140) Cornwell, J. C.; Glibert, P. M.; Owens, M. S. Nutrient Fluxes from Sediments in the San Francisco Bay Delta. *Estuaries and Coasts* **2014**, *37* (5), 1120–1133. https://doi.org/10.1007/s12237-013-9755-4.
(141) Saleh, D.; Domagalski, J. Concentrations, Loads, and Associated Trends of Nutrients Entering the Sacramento–San Joaquin Delta, California. *San Francisco Estuary and Watershed Science* **2021**, *19* (4). https://doi.org/10.15447/sfews.2021v19iss4art6.
(142) Kasak, K.; Espenberg, M.; Anthony, T. L.; Tringe, S. G.; Valach, A. C.; Hemes, K. S.; Silver, W. L.; Mander, Ü.; Kill, K.; McNicol, G.; Szutu, D.; Verfaillie, J.; Baldocchi, D. D. Restoring Wetlands on Intensive Agricultural Lands Modifies Nitrogen Cycling Microbial Communities and Reduces N2O Production Potential. *Journal of Environmental Management* **2021**, *299*, 113562. https://doi.org/10.1016/j.jenvman.2021.113562.
(143) Valach, A. C.; Kasak, K.; Hemes, K. S.; Anthony, T. L.; Dronova, I.; Taddeo, S.; Silver, W. L.; Szutu, D.; Verfaillie, J.; Baldocchi, D. D. Productive Wetlands Restored for Carbon Sequestration Quickly Become Net CO2 Sinks with Site-Level Factors Driving Uptake Variability. *PLOS ONE* **2021**, *16* (3), e0248398. https://doi.org/10.1371/journal.pone.0248398.
(144) Torn, M. S.; Vitousek, P. M.; Trumbore, S. E. The Influence of Nutrient Availability on Soil Organic Matter Turnover Estimated by Incubations and Radiocarbon Modeling. *Ecosystems* **2005**, *8* (4), 352–372. https://doi.org/10.1007/s10021-004-0259-8.
(145) Min, K.; Kang, H.; Lee, D. Effects of Ammonium and Nitrate Additions on Carbon Mineralization in Wetland Soils. *Soil Biology and Biochemistry* **2011**, *43* (12), 2461–2469. https://doi.org/10.1016/j.soilbio.2011.08.019.
(146) Oikawa, P. Y.; Jenerette, G. D.; Knox, S. H.; Sturtevant, C.; Verfaillie, J.; Dronova, I.; Poindexter, C. M.; Eichelmann, E.; Baldocchi, D. D. Evaluation of a Hierarchy of Models Reveals Importance of Substrate Limitation for Predicting Carbon Dioxide and Methane Exchange in Restored Wetlands. *Journal of Geophysical Research: Biogeosciences* **2017**, *122* (1), 145–167. https://doi.org/10.1002/2016JG003438.
(147) Hemes, K. S.; Chamberlain, S. D.; Eichelmann, E.; Knox, S. H.; Baldocchi, D. D. A Biogeochemical Compromise: The High Methane Cost of Sequestering Carbon in Restored Wetlands. *Geophysical Research Letters* **2018**, *45* (12), 6081–6091. https://doi.org/10.1029/2018GL077747.

(148) Rahman, Md. M.; Roberts, K. L.; Grace, M. R.; Kessler, A. J.; Cook, P. L. M. Role of Organic Carbon, Nitrate and Ferrous Iron on the Partitioning between Denitrification and DNRA in Constructed Stormwater Urban Wetlands. *Science of The Total Environment* **2019**, *666*, 608–617. https://doi.org/10.1016/j.scitotenv.2019.02.225.
(149) Cheng, S.; Qin, C.; Xie, H.; Wang, W.; Zhang, J.; Hu, Z.; Liang, S. Comprehensive Evaluation of Manganese Oxides and Iron Oxides as Metal Substrate Materials for Constructed Wetlands from the Perspective of Water Quality and Greenhouse Effect. *Ecotoxicology and Environmental Safety* **2021**, *221*, 112451. https://doi.org/10.1016/j.ecoenv.2021.112451.
(150) Baldwin, D. S.; Rees, G. N.; Mitchell, A. M.; Watson, G.; Williams, J. The Short-Term Effects of Salinization on Anaerobic Nutrient Cycling and Microbial Community Structure in Sediment from a Freshwater Wetland. *Wetlands* **2006**, *26* (2), 455–464. https://doi.org/10.1672/0277-5212(2006)26[455:TSEOSO]2.0.CO;2.
(151) Hemes, K. S.; Chamberlain, S. D.; Eichelmann, E.; Anthony, T.; Valach, A.; Kasak, K.; Szutu, D.; Verfaillie, J.; Silver, W. L.; Baldocchi, D. D. Assessing the Carbon and Climate Benefit of Restoring Degraded Agricultural Peat Soils to Managed Wetlands. *Agricultural and Forest Meteorology* **2019**, *268*, 202–214. https://doi.org/10.1016/J.AGRFORMET.2019.01.017.
(152) Hartman, W. H.; Bueno de Mesquita, C. P.; Theroux, S. M.; Morgan-Lang, C.; Baldocchi, D. D.; Tringe, S. G. Multiple Microbial Guilds Mediate Soil Methane Cycling along a Wetland Salinity Gradient. *mSystems* **2024**, *9* (1), e00936-23. https://doi.org/10.1128/msystems.00936-23.
(153) Poffenbarger, H. J.; Needelman, B. A.; Megonigal, J. P. Salinity Influence on Methane Emissions from Tidal Marshes. *Wetlands* **2011**, *31* (5), 831–842. https://doi.org/10.1007/s13157-011-0197-0.
(154) Al-Haj, A. N.; Fulweiler, R. W. A Synthesis of Methane Emissions from Shallow Vegetated Coastal Ecosystems. *Global Change Biology* **2020**, *26* (5), 2988–3005. https://doi.org/10.1111/gcb.15046.
(155) Cheng, Y.; Elrys, A. S.; Merwad, A.-R. M.; Zhang, H.; Chen, Z.; Zhang, J.; Cai, Z.; Müller, C. Global Patterns and Drivers of Soil Dissimilatory Nitrate Reduction to Ammonium. *Environ. Sci. Technol.* **2022**, *56* (6), 3791–3800. https://doi.org/10.1021/acs.est.1c07997.
(156) Wang, S.; Pi, Y.; Song, Y.; Jiang, Y.; Zhou, L.; Liu, W.; Zhu, G. Hotspot of Dissimilatory Nitrate Reduction to Ammonium (DNRA) Process in Freshwater Sediments of Riparian Zones. *Water Research* **2020**, *173*, 115539. https://doi.org/10.1016/j.watres.2020.115539.
(157) Martínez-Espinosa, C.; Sauvage, S.; Al Bitar, A.; Green, P. A.; Vörösmarty, C. J.; Sánchez-Pérez, J. M. Denitrification in Wetlands: A Review towards a Quantification at Global Scale. *Science of The Total Environment* **2021**, *754*, 142398. https://doi.org/10.1016/j.scitotenv.2020.142398.
(158) Knox, S. H.; Sturtevant, C.; Matthes, J. H.; Koteen, L.; Verfaillie, J.; Baldocchi, D. Agricultural Peatland Restoration: Effects of Land-Use Change on Greenhouse Gas (CO2 and CH4) Fluxes in the Sacramento-San Joaquin Delta. *Global Change Biology* **2015**, *21* (2), 750–765. https://doi.org/10.1111/gcb.12745.

(159) Díaz, R. J.; Rosenberg, R. Introduction to Environmental and Economic Consequences of Hypoxia. *International Journal of Water Resources Development* **2011**, *27* (1), 71–82. https://doi.org/10.1080/07900627.2010.531379.
(160) Fennel, K.; Testa, J. M. Biogeochemical Controls on Coastal Hypoxia. *Annual Review of Marine Science* **2019**, *11* (Volume 11, 2019), 105–130. https://doi.org/10.1146/annurev-marine-010318-095138.
(161) Verhoeven, J. T. A.; Arheimer, B.; Yin, C.; Hefting, M. M. Regional and Global Concerns over Wetlands and Water Quality. *Trends in Ecology & Evolution* **2006**, *21* (2), 96–103. https://doi.org/10.1016/j.tree.2005.11.015.
(162) Marton, J. M.; Creed, I. F.; Lewis, D. B.; Lane, C. R.; Basu, N. B.; Cohen, M. J.; Craft, C. B. Geographically Isolated Wetlands Are Important Biogeochemical Reactors on the Landscape. *BioScience* **2015**, *65* (4), 408–418. https://doi.org/10.1093/biosci/biv009.
(163) Cheng, F. Y.; Van Meter, K. J.; Byrnes, D. K.; Basu, N. B. Maximizing US Nitrate Removal through Wetland Protection and Restoration. *Nature* **2020**, *588* (7839), 625–630. https://doi.org/10.1038/s41586-020-03042-5.
(164) Hansen, A. T.; Dolph, C. L.; Foufoula-Georgiou, E.; Finlay, J. C. Contribution of Wetlands to Nitrate Removal at the Watershed Scale. *Nature Geosci* **2018**, *11* (2), 127–132. https://doi.org/10.1038/s41561-017-0056-6.
(165) Firestone, M. K.; Davidson, E. A. Microbiological Basis of NO and N 2 O Production and Consumption in Soil. *Exchange of trace gases between terrestrial ecosystems and the atmosphere* **1989**, *47*, 7–21.
(166) Herbert, R. A. Nitrogen Cycling in Coastal Marine Ecosystems. *FEMS Microbiology Reviews* **1999**, *23* (5), 563–590. https://doi.org/10.1111/j.1574-6976.1999.tb00414.x.
(167) Palacin-Lizarbe, C.; Camarero, L.; Hallin, S.; Jones, C. M.; Cáliz, J.; Casamayor, E. O.; Catalan, J. The DNRA-Denitrification Dichotomy Differentiates Nitrogen Transformation Pathways in Mountain Lake Benthic Habitats. *Front. Microbiol.* **2019**, *10*. https://doi.org/10.3389/fmicb.2019.01229.
(168) Vymazal, J. Constructed Wetlands for Wastewater Treatment: Five Decades of Experience. *Environ. Sci. Technol.* **2011**, *45* (1), 61–69. https://doi.org/10.1021/es101403q.
(169) Ransom, K. M.; Nolan, B. T.; A. Traum, J.; Faunt, C. C.; Bell, A. M.; Gronberg, J. A. M.; Wheeler, D. C.; Z. Rosecrans, C.; Jurgens, B.; Schwarz, G. E.; Belitz, K.; M. Eberts, S.; Kourakos, G.; Harter, T. A Hybrid Machine Learning Model to Predict and Visualize Nitrate Concentration throughout the Central Valley Aquifer, California, USA. *Science of The Total Environment* **2017**, *601–602*, 1160–1172. https://doi.org/10.1016/j.scitotenv.2017.05.192.
(170) Hansen, J. A.; Jurgens, B. C.; Fram, M. S. Quantifying Anthropogenic Contributions to Century-Scale Groundwater Salinity Changes, San Joaquin Valley, California, USA. *Science of The Total Environment* **2018**, *642*, 125–136. https://doi.org/10.1016/j.scitotenv.2018.05.333.
(171) Rhoades, C. C.; Entwistle, D.; Butler, D. The Influence of Wildfire Extent and Severity on Streamwater Chemistry, Sediment and Temperature Following the Hayman Fire,

ColoradoA. *Int. J. Wildland Fire* **2011**, *20* (3), 430–442. https://doi.org/10.1071/WF09086.
(172) DeLuca, T. H.; MacKenzie, M. D.; Gundale, M. J.; Holben, W. E. Wildfire-Produced Charcoal Directly Influences Nitrogen Cycling in Ponderosa Pine Forests. *Soil Science Society of America Journal* **2006**, *70* (2), 448–453. https://doi.org/10.2136/SSSAJ2005.0096.
(173) Fierer, N.; Schimel, J. P.; Cates, R. G.; Zou, J. Influence of Balsam Poplar Tannin Fractions on Carbon and Nitrogen Dynamics in Alaskan Taiga Floodplain Soils. *Soil Biology and Biochemistry* **2001**, *33* (12–13), 1827–1839. https://doi.org/10.1016/S0038-0717(01)00111-0.
(174) Han, L.; Huang, W.; Yuan, X.; Zhao, Y.; Ma, Z.; Qin, J. Denitrification Potential and Influencing Factors of the Riparian Zone Soils in Different Watersheds,Taihu Basin. *Water Air Soil Pollut* **2017**, *228* (3), 108. https://doi.org/10.1007/s11270-017-3287-7.
(175) Laverman, A. M.; Van Cappellen, P.; van Rotterdam-Los, D.; Pallud, C.; Abell, J. Potential Rates and Pathways of Microbial Nitrate Reduction in Coastal Sediments. *FEMS Microbiology Ecology* **2006**, *58* (2), 179–192. https://doi.org/10.1111/j.1574-6941.2006.00155.x.
(176) Pallud, C.; Meile, C.; Laverman, A. M.; Abell, J.; Van Cappellen, P. The Use of Flow-through Sediment Reactors in Biogeochemical Kinetics: Methodology and Examples of Applications. *Marine Chemistry* **2007**, *106* (1-2 SPEC. ISS.), 256–271. https://doi.org/10.1016/j.marchem.2006.12.011.
(177) Roychoudhury, A. N.; Viollier, E.; Van Cappellen, P. A Plug Flow-through Reactor for Studying Biogeochemical Reactions in Undisturbed Aquatic Sediments. *Applied Geochemistry* **1998**, *13* (2), 269–280. https://doi.org/10.1016/S0883-2927(97)00064-4.
(178) Zhang, Z.; Furman, A. Soil Redox Dynamics under Dynamic Hydrologic Regimes - A Review. *Science of The Total Environment* **2021**, *763*, 143026. https://doi.org/10.1016/j.scitotenv.2020.143026.
(179) Zhang, W.; Li, X.; Liu, T.; Li, F. Enhanced Nitrate Reduction and Current Generation by Bacillus Sp. in the Presence of Iron Oxides. *J Soils Sediments* **2012**, *12* (3), 354–365. https://doi.org/10.1007/s11368-011-0460-2.
(180) Haaijer, S. C. M.; Lamers, L. P. M.; Smolders, A. J. P.; Jetten, M. S. M.; Op den Camp, H. J. M. Iron Sulfide and Pyrite as Potential Electron Donors for Microbial Nitrate Reduction in Freshwater Wetlands. *Geomicrobiology Journal* **2007**, *24* (5), 391–401. https://doi.org/10.1080/01490450701436489.
(181) Burgin, A. J.; Hamilton, S. K. Have We Overemphasized the Role of Denitrification in Aquatic Ecosystems? A Review of Nitrate Removal Pathways. *Frontiers in Ecology and the Environment* **2007**, *5* (2), 89–96. https://doi.org/10.1890/1540-9295(2007)5[89:HWOTRO]2.0.CO;2.
(182) Mavi, M. S.; Marschner, P. Drying and Wetting in Saline and Saline-Sodic Soils—Effects on Microbial Activity, Biomass and Dissolved Organic Carbon. *Plant Soil* **2012**, *355* (1), 51–62. https://doi.org/10.1007/s11104-011-1078-2.
(183) Zhang, G.; Bai, J.; Tebbe, C. C.; Zhao, Q.; Jia, J.; Wang, W.; Wang, X.; Yu, L. Salinity Controls Soil Microbial Community Structure and Function in Coastal Estuarine

Wetlands. *Environmental Microbiology* **2021**, *23* (2), 1020–1037. https://doi.org/10.1111/1462-2920.15281.
(184) Domic, A.; Capriles, J.; Meneses, R.; Pacheco, P. Plant Community Assembly Is Predicted by an Environmental Gradient in High-Altitude Wetlands in the Semiarid Western Bolivian Andes. *Mires and Peat* **2021**, *27*, 12. https://doi.org/10.19189/MaP.2019.JSP.StA.1916.
(185) Mętrak, M.; Chibowski, P.; Sulwiński, M.; Pawlikowski, P.; Suska-Malawska, M. CNP Stoichiometry and Productivity Limitations in High-Altitude Wetland Ecosystems of the Eastern Pamir. *Mires and Peat* **2018**, *21*. https://doi.org/10.19189/MaP.2017.OMB.297.
(186) Huang, J.; Han, M.; Yang, J.; Kappler, A.; Jiang, H. Salinity Impact on Composition and Activity of Nitrate-Reducing Fe(II)-Oxidizing Microorganisms in Saline Lakes. *Applied and Environmental Microbiology* **2022**, *88* (10), e00132-22. https://doi.org/10.1128/aem.00132-22.
(187) Emmerich, M.; Bhansali, A.; Lösekann-Behrens, T.; Schröder, C.; Kappler, A.; Behrens, S. Abundance, Distribution, and Activity of Fe(II)-Oxidizing and Fe(III)-Reducing Microorganisms in Hypersaline Sediments of Lake Kasin, Southern Russia. *Applied and Environmental Microbiology* **2012**, *78* (12), 4386–4399. https://doi.org/10.1128/AEM.07637-11.
(188) Bonin, P.; Rambeloarisoa Ranaivoson, E.; Raymond, N.; Chalamet, A.; Bertrand, J. C. Evidence for Denitrification in Marine Sediment Highly Contaminated by Petroleum Products. *Marine Pollution Bulletin* **1994**, *28* (2), 89–95. https://doi.org/10.1016/0025-326X(94)90544-4.
(189) Thorslund, J.; Jarsjo, J.; Jaramillo, F.; Jawitz, J. W.; Manzoni, S.; Basu, N. B.; Chalov, S. R.; Cohen, M. J.; Creed, I. F.; Goldenberg, R.; Hylin, A.; Kalantari, Z.; Koussis, A. D.; Lyon, S. W.; Mazi, K.; Mard, J.; Persson, K.; Pietro, J.; Prieto, C.; Quin, A.; Van Meter, K.; Destouni, G. Wetlands as Large-Scale Nature-Based Solutions: Status and Challenges for Research, Engineering and Management. *Ecological Engineering* **2017**, *108*, 489–497. https://doi.org/10.1016/j.ecoleng.2017.07.012.
(190) Pezeshki, S. R. Wetland Plant Responses to Soil Flooding. *Environmental and Experimental Botany* **2001**, *46* (3), 299–312. https://doi.org/10.1016/S0098-8472(01)00107-1.
(191) *Ecology of Wetland Ecosystems: Water, Substrate, and Life | Learn Science at Scitable*. https://www.nature.com/scitable/knowledge/library/ecology-of-wetland-ecosystems-water-substrate-and-17059765/ (accessed 2024-04-18).
(192) Chanton, J. P.; Glaser, P. H.; Chasar, L. S.; Burdige, D. J.; Hines, M. E.; Siegel, D. I.; Tremblay, L. B.; Cooper, W. T. Radiocarbon Evidence for the Importance of Surface Vegetation on Fermentation and Methanogenesis in Contrasting Types of Boreal Peatlands. *Global Biogeochemical Cycles* **2008**, *22* (4). https://doi.org/10.1029/2008GB003274.
(193) Picek, T.; Čížková, H.; Dušek, J. Greenhouse Gas Emissions from a Constructed Wetland—Plants as Important Sources of Carbon. *Ecological Engineering* **2007**, *31* (2), 98–106. https://doi.org/10.1016/j.ecoleng.2007.06.008.

(194) Chari, N. R.; Taylor, B. N. Soil Organic Matter Formation and Loss Are Mediated by Root Exudates in a Temperate Forest. *Nat. Geosci.* **2022**, *15* (12), 1011–1016. https://doi.org/10.1038/s41561-022-01079-x.
(195) Dorodnikov, M.; Knorr, K.-H.; Kuzyakov, Y.; Wilmking, M. Plant-Mediated CH_4 Transport and Contribution of Photosynthates to Methanogenesis at a Boreal Mire: A ^{14}C Pulse-Labeling Study. *Biogeosciences* **2011**, *8* (8), 2365–2375. https://doi.org/10.5194/bg-8-2365-2011.
(196) Girkin, N. T.; Turner, B. L.; Ostle, N.; Craigon, J.; Sjögersten, S. Root Exudate Analogues Accelerate CO2 and CH4 Production in Tropical Peat. *Soil Biology and Biochemistry* **2018**, *117*, 48–55. https://doi.org/10.1016/j.soilbio.2017.11.008.
(197) McLaughlin, S.; Zhalnina, K.; Kosina, S.; Northen, T. R.; Sasse, J. The Core Metabolome and Root Exudation Dynamics of Three Phylogenetically Distinct Plant Species. *Nat Commun* **2023**, *14* (1), 1649. https://doi.org/10.1038/s41467-023-37164-x.
(198) Ma, W.; Tang, S.; Dengzeng, Z.; Zhang, D.; Zhang, T.; Ma, X. Root Exudates Contribute to Belowground Ecosystem Hotspots: A Review. *Front. Microbiol.* **2022**, *13*. https://doi.org/10.3389/fmicb.2022.937940.
(199) Chen, Y.; Yao, Z.; Sun, Y.; Wang, E.; Tian, C.; Sun, Y.; Liu, J.; Sun, C.; Tian, L. Current Studies of the Effects of Drought Stress on Root Exudates and Rhizosphere Microbiomes of Crop Plant Species. *International Journal of Molecular Sciences* **2022**, *23* (4), 2374. https://doi.org/10.3390/ijms23042374.
(200) Chai, Y. N.; Schachtman, D. P. Root Exudates Impact Plant Performance under Abiotic Stress. *Trends in Plant Science* **2022**, *27* (1), 80–91. https://doi.org/10.1016/j.tplants.2021.08.003.
(201) Henry, A.; Doucette, W.; Norton, J.; Bugbee, B. Changes in Crested Wheatgrass Root Exudation Caused by Flood, Drought, and Nutrient Stress. *Journal of Environmental Quality* **2007**, *36* (3), 904–912. https://doi.org/10.2134/jeq2006.0425sc.
(202) Hoyos-Santillan, J.; Lomax, B. H.; Large, D.; Turner, B. L.; Boom, A.; Lopez, O. R.; Sjögersten, S. Quality Not Quantity: Organic Matter Composition Controls of CO2 and CH4 Fluxes in Neotropical Peat Profiles. *Soil Biology and Biochemistry* **2016**, *103*, 86–96. https://doi.org/10.1016/j.soilbio.2016.08.017.
(203) Cooper, G. S.; Willcock, S.; Dearing, J. A. Regime Shifts Occur Disproportionately Faster in Larger Ecosystems. *Nat Commun* **2020**, *11* (1), 1175. https://doi.org/10.1038/s41467-020-15029-x.
(204) Waldo, N. B.; Hunt, B. K.; Fadely, E. C.; Moran, J. J.; Neumann, R. B. Plant Root Exudates Increase Methane Emissions through Direct and Indirect Pathways. *Biogeochemistry 2019 145:1* **2019**, *145* (1), 213–234. https://doi.org/10.1007/S10533-019-00600-6.
(205) Akhtar, H.; Lupascu, M.; Sukri, R. S. Interactions between Microtopography, Root Exudate Analogues and Temperature Determine CO2 and CH4 Production Rates in Fire-Degraded Tropical Peat. *Soil Biology and Biochemistry* **2022**, *169*, 108646. https://doi.org/10.1016/j.soilbio.2022.108646.
(206) Verbrigghe, N.; Meeran, K.; Bahn, M.; Fuchslueger, L.; Janssens, I. A.; Richter, A.; Sigurdsson, B. D.; Soong, J. L.; Vicca, S. Negative Priming of Soil Organic Matter

Following Long-Term *in Situ* Warming of Sub-Arctic Soils. *Geoderma* **2022**, *410*, 115652. https://doi.org/10.1016/j.geoderma.2021.115652.
(207) Panchal, P.; Preece, C.; Peñuelas, J.; Giri, J. Soil Carbon Sequestration by Root Exudates. *Trends in Plant Science* **2022**, *27* (8), 749–757. https://doi.org/10.1016/j.tplants.2022.04.009.
(208) Janzen, H. H.; van Groenigen, K. J.; Powlson, D. S.; Schwinghamer, T.; van Groenigen, J. W. Photosynthetic Limits on Carbon Sequestration in Croplands. *Geoderma* **2022**, *416*, 115810. https://doi.org/10.1016/j.geoderma.2022.115810.
(209) Phillips, R. P.; Finzi, A. C.; Bernhardt, E. S. Enhanced Root Exudation Induces Microbial Feedbacks to N Cycling in a Pine Forest under Long-Term CO2 Fumigation. *Ecology Letters* **2011**, *14* (2), 187–194. https://doi.org/10.1111/j.1461-0248.2010.01570.x.
(210) Meier, I. C.; Finzi, A. C.; Phillips, R. P. Root Exudates Increase N Availability by Stimulating Microbial Turnover of Fast-Cycling N Pools. *Soil Biology and Biochemistry* **2017**, *106*, 119–128. https://doi.org/10.1016/j.soilbio.2016.12.004.
(211) Baldocchi, D.; Novick, K.; Keenan, T.; Torn, M. AmeriFlux: Its Impact on Our Understanding of the 'Breathing of the Biosphere', after 25 Years. *Agricultural and Forest Meteorology* **2024**, *348*, 109929. https://doi.org/10.1016/j.agrformet.2024.109929.
(212) Yan, S.; Yin, L.; Dijkstra, F. A.; Wang, P.; Cheng, W. Priming Effect on Soil Carbon Decomposition by Root Exudate Surrogates: A Meta-Analysis. *Soil Biology and Biochemistry* **2023**, *178*, 108955. https://doi.org/10.1016/j.soilbio.2023.108955.
(213) Bethke, C. M.; Sanford, R. A.; Kirk, M. F.; Jin, Q.; Flynn, T. M. The Thermodynamic Ladder in Geomicrobiology. *American Journal of Science* **2011**, *311* (3), 183–210. https://doi.org/10.2475/03.2011.01.
(214) Liu, W.; Xiao, H.; Ma, H.; Li, Y.; Adyel, T. M.; Zhai, J. Reduction of Methane Emissions from Manganese-Rich Constructed Wetlands: Role of Manganese-Dependent Anaerobic Methane Oxidation. *Chemical Engineering Journal* **2020**, *387*, 123402. https://doi.org/10.1016/j.cej.2019.123402.
(215) Segarra, K. E. A.; Comerford, C.; Slaughter, J.; Joye, S. B. Impact of Electron Acceptor Availability on the Anaerobic Oxidation of Methane in Coastal Freshwater and Brackish Wetland Sediments. *Geochimica et Cosmochimica Acta* **2013**, *115*, 15–30. https://doi.org/10.1016/j.gca.2013.03.029.
(216) Beal, E. J.; House, C. H.; Orphan, V. J. Manganese- and Iron-Dependent Marine Methane Oxidation. *Science* **2009**, *325* (5937), 184–187. https://doi.org/10.1126/science.1169984.
(217) Keiluweit, M.; Bougoure, J. J.; Nico, P. S.; Pett-Ridge, J.; Weber, P. K.; Kleber, M. Mineral Protection of Soil Carbon Counteracted by Root Exudates. *Nature Climate Change* **2015**, *5* (6), 588–595. https://doi.org/10.1038/nclimate2580.
(218) Gong, X.; Feng, Y.; Dang, K.; Jiang, Y.; Qi, H.; Feng, B. Linkages of Microbial Community Structure and Root Exudates: Evidence from Microbial Nitrogen Limitation in Soils of Crop Families. *Science of The Total Environment* **2023**, *881*, 163536. https://doi.org/10.1016/j.scitotenv.2023.163536.

(219) Hao, C.; Dungait, J. A. J.; Wei, X.; Ge, T.; Kuzyakov, Y.; Cui, Z.; Tian, J.; Zhang, F. Maize Root Exudate Composition Alters Rhizosphere Bacterial Community to Control Hotspots of Hydrolase Activity in Response to Nitrogen Supply. *Soil Biology and Biochemistry* **2022**, *170*, 108717. https://doi.org/10.1016/j.soilbio.2022.108717.
(220) Moreau, D.; Bardgett, R. D.; Finlay, R. D.; Jones, D. L.; Philippot, L. A Plant Perspective on Nitrogen Cycling in the Rhizosphere. *Functional Ecology* **2019**, *33* (4), 540–552. https://doi.org/10.1111/1365-2435.13303.
(221) Grybos, M.; Davranche, M.; Gruau, G.; Petitjean, P.; Pédrot, M. Increasing pH Drives Organic Matter Solubilization from Wetland Soils under Reducing Conditions. *Geoderma* **2009**, *154* (1), 13–19. https://doi.org/10.1016/j.geoderma.2009.09.001.
(222) Seitzinger, S. P. Linkages between Organic Matter Mineralization and Denitrification in Eight Riparian Wetlands. *Biogeochemistry* **1994**, *25* (1), 19–39. https://doi.org/10.1007/BF00000510.
(223) Yavitt, J. B.; Lang, G. E. Methane Production in Contrasting Wetland Sites: Response to Organic-chemical Components of Peat and to Sulfate Reduction. *Geomicrobiology Journal* **1990**, *8* (1), 27–46. https://doi.org/10.1080/01490459009377876.
(224) Zhu, X.; Yuan, Y.; Wei, X.; Wang, L.; Wang, C. Dissimilatory Iron Reduction and Potential Methane Production in Chagan Lake Wetland Soils with Carbon Addition. *Wetlands Ecol Manage* **2021**, *29* (3), 369–379. https://doi.org/10.1007/s11273-021-09783-y.
(225) Althoff, F.; Jugold, A.; Keppler, F. Methane Formation by Oxidation of Ascorbic Acid Using Iron Minerals and Hydrogen Peroxide. *Chemosphere* **2010**, *80* (3), 286–292. https://doi.org/10.1016/j.chemosphere.2010.04.004.
(226) Peiffer, S.; Kappler, A.; Haderlein, S. B.; Schmidt, C.; Byrne, J. M.; Kleindienst, S.; Vogt, C.; Richnow, H. H.; Obst, M.; Angenent, L. T.; Bryce, C.; McCammon, C.; Planer-Friedrich, B. A Biogeochemical–Hydrological Framework for the Role of Redox-Active Compounds in Aquatic Systems. *Nat. Geosci.* **2021**, *14* (5), 264–272. https://doi.org/10.1038/s41561-021-00742-z.
(227) Hu, J.; Inglett, K. S.; Clark, M. W.; Inglett, P. W.; Ramesh Reddy, K. Nitrous Oxide Production and Consumption by Denitrification in a Grassland: Effects of Grazing and Hydrology. *Science of The Total Environment* **2015**, *532*, 702–710. https://doi.org/10.1016/j.scitotenv.2015.06.036.
(228) Wrage, N.; Velthof, G. L.; van Beusichem, M. L.; Oenema, O. Role of Nitrifier Denitrification in the Production of Nitrous Oxide. *Soil Biology and Biochemistry* **2001**, *33* (12), 1723–1732. https://doi.org/10.1016/S0038-0717(01)00096-7.
(229) Li, Z.; Tang, Z.; Song, Z.; Chen, W.; Tian, D.; Tang, S.; Wang, X.; Wang, J.; Liu, W.; Wang, Y.; Li, J.; Jiang, L.; Luo, Y.; Niu, S. Variations and Controlling Factors of Soil Denitrification Rate. *Global Change Biology* **2022**, *28* (6), 2133–2145. https://doi.org/10.1111/gcb.16066.

Appendix 1

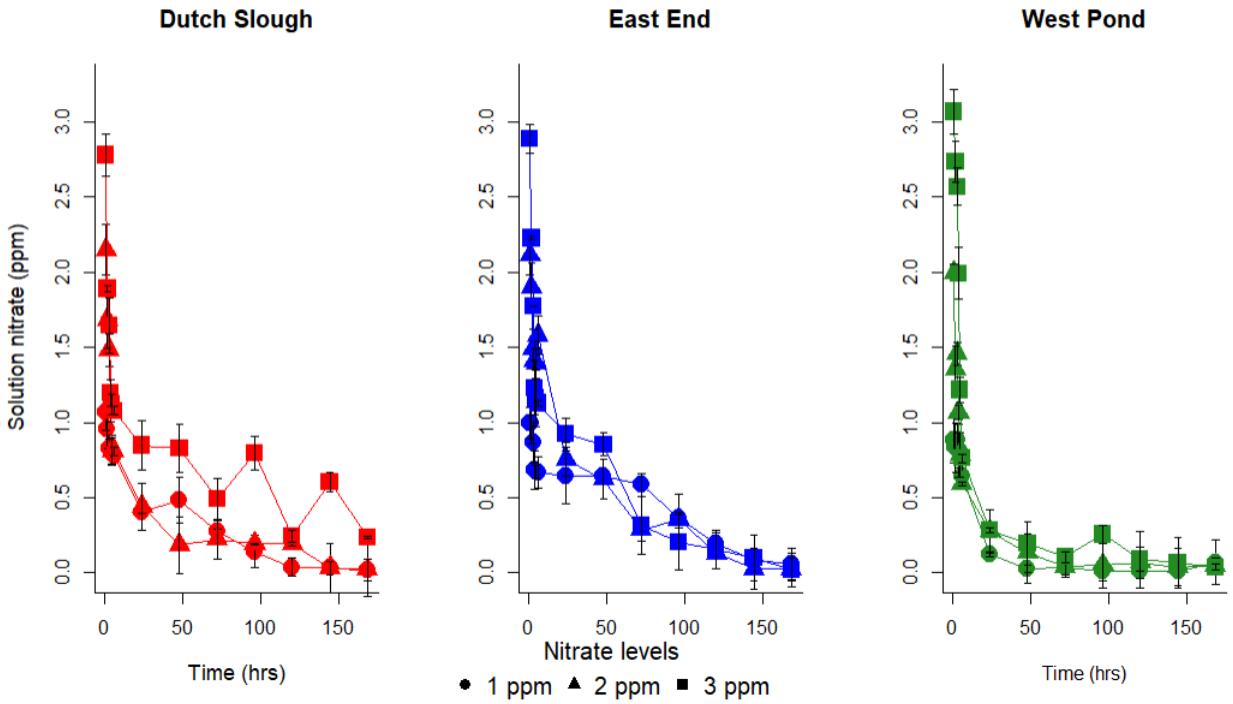

Figure 63. Evolution of nitrate concentrations in the slurry experiments over time.